GEOMETRIC QUANTUM HYDRODYNAMICS AND BOSE-EINSTEIN CONDENSATES: NON-HAMILTONIAN EVOLUTION OF VORTEX LINES

by

Scott A. Strong

A thesis submitted to the Faculty and the Board of Trustees of the Colorado School of Mines in partial fulfillment of the requirements for the degree of Doctor of Philosophy (Applied Physics).

Golden, Colorado

Date _____

Signed: _____
Scott A. Strong

Signed: _____
Dr. Lincoln D. Carr
Thesis Advisor

Golden, Colorado

Date _____

Signed: _____
Dr. Uwe Greife
Professor and Head
Department of Physics

ABSTRACT

Geometric quantum hydrodynamics merges geometric hydrodynamics with quantum hydrodynamics to study the geometric properties of vortex structures in superfluid states of matter. Here the vortex line acts as the fundamental building block and is a topological defect of the fluid medium about which the otherwise irrotational fluid circulates. In this thesis, we show that except for the simplest fluid flows, a vortex line seeks to decompose localized regions of curvature into helical configurations. The simplest flow, known as the local induction approximation, is also an integrable one. Integrability makes the transfer of energy into helical modes impossible. In the following, we demonstrate that any arclength conserving correction to this approximation defines a non-Hamiltonian evolution of the vortex geometry, which is capable of supporting dissipative solitons and helical wavefronts. Quantum turbulence in ultracold vortex tangles relies on energy transfer between helical or Kelvin modes to decay. Thus, models of vortex lines beyond the lowest order integrable cases are vitally important to our mathematical description of free decay of turbulent tangles. To motivate the results of this thesis we connect our theory of vortex line dynamics to continuum fluid mechanics.

The Navier-Stokes equations are a statement of momentum balance for a fluid whose response to shear stress is proportional to the fluid's velocity gradients. Building off of Onsager's rather obscure work in fluid turbulence, others have shown that solutions to Navier-Stokes limit to Euler evolutions of distributional velocity profiles for large Reynolds number. Using this as our context, we show that the Euler equation can be transformed, in an inverse Madelung sense, to the Gross-Pitaevskii equation associated with the mean-field quantum dynamics of a dilute Bose gas. This theory predicts that an irrotational fluid is capable of circulating around regions of density depletion known as vortex lines. Furthermore, if a vortex line is used as the ansatz for the Gross-Pitaevskii equation then it is possible to

show that the Biot-Savart integral over the vortex source results. This connection between the vortex line geometry and the induced velocity field provides the basis for the application of geometric quantum hydrodynamics to Bose-Einstein condensates.

If the Biot-Savart integral is the basis of geometric quantum hydrodynamics, then Hasimoto's transformation is the structure built on top. The fundamental theorem of space curves states that up to rotations and translations, a curve is defined by its curvature and torsion. Through the Hasimoto transformation, it is possible to map flows defined by the Biot-Savart integral to scalar partial differential equations evolving the curvature and torsion of a vortex line. In this thesis, we conduct an asymptotic expansion of the Biot-Savart integral and apply the Hasimoto transformation to show that vortex lines prefer to relax curved abnormalities through the excitation of helical waves along the vortex. Thus, our model predicts a geometric mechanism for the generation of Kelvin waves and corrects a nearly 50 year old result to include the dynamics expected in our most primitive states of fluid matter.

Our derivation begins with the Biot-Savart integral representation of the velocity field induced by a vortex line. We derive an exact representation of the velocity field in terms of the incomplete elliptic integrals by approximating local regions of vorticity with plane circular arcs. The velocity field is shown to be a combination of three fields defining axial flow, circulation and a binormal flow that appears in the presence of non-trivial curvature. The latter flow explains why vortex rings of smaller diameter travel faster than larger rings. Using known asymptotic formulae for the elliptic integrals allows us to move past the lowest order local induction approximation. The asymptotic representations are valid for the regime where the local curvature is small relative to the inverse of the vortex core size and are applicable to vortex lines in Bose-Einstein condensates.

To understand the predictions stemming from our asymptotic representation of the local velocity field, we compute two key quantities. First, we consider the expansion of the local field in powers of curvature to define corrections to the flow when curvature becomes large. Second, we consider the Hasimoto transformation of the general induced binormal flow. The

result is a scalar evolution of the curvature and torsion for configurations of vortex lines with significant bending. Moving past the local induction approximation causes Hasimoto's transformation to map the local flow onto a nonlinear integro-differential equation. Through the use of our asymptotic expansion, this evolution reduces to a nonlinear partial differential equation amenable to both symbolic and numerical analysis.

Our symbolic analysis shows that a specific nonlinear term in the partial differential equation prohibits a Hamiltonian formulation of the problem. Using conservation laws associated with the local induction approximation, we consider how the non-Hamiltonian term gives rise to a dissipative mechanism allowing gain and loss of curvature in the vortex medium. Additionally, we derive a nonlinear dispersion relation predicting that low wavenumber helical modes jettison from locally curved regions. Consequently, curved regions seek to relax their bending through the production of helical structures. If the curvature is created through a vortex reconnection, then helical Kelvin waves couple the vortex to the Bose-Einstein condensate for the purposes of phonon generation and are expected to be the route to decay in free quantum turbulence.

We corroborate these predictions with simulations of corrections to initial states predicted by the local induction approximation. Specifically, we simulate out of plane perturbations of a vortex ring, along with soliton and breathing states. A detailed analysis of the soliton state shows a transition to a log normal distribution where curvature disperses ahead of the traveling wave. On the vortex, this appears as a helical wavefront propagating into an otherwise straight line. The non-Hamiltonian gain mechanism acts to support Kelvin modes as they travel and keeps the initial peak profile from completely eroding, a feature indicative of a dissipative soliton. These dynamics were also seen in both the breathing and ring states. Thus, geometric quantum hydrodynamics predicts that the simplest flow of curved regions on a vortex line generates Kelvin waves providing a route to the anomalous dissipation first predicted by Onsager.

TABLE OF CONTENTS

LIST OF FIGURES

ACKNOWLEDGMENTS

I would like to start by thanking my advisor Dr. Lincoln D. Carr who introduced me to the geometric formulation of vortex motion in Bose-Einstein condensates, which has proven to be a playground of mathematical physics. Without his guidance, dedication, and strength, I would have never completed this work. While it is time to take my next steps, I think fondly of our work together and hope to call him a collaborator and friend long into the future. As I move away from this peak event, I realize that the roller coaster ride was actually fun. Thanks to him for convincing me to do it!

In addition to Lincoln, I would like to acknowledge my thesis committee members. Dr. Paul Martin, Dr. Junko Munakata Marr, and Dr. David Wood who took great care in evaluating my work. Even as I complete this document, I continue to learn from their insightful comments and suggestions. Being an educator myself, I understand how much time is devoted to students and how this often goes unrecognized. I thank each of you for your time, feedback and support. There are five or six educators who have shaped my own practice. Drs. Martin and Wood, the two of you are without a doubt on this list. Specifically, Dr. Martin taught me that in exposition, less is more. On the other hand, Dr. Wood showed me that an altogether different, but equally important, mode of learning occurs when the intensity is taken to eleven. Lastly, Dr. Munakata Marr thank you for coming outside of your home department to support me as I came out of mine. The Mines community would not be the same without you.

I have had so many great educators and colleagues that there is no way that I could produce an exhaustive list. However, I would like to thank Dr. John DeSanto and Dr. Bernard Bialecki. The former taught me that having a multitude of ways to explain a single concept is extremely valuable and the latter made it clear that this is no substitute for knowing one of these ways with clarity. To the members of the Carr group who I have worked with over

the years, your feedback is appreciated and has proven quite useful in building the topics of this thesis. Michael Wall, Laith Haddad, and Anastasia Gladkina your encouragement over the years has been greatly appreciated. To the members of the Department of Applied Mathematics and Statistics, thank you for your understanding and support as I have worked towards completing this degree.

Since 2001, I have had the opportunity to teach several thousand Colorado School of Mines undergraduate students topics from mathematics to computer science. Some days I remember students who I taught years ago, while other days it is someone who I have interacted with quite recently. With so many memories, there is no way to fairly distribute the acknowledgment and so let me just say that I would not be here today without these numerous positive student interactions. As a group, they have pushed me to explain concepts without being overly bound to the perspective of my training. At the same time, their open and honest conversations have provided the support necessary for me to get out of my comfort zone. As they are who I am thinking of as I write, their influence can be seen throughout this thesis.

I will never be able to properly thank my family and friends for all they have given me. Gus Greivel, Holly Eklund, and Terry Bridgman, thanks for listening to the rants, the excitement, and the disappointments. Alex Yuffa, thanks for always being there, I think of you as a brother. To my actual brother, Kenny Strong, thanks for always believing in me. To my parents, Kenneth and Mei-Yeuh Strong, I am a difficult personality to support but your unconditional love and encouragement are exactly what I needed. Jala and Mona, thanks for making me play with dolls and color pictures. For the record, the pictures I drew were equations. Some even appear in this thesis! Thanks for thinking they were cool. None of this would have been possible without Jennifer Strong: you will have my thanks for the rest of time.

Square One

Had to find some higher ground
Had some fear to get around
You can't say what you don't know
Later on won't work no more
Last time through I hid my tracks
So well I could not get back
Yeah my way was hard to find
Can't sell your soul for piece of mind
Square one, my slate is clear
Rest your head on me, my dear
It took a world of trouble, a world of tears
Took a long time... to get back here

Try so hard to stand alone
Struggle to see past my nose
Always had more dogs than bones
I could never wear those clothes
It's a dark victory
You won and you also lost
Told us you were satisfied
But it never came across
Square one, my slate is clear
Rest your head on me, my dear
It took a world of trouble, a world of tears
Took a long time... to get back here

Tom Petty - 2006

CHAPTER 1

QUANTUM HYDRODYNAMICS, BOSE-EINSTEIN CONDENSATION, TURBULENCE AND GEOMETRY

Geometric hydrodynamics is the application of differential geometry to fluid mechanics and originates from a 1966 paper written by V. I. Arnold. [1] In this work, Arnold demonstrates that the evolution of an incompressible and inviscid fluid defines a geodesic flow in the space of invertible deformations of the fluid body. Through this abstraction, he provides a connection to Euler's rotation equations associated with rigid rotating bodies. This collaboration between mathematical analysis and geometry has furthered our understanding of hydrodynamic stability, as well as the relationship between Newton's equations and Schrödinger evolutions. [2, 3] Quantum hydrodynamics is the study of a subset of fluid phenomena having quantum characteristics. In abstraction, it applies to the fields of semiconductor devices, quantum chemistry, superfluidity, astrophysical dynamics in neutron stars, and quark-gluon plasmas. [4] We call the merger of these two distinct theories Geometric Quantum Hydrodynamics. A goal of this theory is to understand the behavior of quantized vortices common to the previous phenomena. In the field of quantum turbulence, the vortices provide a geometric structure to the flow making a complete understanding of vortex line dynamics vitally important to the field.

Geometric quantum hydrodynamics starts with the early 20^{th} century work of Da Rios, a student of Levi-Civita, who first demonstrated that points on a vortex line flowed in the local binormal direction and at a speed proportional to the local curvature. [5] While the result was repeatedly rediscovered throughout the 20^{th} century [6, 7], it was the work of Hasimoto in 1972 [8] which truly brought the study of line dynamics back to its roots in differential geometry. In this framework, one can study how an ambient fluid flow affects embedded vortex lines in terms of the line's curvature and torsion. Hasimoto showed that

the vortex geometry is evolved by a cubic focusing one-dimensional nonlinear Schrödinger equation, which is both Hamiltonian and integrable. This connection to integrable dynamics increased the type and number of tools that could be used to study the geometry of a vortex line. However, between the incredible balance necessary to sustain integrability and the lack of available experimental fluids adequately modeled by vortex lines, Hasimoto's work resulted mostly in symbolic analysis. Twenty-years of sophisticated experimentation with Bose-Einstein condensation with a quantitatively correct mathematical model stands to change all of this. Additionally, it is now known that Hasimoto's transformation is a manifestation of Madelung's 1926 transformation between Schrödinger's equation [9] and the Newtonian momentum balance defined by the Euler evolution of a fluid continuum. [3] One goal of this thesis is to connect these continuum principles to the Hamiltonian flow of vortex lines.

In this thesis, we build on this line of research specifically as it relates to the dynamics of vortices in Bose-Einstein condensates. Our ability to engineer and control the dynamics of vortex states coupled to imaging the system through standard optical methods, and the appropriateness of vortex line models, make Bose-Einstein condensates unlike any other experimental fluid system. In brief, the body of this thesis generalizes the asymptotic theory of binormal flow to derive a scalar partial differential equation that is capable of relaxing localized regions of curvature into traveling packets of helical waves known as Kelvin waves. In a quantum liquid, the reconnecting vortices provide moments where curvature can become locally large. The generation of Kelvin waves from these events is a necessary ingredient for the complete understanding of decay in quantum turbulence and is an example of the anomalous dissipation of kinetic energy first conjectured by Onsager in 1949. [10] In this introduction, we provide an impression of quantum hydrodynamics and its geometric tools. We assume that the reader is a student of mathematics or physics and is starting their advanced training in either discipline. Since many prospective readers may never have studied fluid or quantum mechanics, we quickly provide some key features of the fields.

After this, we discuss a mathematical model associated with Bose-Einstein condensation and through a direct analogy with electromagnetism, we discuss geometric aspects of quantum hydrodynamics. We conclude with how these results can be applied to quantum turbulence and review the current status of experiments. After our conclusions, we present an outline of the contents of this thesis.

1.1 Fluid Turbulence, Reynolds Number and Quantum Mechanics

Elements of fluid mechanics are present in a simple first order autonomous ordinary differential equation modeling the free fall of a particle flowing through a fluid medium. Newton's second law gives

$$\frac{d}{dt}\left(mv\right) = mg - \gamma_1 v - \gamma_2 v^2,\ m, g, \gamma_1, \gamma_2 \in \mathbb{R}^+, \tag{1.1}$$

where $v : \mathbb{R}^+ \to \mathbb{R}_0^+$ and γ_1, γ_2 are drag coefficients given by Einstein-Stokes [11] and Lord Rayleigh [12], respectively. While it is interesting to note how the form of the solution is significantly more complicated in the nonlinear case than the linear case, it is more important for our purposes to non-dimensionalize the equation and pit the velocity terms against each other. Doing so one finds that the nonlinear drag term dominates the dynamics when

$$R_{\mathrm{e}} \propto \frac{\gamma_2 \tilde{v}}{\gamma_1} = \frac{\rho C_d A \tilde{v}}{12\pi\mu r} \gg 1. \tag{1.2}$$

In the numerator, we have the mass density of the fluid, ρ, the characteristic velocity of the flow, $\tilde{v}$, incident on a cross-sectional area, A and a non-dimensional drag coefficient, C_d, which is experimentally tuned to the object and fluid. In the denominator, we have the fluid viscosity, μ, and the Stokes radius, r, given by the size of a spherical particle used to define the diffusivity within the fluid. This ratio defines the Reynolds number, R_{e}. An inspection of the dimensions shows that Reynolds number determines whether energy transfer via momentum exchange or viscous drag dominates the flow dynamics. For large Reynolds number, the fluid does little to oppose shear stress and, consequently, supports the creation

of stagnation points and turbulent eddy formation. For small Reynolds number, the flow around the falling object tends to be laminar forming smooth streamlines. The difference between these two regimes may be understood through the classic skydiver problem. [13] Prior to parachute deployment, the flow is mostly laminar. After the canopy is unfurled, the fluid flow becomes highly turbulent. This thesis is concerned with fluids whose Reynolds number is so large that it can be treated as formally infinite. Such fluids are created at low temperatures where quantum mechanical effects are non-negligible.

A Bose-Einstein condensate is a state of matter, first predicted in 1924 [14, 15] and realized in experiments roughly 70 years later. [16] It consists of a preparation of bosonic matter cooled to a point where a large fraction of the particles occupies the lowest quantized energy state. To understand the mathematical model of the condensate, one must be exposed to a modicum of quantum mechanics, a topic often not covered in most mathematics sequences. Consequently, we quickly build quantum mechanics from the perspective of a dynamical system common to the undergraduate science curriculum.

Recall that the dynamics of an object of constant mass connected to a Hookean spring which is subjected to neither drag nor an external force is given by $m\ddot{y} + ky = 0$ where $m, k \in \mathbb{R}^+$ and $y = y(t)$ measures the displacement of the mass from its equilibrium position $(y, \dot{y}) = (0, 0)$ in the phase space spanned by the y and $\dot{y}$ vectors. Trajectories in this phase space correspond to level curves of the Hamiltonian energy surface given by $H(y, \dot{y}) = m\dot{y}^2/2 + ky^2/2$, where the terms represent kinetic, T, and potential, V, energies, $H = T + V$. Dissipation given by linear/laminar drag manifesting from the motion of the mass relative to a fluid background, say through a shock absorber where a paddle is pushed through a viscous fluid, continuously drains energy from the system and eventually returns it to equilibrium.

The conservative problem can be reformulated by defining the subtraction of the kinetic and potential energies and is known as the Lagrangian, $L = T - V$. This quantity then defines an action functional, $S(y, \dot{y}) = \displaystyle\int_{t_0}^{t_1} L(y, \dot{y})\, dt$, acting on the space of all possible

trajectories connecting $y(t_0)$ and $y(t_1)$. The principle of least action asserts that the solution to this mass spring problem is the function that minimizes the variation of this action. For $m = k = 1$, one can quickly see that the two trajectories $y_1(t) = \cos(t)$ and $y_2(t) = 1 - 2t/\pi$ give very different actions on the interval $0 \leq t \leq \pi$ with y_1 being smaller. If we trust the principle of least action, then our intuition over the mass spring system tells us that y_1 is a minimizer of the action. A more powerful perspective is found through the application of the calculus of variations which states that the path minimizing the action functional must also satisfy the Euler-Lagrange equations, $\frac{d}{dt}\left(\frac{\partial L}{\partial \dot{y}}\right) = \frac{\partial L}{\partial y}$, which recovers Newton's second law, $\frac{d}{dt}(m\dot{y}) = -\nabla V$ where $V = V(y)$. It is this modern perspective of mechanics which has allowed inroads connecting quantum and classical physics.

Starting with the work of Dirac, Feynman realized that quantum mechanics could be recovered from the Lagrangian formulation of classical mechanics. [17] He assumed that the probability amplitude of a quantum process, also known as a wave function, ψ, was defined by the contributions of all possible paths joining two points in configuration space and that each path contributed to the wavefunction by an amount proportional to $e^{iS/\hbar}$, where Planck's constant, $\hbar$, is introduced to non-dimensionalize the exponent. Feynman began by summing the individual contributions over all configurations and time evolved the wave function an infinitesimal amount. Power expanding the wave function in the spatial variable and retaining only linear terms in the time perturbation yields an evolution of the wave function given by $i\hbar\psi_t = -\hbar^2 \triangle \psi/2m + V\psi$, which is Schrödinger's equation, where $\triangle = \partial_{xx} + \partial_{yy} + \partial_{zz}$. While the classical particle definitely takes a path that minimizes the action, the quantum particle takes all paths and those with large action define highly oscillatory integrands that tend to cancel themselves out when integrated over the configuration space. Consequently, the square of the complex modulus of the Feynman's probability amplitude defines a probability density function dominated by those states whose action is small.

A typical example is to contrast the classical harmonic oscillator with its quantum analog, $i\hbar\psi_t = \hat{H}\psi = -\hbar^2\psi_{xx}/2m + m\omega x^2\psi/2$. [18, 19] Both cases model a dynamical point particle

near a potential energy minimum. However, one finds that while the classical oscillator can assume any energy from a continuously infinite spectrum bounded below by zero, the quantum harmonic oscillator can only access a countably infinite set of non-trivial energies. The concept of quantization of an observable with a well-defined lowest energy state has useful analogs in the setting of quantum hydrodynamics. However, since a single particle is far from a fluid state, we must consider a dilute Bose gas cooled to a point where quantum effects manifest.

1.2 Mean-Field Dynamics and Quantum Hydrodynamics

The quantum many-body problem, defined by a vector Schrödinger equation, is intrinsically a linear one and though it does not suffer from the same problems as classical chaos, realistic interacting systems are generally intractable due to the large number of degrees of freedom. For example, dilute Bose-Einstein condensates can have on the order of 10^6 particles, or more, and bosonic stars have 10^{30}. Both systems yield intractable symbolic and numerical problems unless the particle interactions are turned off. The goal is to introduce interactions in such a way that an effective evolution equation can be found. [20, 21] Specifically, a system of N identical bosons with mass m are subjected to the external potential field $V(\mathbf{x})$ and permitted to undergo two-body interactions defined by point-like particle interactions. The Born approximation provides an effective two-body interaction strength related to the scattering length, which is constant in momentum space. The interaction potential in configuration space is related by Fourier transform and is therefore given by a Dirac function. The many-body Hamiltonian for such a system is given by,

$$H = \sum_{i=1}^{N} -\frac{\hbar^2}{2m}\triangle_{\mathbf{x}_i} + V(\mathbf{x}_i) + \frac{U}{2}\sum_{i\neq j}\delta(\mathbf{x}_i - \mathbf{x}_j). \tag{1.3}$$

The energy of the system is given by the quadratic form defined by the integration, $E = \int \bar{\Psi} H \Psi d\mathbf{x}_1\mathbf{x}_2\mathbf{x}_3 \ldots d\mathbf{x}_N$, where $\bar{\Psi}$ is the complex conjugate of the many-body eigenvector associated with the operator equation $H\Psi = E\Psi$. If all bosons are in the condensed state,

then the many-body wave function can be written as the product of normalized single-particle wave functions, ψ,

$$\Psi(\mathbf{x}_1, \mathbf{x}_2, \mathbf{x}_3, \ldots, \mathbf{x}_N) = \prod_{i=1}^{N} \psi(\mathbf{x}_i), \quad \int_{\mathbb{R}^3} d\mathbf{x}\, \psi(\mathbf{x}) = 1. \tag{1.4}$$

The normalized many-body wave function is then given by $\Psi = \sqrt{N}\psi$. Substituting this into energy functional defined by the Hamiltonian operator gives

$$E = \int d\mathbf{x} \bar{\Psi} \left[-\frac{\hbar^2}{2m} \triangle + V(\mathbf{x}) + \frac{U}{2} |\Psi|^2 \right] \Psi. \tag{1.5}$$

Minimizing the variation of this energy with respect to $\bar{\Psi}$, subject to the normalization constraint, defines a Lagrange multiplier problem, which is solved by requiring that

$$\left[-\frac{\hbar^2}{2m} \triangle + V(\mathbf{x}) + \frac{U}{2} |\Psi|^2 \right] \Psi = \mu \Psi \tag{1.6}$$

where μ is the thermodynamic quantity describing the change in energy associated with particle occupancy number known as the chemical potential. Equation (1.6) defines the time-independent Gross-Pitaevskii equation and the condensate wave function associated with the eigenvalue μ describes a collection of bosons sharing the same chemical potential. In analogy with Schrödinger evolutions, the time-dependent Gross-Pitaevskii equation is given by

$$i\hbar \frac{\partial \Psi}{\partial t} = -\frac{\hbar^2}{2m} \triangle \Psi + V(\mathbf{x})\Psi + \frac{U}{2} |\Psi|^2 \Psi. \tag{1.7}$$

The connection between the time-independent and time-dependent equations is found in the relationship between the chemical potential and the phase factor associated with the destruction of ground state particles in the large particle number limit. Additionally, it is possible to derive the time-dependent Gross-Pitaevskii equation using the principle of least action for a Lagrangian formulation where the energy density Hamiltonian is fourth order in

the condensate wave function. Both cases are too technical for our needs. Instead, we note that this equation is a Schrödinger equation where the external potential V is augmented by a nonlinear term that averages the condensate field where the interaction energy felt by an atom is replaced by the condensate density multiplying an effective interaction. For the reasons above, Eq. (1.7) is defined as a mean-field equation and is accurate when the condensate fraction is close to 100%.

In 1926 Erwin Madelung transformed the Schrödinger equation into a system of hydrodynamic equations. [9] In doing so, he gave birth to the field of quantum hydrodynamics relating the dynamics of a single quantum particle to a mass conserving inviscid flow. Here the probability density field corresponds to the fluid mass density which is evolved by a velocity field satisfying Euler's equations. While a single point does not make a fluid, a collection of bosons condensed into a gas evolved by the Gross-Pitaevskii equation does. Madelung's transformation begins by assuming that $\Psi = \sqrt{\rho}\, e^{i\phi}$ and separates Eq. (1.7) into real and imaginary parts yielding the following equations,

$$\frac{\partial \rho}{\partial t} + \nabla \cdot (\rho v) = 0 \tag{1.8}$$

$$\frac{\partial \phi}{\partial t} + \frac{1}{2m}|\nabla \phi|^2 = \frac{\hbar^2}{2m}\frac{\triangle \sqrt{\rho}}{\sqrt{\rho}} - \rho \tag{1.9}$$

where $\mathbf{v} = \nabla \phi$. Taking the gradient of Eq. (1.9) shows that the Madelung transformation describes a Bose-Einstein condensate as an inviscid barotropic fluid whose evolution is given by a mass conserving Euler equation. This flow is manifestly potential and therefore irrotational. That is, if curl defines the axis of rotation at a point in the fluid, then a potential flow has trivial vorticity on its domain, $\boldsymbol{\omega} = \nabla \times \mathbf{v} = \nabla \times \nabla \phi = \mathbf{0}$. That said, it is clear from both experiments and simulations that turbulent states of this fluid exist and are structured about its vorticity. If the system has trivial curl throughout, then what vorticity does this system possess? To resolve this question, we mention a common problem posed to calculus students which is focused on subtleties of the hypotheses of Stokes' theorem. Here one finds that manipulation of the fluid geometry allows for a vortex state to exist, manifesting as pure

circulation. In the next section, we investigate this problem while utilizing a little bit of electromagnetic theory to contextualize the result.

1.3 Geometric Aspects of Quantum Hydrodynamics

Assuming an undergraduate background in the physical sciences, we draw on an analogy with electromagnetism to incorporate a discussion of the geometric elements of fluid mechanics. Specifically, Maxwell's equations define how the coupled electric and magnetic fields are capable of inducing dynamics on each other. While this is not a fluid system, it is a common one and provides an excellent analogy to the hydrodynamics discussed in this thesis. Specifically, the Maxwell-Faraday equation tells us that the flux of a magnetic field can induce a current along the boundary of a smooth orientable surface. From this mechanism of action, one suspects that a steady current flowing along a one-dimensional curve can induce a magnetic field. The Biot-Savart integral is the mathematical counterpart to this intuition and, in principle, allows one to write down the magnetic field given the geometry of the wire on which the current steadily flows. The connection between these statements and fluid mechanics is provided by the abstraction of vector analysis, which is the language used to describe both theories. In the setting of fluid mechanics, vorticity plays the role of current and the field which it induces is not magnetic but, instead, the fluid velocity. A typical problem in a multivariate calculus class is to demonstrate that the field $\mathbf{F} = -\dfrac{y}{x^2+y^2}\hat{\mathbf{i}} + \dfrac{x}{x^2+y^2}\hat{\mathbf{j}}$ satisfies the condition $\nabla \times \mathbf{F} = 0$ everywhere in the domain of $\mathbf{F}$, but defines the circulation $\oint_C \mathbf{F} \cdot d\mathbf{r} = 2\pi$, which is seemingly in contradiction with Stokes' theorem. The problem is resolved when one notices that $\mathbf{F}$ is not defined at the origin. This breaks down the simple connectivity of the plane and not every closed path in $\mathbb{R}^2$ defines a region whose points lie in the domain of the field $\mathbf{F}$. The non-zero circulation about the singularity of the otherwise irrotational field, $\mathbf{F}$, leads one to interpret $\mathbf{F}$ as a simple source known as a point vortex. [22] Moreover, the non-triviality of the fundamental group on this topological space leads to the convention of calling this vortex a topological defect of $\mathbb{R}^2$. While this is not the most interesting example, one can think of joining a continuum of these defects into a vortex line in

$\mathbb{R}^3$. As the analog of a steady line current, the Biot-Savart integral can be used to accumulate the vorticity over the line source to recover the induced velocity field. For fluids, we find that the circulatory field is capable of causing the vortex to flow through the ambient space while altering its curvature and torsion.

The theorems of Kelvin and Helmholtz state that the motion of a vortex line is that of the ambient fluid in which it is embedded. [23, 24] Vector analysis tells us that the incompressible component of the velocity field induced by the vortex has a representation through the Biot-Savart integral. [25] Generally, the autonomous flow generated by a planar vortex line can be decomposed into three components representing the axial/tangential, circulatory and binormal flows, the latter two vanishing if the vortex has trivial curvature. A rich and useful theory can be constructed around the assumption that each segment of vorticity can be well approximated by a planar vortex line. Specifically, by focusing our analysis on the fluid flow manifesting from a curvature dependent binormal flow, one can define a class of wave motions described by the geometric deformations along the vortex. In this thesis, we study this theory and report on new results predicting that binormal motion endows the vortex medium with dispersion and gain/loss mechanisms which are necessary to support helical wave generation sourced by locally curved regions. This generation of Kelvin waves on a vortex line is important to the decay mechanisms of quantum turbulence. [26, 27] Our key point is that any amount of correction to the most primitive motion of a vortex line results in the generation of Kelvin waves. As these Kelvin waves are important to our understanding of quantum turbulence, models incorporating this dynamic are vital for future development of the field. From the creation of the froth that tops our macchiato, to passing large trucks while driving, our everyday experience provides many examples of classical turbulence. Quantum turbulence is different enough to warrant a focused discussion. In the following, we give an overview of the phenomenon and review the current status of experiments in Bose-Einstein condensates.

1.4 The Anatomy of a Vortex Line and Kelvin Waves

If the principal character of this thesis is a vortex line, then it makes sense to discuss its features with an emphasis on its geometric properties. First, we consider the density profile of a vortex line. Similar to a classical hydrodynamic vortex created by emptying a column of water, a quantized vortex in a Bose-Einstein condensate is a region of low density. However, a significant difference between the two is in how the density tends to zero as we approach the vortex. In 2004 Berloff applied a Padé approximation to the nonlinear Bessel equation defined by the radial component of the time-independent Gross-Pitaevskii equation. Doing so, she arrived at an approximation to the density profile of a straight line vortex in a uniform condensate. Aligning the vortex with the z-axis implies that every planar cross-section perpendicular to this axis has the same density profile. Assuming that the density vanishes at $r = 0$ in an arbitrary planar cross-section and that the density tends to one as $r \to \infty$, defines a profile given in Figure 1.1a. The healing length or vortex core size is defined by the characteristic length needed for the condensate to return to the bulk density, In Figure 1.1b we plot the radial distance from the vortex line as a function of condensate density. Though the far-field density profile changes considerably for trapped condensates, our derivations assume that the condensate is so large that boundary conditions contribute negligibly to the vortex density profile.

A general vortex line is a one dimensional topological defect of the condensate cloud with a cross-sectional density profile as approximated in the work of Berloff. We consider now how differential geometry describes the vortex. In Figure 1.2 we depict the vortex line, its osculating plane, curvature profile and normal plane. The vortex line is a function of arclength s and time t. At each point on the vortex there is a local orthogonal coordinate system, known as the Frenet frame, consisting of the tangent ($\mathbf{T}$), normal ($\mathbf{N}$), and binormal ($\mathbf{B}$) vectors. Additionally, at each point, two scalar quantities are defined. The curvature, κ, defines how the vortex fails to be straight, and the torsion, τ, describes how the vortex fails to be planar. Differential geometry tells us that the linear system of non-autonomous ordinary

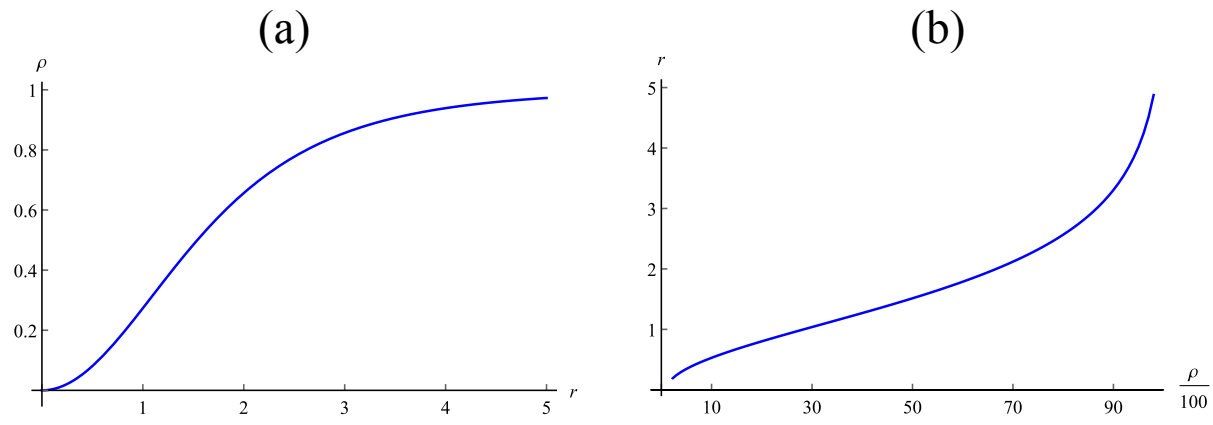

Figure 1.1: Vortex Line Density Profile. (a) The Padé approximation of the cross sectional density profile of a straight line vortex in an uniform Bose-Einstein condensate. We see a smooth return from the density depletion defining the vortex line at the radial origin to a bulk value $\rho(r) \to 1$ as $r \to \infty$, in non-dimensional variables. (b) The radial distance as a function of percentage of the bulk. This approximation predicts that it takes roughly 3.41636 non-dimensional radial units to return to 90% of the bulk value.

differential equations, known as the Frenet-Serret equations, recovers the local tangent vector from the curvature and torsion. With this known, integration can be used to recover the vortex line. In other words, a vortex line is described by the point to point changes given by Frenet circles. The radius of this circle defines the reciprocal of curvature, $R = \kappa^{-1}$. Additionally, we depict the vortex core size, ξ, and associate the embellished girth given to the vortex in the figure with the density profile given in Figure 1.1. The vortex line depicted is such that $\tau = 1$ and $\kappa = 2\,\mathrm{sech}(s)$. This corresponds to a vortex line with a traveling kink. Kelvin showed that a helical deformation of a vortex line propagates as a wave. In this thesis, we show that curvature abnormalities on an otherwise straight vortex seek to decompose themselves into propagating helical/Kelvin waves.

Kelvin waves are fundamental objects in hydrodynamic flows but have different behaviors depending on the dimensionality of the system. This has a strong connection to turbulence, which we explain here. A two dimensional Kelvin wave occurs at the geophysical level when a warm water anomaly in the Pacific Ocean near the north coast of Australia is built by the west moving trade winds. An upwelling of cold water near South America occurs to

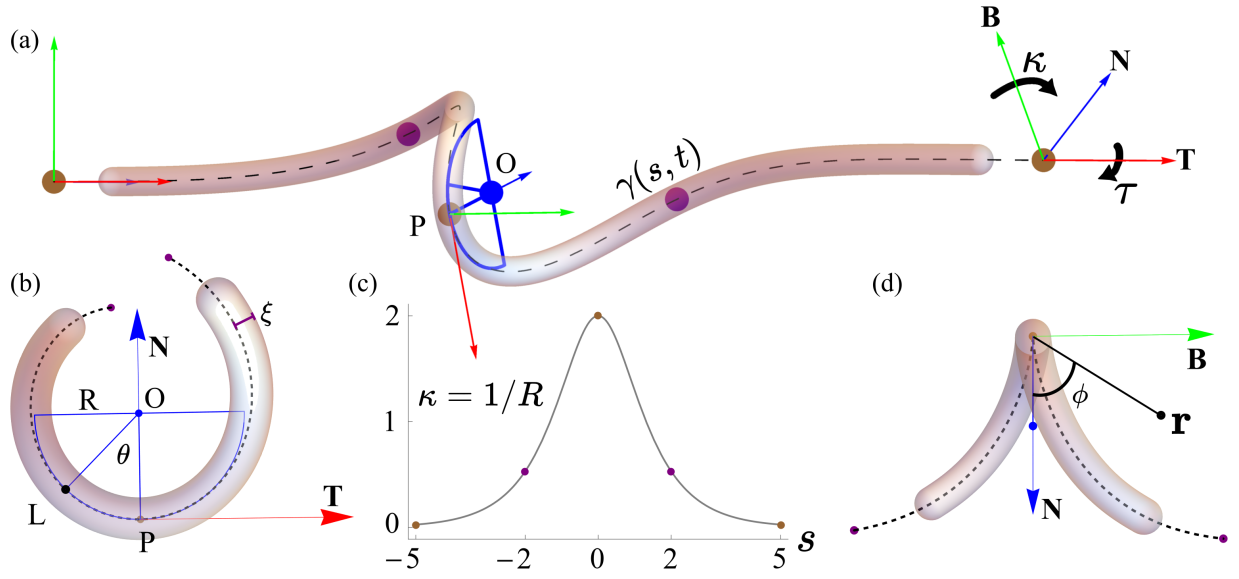

Figure 1.2: Vortex Line Geometry. This graphic appears in Chapter 5, as Figure 5.1. (a) The local orthogonal frame, tangent (red, $\mathbf{T}$), normal (blue, $\mathbf{N}$) and binormal (green, $\mathbf{B}$) vectors, at the initial, middle and terminal points (brown) of the vortex line, $\boldsymbol{\gamma}(s,t)$, with embellished width. At the reference point P we have a local description of the vortex given by a blue semi-circle. Changes to the Frenet frame from point to point are described by the curvature, κ, and torsion, τ. (b) View down the long axis of $\boldsymbol{\gamma}$ where we see the osculating plane spanned by the tangent and normal vectors. The local geometry at P is defined by the radius of curvature R, which is related to the curvature by $\kappa = R^{-1}$. The angle θ sweeps out an arclength from 0 to L providing a local parameterization to $\boldsymbol{\gamma}$ about P. The core scale is defined as ξ; in Bose-Einstein condensates taken as the superfluid healing length. (c) The curvature distribution associated with the vortex line in (a) with unit torsion. (d) The normal plane is spanned by $\mathbf{N}$ and $\mathbf{B}$, with observation point, $\mathbf{r} = (0, x_2, x_3)$, placed in this plane and defined by the polar angle ϕ.

compensate for this. This structure is normally stationary and sits in positive feedback with a circulatory atmospheric cycle of warm moist rainfall in the east and cool dry air in the west. However, if the east to west moving trade winds loses their strength, then it is possible for the warm water to diffuse into the cold region. When the balance is broken a global dynamic is created where Rossby waves, gigantic undulations of the ocean water, transport the cold water west. [28, 29] The warm water responds by traveling east, a motion further supported by the Coriolis force causing the Equator to act as a waveguide. The non-dispersive region of warm water steadily moving west forms an equatorial Kelvin wave. The large-scale release

of warm water causes an El Niño, which brings strong rain systems to the Americas. This Rossby-Kelvin interplay occurs generally and causes a strong delineation between circulatory flows in the northern and southern hemisphere, which leads to concentration of persistent surface structures. Specifically, vorticity in two dimensions tends to concentrate leading to long-scale persistent structures, like the great Pacific garbage patches and the Great Red Spot on Jupiter. [30] Specifically, in two dimensions vorticity injected into the system at small scales is capable of consolidating rotational energy into larger structures. This inverse cascade process is not present in three dimensions where the rotational energy of large eddies cascades to smaller length scales so that dissipation manifesting from molecular diffusion can relax the turbulent state. In Onsager's only published paper on turbulence theory, both cascade processes are discussed. [10] Interestingly, he conjectures a route to dissipation expected to arise in systems with negligible viscosity. At this time, Kelvin waves on a vortex line are expected to play a key role. In three dimensions, Kelvin showed that waves could live on vortex media and that helical deformations of a line of vorticity propagate along the vortex. [31] These helical distortions are fundamental modes of the hydrodynamic phenomenon and instead of concentrating energy, in a Bose-Einstein condensate, they act to excite acoustic waves traveling through the gas away from the vortex line in an effort to relax turbulent states. The generation of these modes from localized curvature abnormalities and their connection to continuum hydrodynamics is the focus of this thesis. In the next section we describe the manifestation of vortex lines in Bose-Einstein condensates and their subsequent turbulent state.

1.5 Quantum Turbulence and Experimental Bose-Einstein Condensates

In classical flows, turbulence is often contrasted with laminar flows. Laminar flows are defined by layered flows where the velocity and pressure fields see minimal disruption between these layers. Classical turbulence, instead, exhibits chaotic changes over the medium. Fundamental to this phenomenon is the formation of vorticity within the fluid, which is absent in the laminar regime as the flow lines are not permitted to circle back into themselves.

The classic example here is the turbulent breakdown of a flow of a fluid past an obstacle. As we move away from the laminar regime instabilities in the flow result in vortex shedding downstream of the cylinder producing von Kármán vortices. [32] Experiments show that the rotational energy of the vortices dissipates further downstream. In 1922 Lewis Richardson characterized the energy cascade process through which the dissipation is achieved with the following poem, "Big whirls have little whirls, that feed on their velocity, and little whirls have lesser whirls and so on to viscosity." [33] The life cycle of these vortices ends when they have reached length scales small enough to allow for molecular diffusion permitting viscous dissipation of angular momentum. If this is the characterization of classical hydrodynamic turbulence, then what can be said about quantum turbulence? To answer this question, we should first consider what a quantized vortex is and how one can achieve this state in the laboratory.

While the hypothesized state of matter known as Bose-Einstein condensation (1924-1925) predates the 1927 roll-out of the Model-A, Ford Motor Company's successor to the Model-T, experimental realization of this phenomenon did not occur until roughly 70 years later, June 5^{th}, 1995. This also happened to be the sixteenth birthday of the author who was enjoying his first solo drive as a new state of matter emerged on planet Earth. This achievement was celebrated six years later with a Nobel Prize shared between Eric Cornell and Carl Wieman, both affiliated with the University of Colorado at Boulder, and Wolfgang Ketterle of the Massachusetts Institute of Technology. [16] Since that time there has been a sustained interest in modeling, simulating and experimenting with what is essentially an extremely primitive continuum fluid that is capable of possessing quantum mechanical effects existing at macroscopic length scales.

A Bose-Einstein condensate is a dilute gas of atoms where the delocalized wave-like nature of the particles, as characterized by the de Broglie wavelength, is larger than the average interparticle spacing. In this case, the individual atoms collectively assume the ground state wave function of the Gross-Pitaevskii equation, Eq. (1.7). Production of this

degenerate gas begins with the collection of billions of atoms, or more, into a magneto-optical trap. This trap consists of an anti-Helmholtz coil used to create an almost fixed magnetic quadrupole field whose center is the focal point of counterpropagating lasers aligned along the coordinate axes. Atoms at this focal point lose momentum through interacting with the photons comprising the laser light and are thus cooled. As atoms move away from this focal point, the magnetic field shifts the atoms back to the resonant frequency of the laser light and they return to the slow-moving collection at the trap center. The subsequent free state is known as optical molasses where the billions of atoms exist in a region of space on the order of a cubic millimeter at temperatures around 10 milliKelvins. This slow collection of atoms is then cooled further through evaporation which can decrease the temperature by three orders of magnitude attaining the condensed state, while typically reducing the number of atoms to 10^5 to 10^7 depending on the experiment. The trap is then raised and after the hot particles thermalize with the cloud, the trap is lowered again to allow for evaporation. The end result of this process is a cloud of atoms that are significantly cooler, typically a few hundred nanoKelvin. While many of the atoms in the "molasses" are lost through evaporation, an experimentally viable Bose-Einstein condensate is left behind. [34]

A prepared Bose-Einstein condensate, can be supplied with angular momentum through rotation of the background potential. The resulting gaseous cloud of atoms roughly forms an ellipsoid and using the Gross-Pitaevskii equation to define an energy functional, one can numerically demonstrate that, away from the boundaries, the condensate will seek to form a lattice of vortices whose inter-vortex spacing is defined so as to minimize the system energy. Experimentally, it is observed that vortices will nucleate at the periphery of the condensate, move towards the bulk and arrange themselves into the predicted lattice. Such stable configurations of vortices were first proposed by Abrikosov in the setting of superconductivity. [35] There are, of course, several other ways to nucleate the vortices, e.g., wavefunction engineering, optical stirring, and synthetic magnetic fields that exploit equivalence between the Lorentz force and the Coriolis force. [36, 37] In 2001 an optically

stirred condensate produced a sample with 15 vortices [38] and just two years later rapidly rotating magnetic traps were used to produce over 4 to 10 times the number of vortices. [39, 40]

The oblate cloud of atoms making up the Bose-Einstein condensate is roughly 100 micrometers tall and twice the width. A vortex inside this cloud has a core width that is nearly two orders of magnitude smaller. [41] If the cloud was as wide as the Great Pyramid of Giza, then the vortex would be as wide as a Volkswagen Beetle. In superfluid helium, the system size is significantly larger by up to two orders of magnitude. If the condensate is the Pyramid of Giza then the superfluid helium system is the deepest point in the Mariana Trench. In superfluid helium, tracer particles are trapped inside the vortices and standard imaging processes are used. Nevertheless, for the much smaller Bose-Einstein condensates we have several avenues of quantitative imaging of the vortices. Most imaging techniques involve destroying the condensate through optical absorption. This can be done either *in situ* or during the expansion of the cloud after the trap has been turned off. In both cases the cloud is probed with a laser tuned to be absorbed by the atoms. The light making it through the cloud is imaged and the condensate features appear as a shadow which is recorded with a CCD camera. Spontaneous emission from the atoms occurs after the probing and eventually the system is destroyed through heating. Consequently, the condensate dynamics must be recovered by averaging multiple experimental runs. While this is certainly different than the ballistic expansion, true *in situ* images must be created through non-destructive means. Dispersive imaging is a method where off-resonance laser light is scattered by the cloud and analyzed separate from the incident light. The amount of heat deposited into the cloud is roughly 300 times less than that given by an on resonance probe. This allows for repeated imaging of the cloud dynamics that is far less destructive. [34, 42, 43] Additionally, a stroboscopic technique can be employed that sends in a microwave pulse, which jostles 1% to 10% of the atoms free from the condensate. As the dislodged atoms fall, the cloud they form expands to a point where standard digital optical methods are used. [44, 45]

A 2015 experiment in Trento, Italy, produced vortices in an oblate condensate comprised of roughly 10^7 sodium atoms confined to a harmonic trap by cooling the system through the Bose-Einstein condensate transition point to 200 nanokelvin, leveraging the Kibble-Zurek mechanism. In this scenario an atomic gas is cooled to a point where low energy modes are occupied before the gas undergoes the condensate phase transition. These high occupation but low energy states act as large amplitude waves which have random phases consistent with their still present thermal properties. The nodes of the superposition of these modes form density depletions that persist in the form of vortices when the system is rapidly quenched through the phase transition. [41, 46, 47] Using stroboscopic imaging techniques the precession dynamics were observed, as well as interactions between the vortex lines. It was found that the precession of a vortex about the trap center was minimally affected by the presence of multiple vortices. To explain this the authors put forward the hypothesis that either the vortices do not reconnect or a rapid double reconnection process ensues so that the overall dynamics are relatively unaffected. In a later collaboration with members of the Joint Quantum Centre in Newcastle, a similar condensate was prepared and compared against numerical simulations. [48] In this experiment, double reconnections along with near crossing rebound events for small relative velocities and ejection of vortices from the cloud were observed. They concluded that these dynamics were result of the inhomogeneous confined nature of the trapped cloud.

Two vortices do not make a vortex tangle, nor does an Abrikosov lattice of vortices constitute turbulence. The first experiment designed to explore quantum turbulence in Bose-Einstein condensates was a 2009 collaboration between researchers from the Universidade de Saõ Paulo, Brazil, with members from Universita di Firenze, Italy. Together they condensed roughly 10^5 rubidium atoms in a cigar-shaped trap in which vortices were nucleated by both shaking and spinning the trap. [49, 50] Contrary to the energy minimizing lattice, a disordered arrangement of vortices was observed through standard imaging techniques. A second indication that the cloud had achieved a turbulent state was given by its atypical

expansion that matched neither a quantum condensed state nor a thermalized state. More recently, the same group working with a similar experimental apparatus further demonstrated the ability to image quadrupolar modes, scissors modes, and ultimately vortices which evolved into a tangle. [51] In a 2014 review article, the Newcastle group summarizes the current state of turbulence in Bose-Einstein condensates and questions whether our experimental realizations with a relatively limited number of atoms, 10^3 to 10^9, can sustain the number of vortices needed to really become turbulent. [52] That year, the same authors reported on numerical simulations supporting the notion that optically stirring a spherically symmetric condensate with a Gaussian profiled laser provides an efficient means to generate a quantum tangle in a condensate, while minimally affecting the net transfer of angular momentum into the system. Establishing quantum turbulence in experimental Bose-Einstein condensates is difficult due to the limited number of vortices the cloud can support, a problem not shared by superfluid helium. [53] On the other hand, superfluid helium does not have a quantitatively correct model that can be used in conjunction with experimental data, where condensates have the Gross-Pitaevskii equation. The fundamental difference is in the nature of interactions. The two-fluid picture of quantum hydrodynamics decomposes the liquid into superfluid and normal states. While nearly 100% of the atoms in an experimental Bose-Einstein condensate are in the superfluid state, only a few percent of liquid helium atoms are superfluid. The Bogoliubov theory of excitations describes the momentum distribution of particles. The prediction is that the superfluid fraction is large for dilute liquids, in the sense that the length of interparticle spacing dominates the interaction length. This diluteness criterion cannot be maintained in liquid helium. Consequently, the superfluid fraction in liquid helium is depleted. [54] That said, simulations indicate that a vortex line model is an appropriate building block in both physical contexts.

In a 2017 review article, Tsubota outlines three environments for the simulation of quantum turbulence. [55] The first, and likely the oldest, is the vortex filament method, which assumes a line source of vorticity in an incompressible fluid and evolves the vortex structure in

accordance to its local flow expressed by either the Biot-Savart integral or approximations to it. The second method is a direct simulation of the continuum model given by Gross-Pitaevskii, which natively handles core-related phenomenon at the cost of simulating the entire fluid. The third method is due to Hall, Vinen, Bekharevich, and Khalatnikov and is based on the two-fluid model where a superfluid coexists with a normal Navier-Stokes like fluid. In this model, the interaction of the two components introduces a dissipative mechanism. Tsubota ends the article with open problems in numerical studies of quantum turbulence in both atomic gases and helium. From this list of open problems, it is clear that there is no single model can answer all of the questions that exist. A prominent question is the nature of energy cascades in turbulent tangles, which is currently reliant on initial states comprised of bundles of vortex lines forming the equivalent of a vortex tube. [56, 57] In simulations, these bundles decompose into a tangle according to a reasonable script beginning with a classical story. [58]

Conceptually, quantum turbulence differs from classical turbulence through the constrained nature of quantized vortex lines which are non-diffusive regions devoid of the superfluid. The circulation they support is further restricted to take on values from a discrete rather than continuous set and when this value is decided it remains the same along all vortex lines in the quantum fluid. That is, whenever $\rho \neq 0$ in Eq. (1.7), the associated velocity field is defined by a scalar potential and therefore irrotational, $\nabla \times \nabla\phi = 0$. However, regions where $\rho = 0$ may define a topological defect of the fluid space leading to a purely circulatory flow about the vortex line. Quantization of the circulation is a consequence of the relationship between the velocity and the phase of the mean-field wave function. Turbulent states can be manufactured by spinning up the fluid so that a large circulation will prefer to decompose itself into a lattice of vortex lines, each possessing a quantum of circulation. Once the transfer of angular momentum into the system is stopped, any small deviations to this metastable bundle will induce turbulence in the form of a quantum tangle.

As the collimated tube of vortices begins to decompose, smaller self-similar regions of tubes may form which is indicative of a classical Richardson cascade. This cascade cannot last

forever and the vortices will begin to interact. While they push and pull on one another, some will naturally intersect with themselves or others forming the tangle. Vortex reconnections are preceded by the creation of a cusp where the curvature becomes large. After the reconnection event, a region of highly localized curvature remains. The vortex line proceeds to relax this region through the excitation of helical modes along the vortex, which are a type of Kelvin wave. The Kelvin waves allow the vortex line to couple to the quantum fluid so that the turbulent energy can relax through the excitation of acoustic modes. This dynamic is unique to the turbulent quantum tangle and hypothesized to resolve the conjecture by Onsager who anticipated "a mechanism of dissipation in which the role of the viscosity is altogether secondary." In review, the biography of the tangle begins with an ordered lattice that transitions to a self-similar state through a Richardson cascade transferring large scale properties to finer scales. A quantum tangle is then born after the Richardson cascade, when the large scale structure has been decomposed to the point where the tangle appears random. This quantum turbulence is marked by repeated reconnections that drive Kelvin waves and phonon emission in the quantum fluid. This continues until vortices live the majority of their life in isolation, at which point the tangle is said to have relaxed and the turbulence abated. Currently, there does not exist an analytic model that connects the local flow directly to the vortex line geometry. The work in this thesis solves this outstanding problem.

Starting with the Biot-Savart integral, we derive a model that predicts the generation of Kelvin waves from curved abnormalities on an isolated vortex line. This result is complementary to the body of work which models the kinetics of Kelvin waves that seek to understand the statistical properties of a Kelvin wave cascade. [59] That being said, the techniques we develop within this thesis are quite general and can be used whenever the dynamics of a vortex tube are well approximated by the behavior of the vortex line at its center, i.e., if the deformations of the vortex core are negligible. In Chapter 6 we conclude with an outlook of the future utility of these methods.

1.6 Thesis Organization

This thesis contains chapter material that is original work either published in or submitted to peer-reviewed journals. In addition, to these chapters, we have provided an introduction to the thesis in Chapter 1, and Chapter 2 provides preparatory material for understanding Chapters 3 through 5. Chapter 2 focuses on the equations of fluid dynamics and their connection to the Biot-Savart formalism in which the results of the main body are rooted. Specifically, the continuum theory of viscous thermal fluids in the large Reynolds number limit is reduced to the Biot-Savart integral through the use of two pre-existing results and a scaling argument which we develop. Chapter 3 studies the velocity induced by a plane circular arc of vorticity and derives an exact representation of the field in terms of incomplete elliptic integrals. Chapter 4 is a review of the key results of a Hasimoto transformation of the asymptotic analysis of the exact velocity field derived in Chapter 3. Specifically, we find that the non-Hamiltonian evolution of the curvature and torsion drives the system to relax regions of localized curvature into helical waves. In Chapter 5, we present the details of the calculation justifying the previous results. We conclude the thesis with a summary and a discussion of possible avenues of future research in Chapter 6.

In talks leading up to the defense of this dissertation, a mind map was used to outline the interconnections between various topics unified by geometric quantum hydrodynamics. We include this graphic in Figure 1.3 below. The embedded images are in the public domain and a list of attributions appears in Appendix C. Additionally, a brief overview of the key points in this thesis was provided in a handout disseminated at the defense. This handout is reproduced in Appendix A.

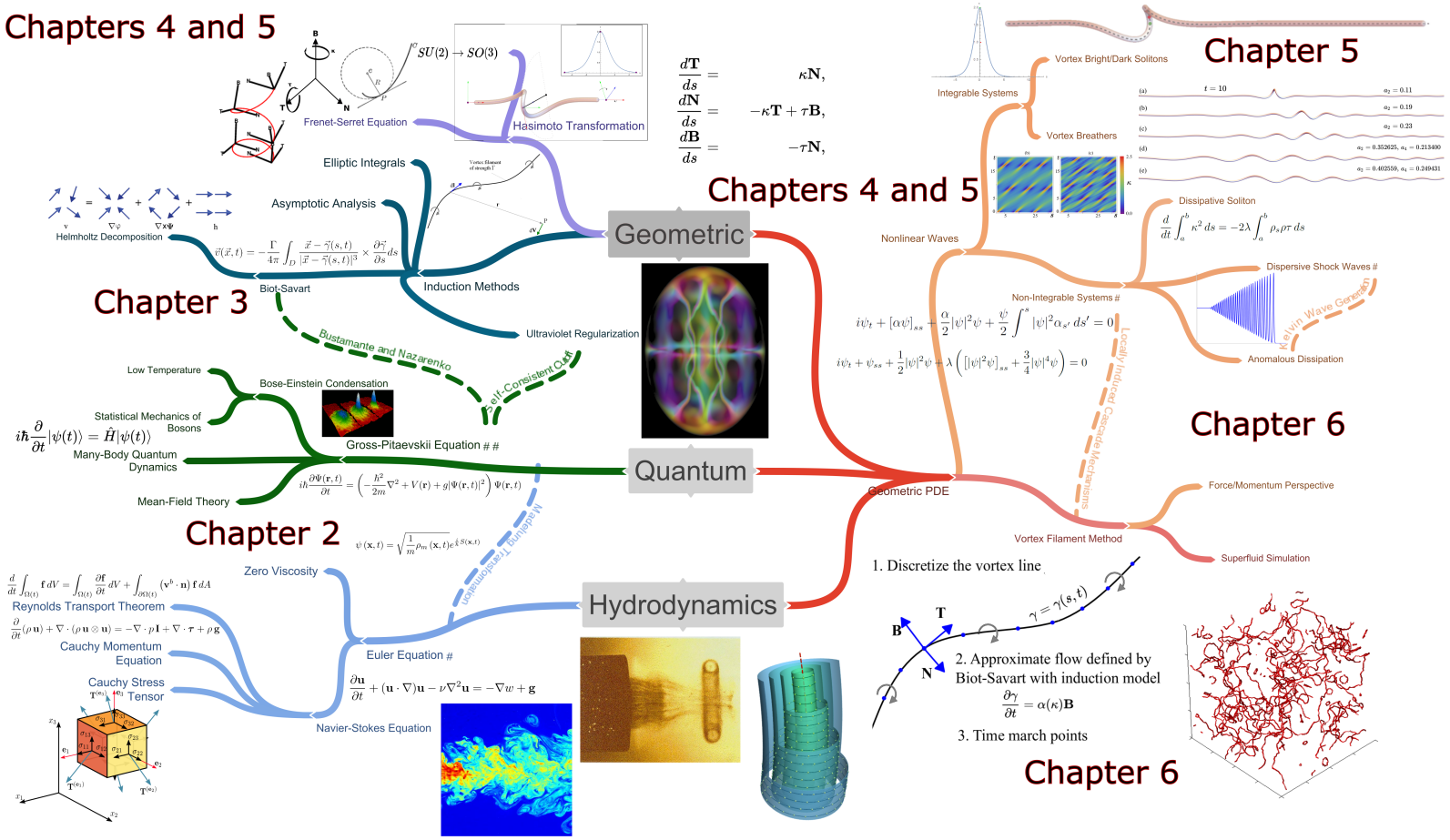

Figure 1.3: Geometric Quantum Hydrodynamics - Mind Map. In Chapter 2 we present the basis of Geometric Quantum Hydrodynamics, which connects the Biot-Savart integral to Navier-Stokes evolution of potential flows in the high Reynolds number limit. Chapter 3 is the reproduction of a paper where an exact representation of the velocity field induced by a plane circular arc is derived. Chapters 4 and 5 present a detailed asymptotic analysis of the Biot-Savart representation of the induced velocity field and its Hasimoto transformation. Additionally, these chapters discuss the nonlinear wave motions produced on the vortex line in terms of symbolic predictions and numerical simulations. Lastly, 6 discusses various applications of the theory of geometric quantum hydrodynamics. References for the images contained within this mind map are given in Appendix C.

CHAPTER 2

THE BASIS FOR GEOMETRIC QUANTUM HYDRODYNAMICS

The study of Kelvin waves on vortex lines in quantum liquids is currently undergoing a renaissance. Recently several lines of theory and experiments have emerged which are focused on addressing open questions concerning the energy spectra of wave motion on vortex lines as it relates to turbulence and its conjectured decay. These avenues of research are currently operating independently. The objective of this chapter is to weave them together to form a basis for the analysis of Chapters 3, 4, and 5. Specifically, we review two results that allow us to directly connect continuum fluid mechanics to the Biot-Savart integral, which is the starting point in our derivation of Kelvin wave generation on a vortex line. To make this connection, we will need to supply an intermediate step relating the Euler equations to the Gross-Pitaevskii equation. Geometric quantum hydrodynamics is completed by joining the continuum models of hydrodynamics to the geometric partial differential equations modeling vortex motion through the dynamics of its curvature and torsion. This geometric description comes about from the 1972 transformation of Hasimoto which maps the local flow of the vortex line to a scalar partial differential equation evolving the curvature and torsion along the vortex line. [8] This transformation was originally used by Madelung in 1926 to map Schrödinger equation to Newton's laws applied to continuum fluids. [9] This ever-growing connection between Newton's second law and the Schrödinger equation, first developed by Arnold in 1966, plays a fundamental role in the generation of Kelvin waves and the energy dissipation in our most primitive fluids. [1]

The mean-field theory of Bose-Einstein condensation predicts that a collection of weakly interacting condensed bosonic matter obeys a nonlinear Schrödinger evolution known as the Gross-Pitaevskii equation. This theory precludes internal rotation about anything other than a region of depleted density forming a topological defect of the fluid continuum in accordance

with the vortex filament theorems of Helmholtz. The statistical mechanics of indistinguishable particles is achieved by cooling a collection of identical atoms to the ultracold Bose-condensed regime. The quantum nature of the fluid is realized as a quantization of circulation about any vortex state. This phenomenon is a consequence of a large fraction of the bosons occupying the same averaged many-body wave function defined by the Gross-Pitaevskii equation. Consequently, turbulence must be constrained to a non-diffusive one-dimensional sub-structure of the ambient fluid and has a homogeneous circulation throughout. This medium is capable of supporting scalar wave motions akin to those of elastic strings. It is expected that the life cycle of turbulence begins with a Richardson cascade that takes turbulent energy from the large-scale collection of vortex lines to smaller scales until the vortices appear randomly configured. At this point, vortex-vortex interactions, occurring when the inter-vortex spacing is commensurate with the core size, drives Kelvin wave motion of the vortex lines coupling the vortex medium to the fluid allowing for the generation of phonons. As the frequency of interactions decreases, the remaining vortices spend most of their time in isolation and the turbulent tangle is said to have relaxed. Here the dissipation of kinetic energy is achieved without the support of molecular diffusion consistent with the 1949 conjecture of Onsager. [10]

In a series of papers, [60], [61], and [62], we study the wave motions of an isolated vortex line in an unbounded mean-field Bose-Einstein condensate. Starting with the Biot-Savart integral, we derive an exact expression for the velocity field induced by a plane circular arc of vorticity. This result can be simplified through the use of known asymptotic approximations to the incomplete elliptic integrals near their logarithmic singularity. Using the cutoff defined by Bustamante and Nazarenko [63], this representation is regularized so that only the first order contributions of the vortex core are considered. Once this is done an expression for the speed of the vortex in the binormal direction can be expanded in powers of curvature, with the well known local induction approximation resulting as a linear approximation to this speed. Using this expansion, it is possible to study the evolution of the curvature and torsion

of a vortex line through the Hasimoto transformation. The result is a modified nonlinear Schrödinger equation that gives rise to a non-Hamiltonian gain/loss mechanism and enhanced dispersion along the vortex. [61] The theory predicts that soliton solutions arising from the linear approximation of the binormal speed decompose themselves into packets of helical waves, known as Kelvin waves. While this result provides useful insights into the generation of Kelvin waves, we first discuss the relationship between the Biot-Savart integral and the equations of continuum fluid mechanics.

The following discussion is organized as follows. In Sec. 2.1 we outline the derivation of the Navier-Stokes equation from continuum mechanics. In Sec. 2.2 we review the Onsager conjecture and recent progress in its theoretical implications that define a relationship between the Navier-Stokes equation and Euler equations in the limit of large Reynolds number. Section 2.3 states the conditions necessary to derive the Gross-Pitaevskii equation from the Euler equation. After this, we review recent work that connects the Gross-Pitaevskii equation to a regularization of the Biot-Savart integral that is consistent with Bose-Einstein condensation. [63] Lastly, we summarize the results of this chapter and provide an outlook on future avenues of work.

2.1 The Navier-Stokes Equation

The Navier-Stokes equations describe changes to the momentum at points in a fluid continuum whose intensive properties like density, temperature, and pressure are well defined on infinitesimal volumes, which are small with respect to system size but large compared to the characteristic length scale of the molecular constituents comprising the fluid. This assumption breaks down for a non-small Knudsen number, which is the ratio of the Mach number and Reynolds number scaled by the heat capacity ratio. At this point, the average distance traveled by a molecule between collisions becomes comparable to the system size, signifying that continuum theories must give way to statistical methods. In the following, a small Knudsen number is assumed and the Navier-Stokes equations for a continuum fluid are derived. We include this derivation to make clear the connection between fluid continua and

Newton's second law. Those familiar with the derivation can proceed directly to Sec. 2.2 where literature discussing the connection between Navier-Stokes equations and the Euler equations in the limit of large Reynolds number is summarized.

The Cauchy momentum equation describes the non-relativistic momentum transport in an arbitrary continuum and derives from the application of Newton's second law to a region of fluid or fluid parcel. We let $\mathbf{v} : \mathbb{R}^{3+1} \to \mathbb{R}^3$ be the velocity of the fluid at any point and define $\Omega \subset \mathbb{R}^3$ to be a parcel of fluid permitted to flow through the continuum. There are two perspectives to take when considering the dynamics of this fluid parcel. If you move along with the fluid parcel, for instance like a weather balloon in the atmosphere, then you are describing the flow in a Lagrangian reference frame. A moving measurement is difficult to achieve in a laboratory setting and one instead probes the field at a fixed location adopting a Eulerian reference frame. In the setting of gravitation, the Eulerian perspective is that of the vector field describing gravitational forces at points in space, while the Lagrangian frame would specify the forces felt by a particle moving through this field. While the physical field and outcomes are the same, the two mathematical descriptions are not the same as a Lagrangian parcel would encounter many Eulerian probes as it travels. The only time the two descriptions are the same as when the flow lines are steady and parallel. We would like to understand changes experienced by the fluid parcel during its motion represented in the laboratory coordinates, which is tantamount to connecting the Eulerian and Lagrangian descriptions.

During the fluid parcel's flow, it will encounter some Eulerian probe. We associate with this probe a reference configuration which we denote with $\Omega_0 = \Omega(0)$. The flow that brings this parcel to the Eulerian probe is defined as the one-to-one and invertible mapping $\boldsymbol{\chi} : \mathbb{R}^{3+1} \to \mathbb{R}^3$. It can be shown that for such a mapping the reference configuration is arbitrary, which is to say that we have total control over where we conduct our Eulerian measurements. Consequently, to understand the dynamics of the fluid parcel in the laboratory frame, one only needs information about the reference configuration, Ω_0, the current configuration, $\Omega(t)$

and the flow, $\boldsymbol{\chi}$, joining them. In terms of our mapping, we have $\mathbf{y} = \boldsymbol{\chi}(\mathbf{x}, t)$ where $\mathbf{x} \in \Omega_0$ is a point in the reference configuration that is mapped by the flow $\boldsymbol{\chi}$ onto a point, $\mathbf{y} \in \Omega(t)$, in the current configuration. To get from $\mathbf{x}$ to $\mathbf{y}$, the material point must move with speed $\mathbf{v} = \partial\boldsymbol{\chi}/\partial t$.

If we define a scalar field on $\Omega(t)$, then we would like to know its dynamics when accumulating over the fluid parcel in the current configuration. As the parcel may change its shape during its movement, this calculation is difficult because of the explicit time dependence in the domain of integration. However, if we could transform into the reference configuration, then the domain would become static at the cost of explicit time variation of the material trajectories inside the parcel. This transformation between Eulerian and Lagrangian perspectives of the fluid parcel is known as the Reynolds transport theorem. It can be thought of as a higher dimensional generalization of the Leibniz differentiation under the integral, which itself is a manifestation of the fundamental theorem of calculus. The derivation of the theorem is technical, requiring a few results from tensor analysis. However, assuming a familiarity with linear algebra, we can minimize the amount of tensorial work and notation.

In addition to the mapping between the reference and current configurations, we will need the deformation gradient, which describes how the flow changes across the reference configuration,

$$\mathbf{F} = \nabla\boldsymbol{\chi}, \quad \mathbf{F}_{ij} = \frac{\partial \chi_i}{\partial x_j}. \tag{2.1}$$

We also have the velocity gradient, which is the Jacobian matrix of the velocity field in the current configuration,

$$\mathbf{L}_{ij} = \frac{\partial v_i}{\partial y_j}. \tag{2.2}$$

The Reynolds transport theorem considers time dynamics of the deformation gradient in the current configuration as opposed to the reference configuration. We derive this relationship and avoid tensorial notation by considering the element level description of the deformation gradient,

$$\frac{\partial \mathbf{F}_{ij}}{\partial t} = \frac{\partial}{\partial t}\frac{\partial \chi_i}{\partial x_j} \tag{2.3}$$

$$= \frac{\partial}{\partial t}\frac{\partial \chi_i}{\partial y_k}\frac{\partial y_k}{\partial x_j} \tag{2.4}$$

$$= \frac{\partial}{\partial t}\frac{\partial \chi_i}{\partial y_k}\frac{\partial \chi_k}{\partial x_j} \tag{2.5}$$

$$= \frac{\partial v_i}{\partial y_k}\mathbf{F}_{kj} \tag{2.6}$$

which implies that $\partial_t \mathbf{F} = \mathbf{L}\mathbf{F}$ and $\mathbf{L} = (\partial_t \mathbf{F})\mathbf{F}^{-1}$. We would like to now consider the dynamics of the total momentum in our material body at the current configuration. To process this integral, we convert to the reference configuration, so that the domain of integration is static in time, which introduces a change of variables given by the deformation gradient. Taking the time derivative of the integrand and applying the Jacobi formula, we transform back to find the Cauchy momentum equation. In detail we have

$$\frac{d}{dt}\int_{\Omega(t)} \rho(\mathbf{y},t)\mathbf{v}(\mathbf{y},t)\,d\mathbf{y} = \int_{\Omega_0} \frac{\partial}{\partial t}\left[\rho(\mathbf{x},t)\mathbf{v}(\mathbf{x},t)\,\det\left(\mathbf{F}(x,t)\right)\right] d\mathbf{x} \tag{2.7}$$

$$= \int_{\Omega_0} \left[\det\left(\mathbf{F}\right)\frac{\partial}{\partial t}\left(\rho\mathbf{v}\right) + \rho\mathbf{v}\frac{\partial}{\partial t}\det\left(\mathbf{F}\right)\right] d\mathbf{x} \tag{2.8}$$

$$= \int_{\Omega_0} \left[\frac{\partial}{\partial t}\left(\rho\mathbf{v}\right) + \rho\mathbf{v}\,\mathrm{tr}\left(\frac{\partial \mathbf{F}}{\partial t}\mathbf{F}^{-1}\right)\right]\det\left(\mathbf{F}\right) d\mathbf{x} \tag{2.9}$$

$$= \int_{\Omega(t)} \left[\frac{\partial}{\partial t}\left(\rho\mathbf{v}\right) + \left(\nabla\rho\mathbf{v}\right)\cdot\mathbf{v} + \rho\mathbf{v}\,\mathrm{tr}\left(\mathbf{L}\right)\right] d\mathbf{y} \tag{2.10}$$

$$= \int_{\Omega(t)} \left[\frac{\partial}{\partial t}\left(\rho\mathbf{v}\right) + \left(\nabla\rho\mathbf{v}\right)\cdot\mathbf{v} + \rho\mathbf{v}\left(\nabla\cdot\mathbf{v}\right)\right] d\mathbf{y} \tag{2.11}$$

$$= \int_{\Omega(t)} \left[\frac{\partial}{\partial t}\left(\rho\mathbf{v}\right) + \nabla\cdot\left(\rho\mathbf{v}\mathbf{v}^{\mathrm{T}}\right)\right] d\mathbf{y}. \tag{2.12}$$

The last equality is given by the application of a tensor contraction formula which relates the divergence of an outer product to standard vector calculus statements, $\nabla \cdot (\mathbf{a}\mathbf{b}^{\mathrm{T}}) = \nabla\mathbf{a} \cdot \mathbf{b} + \mathbf{a}\,(\nabla \cdot \mathbf{b})$. The key to understanding this result is recognizing that we have a formula for the momentum dynamics of the material body in terms of space-time changes to the density and velocity fields in the Eulerian frame. Moreover, if the integral vanished, then upon manipulation of the second term with the divergence theorem, we would find the sensible result that momentum change inside the material body is related to the flux of momentum through its boundary. Since the fluid parcel is arbitrary, this momentum balance over Ω, under a continuum assumption, is true locally on all fluid material points. Thus, we define the local momentum balance on material points as

$$\frac{D}{Dt}\,(\rho\mathbf{v}) = \frac{\partial}{\partial t}\,(\rho\mathbf{v}) + \nabla \cdot (\rho\mathbf{v}\mathbf{v}^{\mathrm{T}}) = \mathbf{s} \tag{2.13}$$

where $\mathbf{s}$ is a point source of momentum and D/Dt is called the material derivative. To conceptualize the material derivative, suppose the material body is an elastic ball and that it is impacting a solid body. The momentum changes observed as the body deforms are given in terms of two features experienced by the material points. The first contribution is due to changes in momentum and the second is due to deformations occurring relative to a material point. The material derivative, therefore, defines the momentum change in the reference configuration through the motion of its material points. We now consider sources of momentum for the previous balance equation.

Momentum changes can arise from body forces acting over the material, such as gravity, and surface forces acting on the geometry of the configuration. Specifically,

$$\mathbf{s} = \nabla \cdot \sigma + \mathbf{f} \tag{2.14}$$

where the surface forces are described by the Cauchy stress tenor σ, which can be further decomposed into

$$\sigma_{ij} = \begin{pmatrix} \sigma_{xx} & \tau_{xy} & \tau_{xz} \\ \tau_{yx} & \sigma_{yy} & \tau_{yz} \\ \tau_{zx} & \tau_{zy} & \sigma_{zz} \end{pmatrix} = \begin{pmatrix} \sigma_{xx} + p & \tau_{xy} & \tau_{xz} \\ \tau_{yx} & \sigma_{yy} + p & \tau_{yz} \\ \tau_{zx} & \tau_{zy} & \sigma_{zz} + p \end{pmatrix} - \begin{pmatrix} p & 0 & 0 \\ 0 & p & 0 \\ 0 & 0 & p \end{pmatrix} = \boldsymbol{\tau} - pI \quad (2.15)$$

where the components σ_{ij} correspond to normal stresses and shear stresses, $\boldsymbol{\tau}$, both of which act on the material volume. For example, $\sigma_{12} = \tau_{xy}$ represents the magnitude of the force acting across one of the three principle faces of the characteristic volume orthogonal to the local normal vector. Extracting the mechanical pressure, p, from the Cauchy stress tensor leaves behind deviatoric stress tensor $\boldsymbol{\tau}$. The pressure acts normal to the principle faces. The deviatoric stresses are only present when the material volume is in motion and describes the tendency of the volume to distort. At this point our momentum balance law is,

$$\frac{D\left(\rho \mathbf{v}\right)}{Dt} = -\nabla p + \nabla \cdot \boldsymbol{\tau} + \mathbf{f}. \quad (2.16)$$

A Newtonian fluid is one whose deviatoric stress tensor is invariant with respect to the direction observed and is linearly proportional to the velocity gradients.[1] This tensor characterizes distortions of the body due to straining and changes in volume. Small displacements of the fluid can be represented as the linear approximation to the velocity field given by the Jacobian matrix of the velocity field. [64] The symmetric component of this matrix defines the strain on the material volume. So that the deviatoric stress tensor is zero when the fluid is static, is main diagonal is subtracted away. Specifically, if we have the Jacobian, $\mathbf{J}_{ij} = [\nabla \mathbf{v}]_{ij} = \partial v_i / \partial x_j$ then the deviatoric stress tensor has the representation,

$$\boldsymbol{\tau} = \mu(\nabla \mathbf{v} + (\nabla \mathbf{v})^{\mathrm{T}}) - \frac{2\mu}{3}\left(\nabla \cdot \mathbf{v}\right)\mathbf{I} + \lambda\left(\nabla \cdot \mathbf{v}\right)\mathbf{I}, \quad (2.17)$$

where $\mathbf{I}$ is the three-by-three identity matrix. The shear viscosity, μ, is a parameter which defines how the fluid opposes this deformation. The compressibility of the fluid may also alter

[1] All fluids considered in this work are isotropic with observable volumes having with a linear response to shear stress, i.e., they are all Newtonian fluids. Examples of non-Newtonian fluids are highly composite materials in liquid suspension like cornstarch in water, blood, paint, ketchup and liquid polymers which experience shear thinning and thickening.

its response to shear stresses and comes about through both shear viscosity and bulk viscosity, λ, which is related to the vibrational energy of molecular aggregates. Assuming that the mass density is conserved, then application of the tensor contraction used in the derivation of the Cauchy momentum equation provides the following reduction to the material derivative,

$$\frac{D}{Dt}(\rho\mathbf{v}) = \frac{\partial\rho}{\partial t}\mathbf{v} + \rho\frac{\partial\mathbf{v}}{\partial t} + \mathbf{v}\,\nabla\cdot(\rho\mathbf{v}) + (\rho\mathbf{v}\cdot\nabla)\,\mathbf{v} \tag{2.18}$$

$$= \left(\frac{\partial\rho}{\partial t} + \nabla\cdot(\rho\mathbf{v})\right)\mathbf{v} + \rho\frac{\partial\mathbf{v}}{\partial t} + (\rho\mathbf{v}\cdot\nabla)\,\mathbf{v} \tag{2.19}$$

$$= (\rho\mathbf{v}\cdot\nabla)\,\mathbf{v}. \tag{2.20}$$

Assuming conservation of mass, then we have the Navier-Stokes equations,

$$\frac{D}{Dt}(\rho\mathbf{v}) = -\nabla p + \nabla\cdot[\mu(\nabla\mathbf{v} + (\nabla\mathbf{v})^{\mathrm{T}})] + \nabla\cdot\left[\left(\lambda - \frac{2\mu}{3}\right)(\nabla\cdot\mathbf{v})\,\mathbf{I}\right] + \mathbf{f}. \tag{2.21}$$

The left hand side is the change in momentum in an isotropic Newtonian fluid created by pressure gradients, shear forces, compressibility effects, and body forces on the right hand side, respectively. Standard tensor operations show that the incompressible shear viscosity component reduces to $\mu\triangle\mathbf{v}$, where $\triangle = \partial_{xx} + \partial_{yy} + \partial_{zz}$, bringing the equation to the most common form of the Navier-Stokes equations. However, since the next section is about an abstract relationship between this equation and the Euler equations where all viscous terms are neglected, we omit the final reduction so no further tensor calculus is introduced.

2.2 Onsager's Conjecture and the Dissipation Anomaly in Three-Dimensional Turbulence

It is a well-established fact that the drag applied to an object moving through a fluid derives from two terms. The first is associated with viscous drag imparted through a laminar flow whose force is linear with respect to velocity. The second contribution is a quadratic enhancement due to fluid turbulence and exists even in the absence of viscosity. [13] While Lars Onsager's publications in the field of hydrodynamic turbulence were limited to an abstract [65], and a single publication [10] there existed considerable work in his private

journals on fluid turbulence. [66] It has taken the scientific community roughly half of a century to assimilate and further his work. Of particular interest is the conjectured dissipative anomaly which was reported on in the second half of his 1949 paper. In this work, he states that turbulent dissipation could take place without the "final assistance from viscosity" and that "conservation of energy does not apply because the field does not remain differentiable." As compared to drag on moving bodies in high Reynolds number flows, dissipation of fluid turbulence in the absence of viscosity is likely less than intuitive. In fact, researchers struggle with understanding the mathematical structure and physical implications associated with the relationship between the Navier-Stokes and Euler equations in the large Reynolds number limit. While we do not speak to aspects of the mathematical analysis, we do put forward the vortex line model as a suitable setting to investigate aspects of the dissipative anomaly further. Specifically, we provide a context for his conjecture and review historical placement of the formal statement before concluding with a review of the current status of the theory and how it fits into geometric quantum hydrodynamics.

Following the publication of an abstract in 1945 that independently predicted the Kolmogorov 5/3 law, Onsager addressed the participants of the International Union of Pure and Applied Physics conference on statistical mechanics in Florence, Italy in 1949. Here he announced quantization of circulation in superfluids and a theory of energy dissipation for turbulence in three dimensions that relies on the development of singularities in the Euler equations. A review of Onsager's presentation comments that it was elegant, spartan, deep, and decidedly cryptic. [67] In this presentation and follow up paper Onsager states that dissipation can remain even in the absence of viscosity. It is hypothesized that this work remained underutilized by the community and a priority was given to the contemporary work of Burgers and Kolmogorov. Consequently, it is the work of Kolmogorov that the community associates with fluid turbulence. [68–70] This theory is the mathematical formulation of the poetic description of turbulence offered by Richardson, who describes the generation of eddies at decreasingly small scales until a Kolmogorov scale is reached where viscosity can dissipate

turbulent kinetic energy into heat. Between the scale containing the largest eddies, where the majority of kinetic energy resides, and the small scale where molecular diffusion dissipates the system, Kolmogorov defines an inertial subrange. In the inertial subrange, neither the direct forcing of the flow leading to large eddy formation nor the viscous dissipation caused by molecular diffusion is apparent. Kolmogorov hypothesized that this intermediate range well separated the large and small scales and defines a flow dominated by the unrestricted nonlinear transfer of energy from large to small scales. Kolmogorov quantifies Richardson's qualitative description of turbulence by stating a universal form for the cascade of energy. The energy of eddies in the intermediate range obey $E(k) \propto k^{-5/3}$ where k is the wavenumber and can be thought of as the reciprocal of the eddy diameter. Thus, energy in the inertial subrange is independent of viscosity and obeys a power law dependence such that eddies of smaller diameter contain a decreasing amount of energy. The theory therefore says that Richardson decay is a process where kinetic energy in large scale eddies is transported through an intermediate scale where self-similar eddy formation breaks large scale energy into smaller eddies so that viscous dissipation eventually heats the fluid. In this case, what did Onsager mean when he said that this process could complete itself without a final assist from fluid viscosity?

Before the formal statement and its current state in the literature, we note that both experiments and simulations indicate that as Reynolds number increases, the energy dissipation rate asymptotically approaches a non-zero constant value. [71] Thus, the kinetic energy present in the eddies formed at a large length scale cascading to smaller scales decays at rate seemingly independent of viscosity. Onsager's original conjecture [10] asserts that the only way to permit kinetic energy dissipation as $R_{\mathrm{e}} \to \infty$ is to allow the velocity gradients to become arbitrarily large. Moreover, his statement specifies a condition allowing for this in terms of a loss of smoothness within the velocity field. In the following paragraph, we describe the loss of smoothness in terms of Hölder regularity, corresponding to a Hölder exponent of 1/3. In light of this, it makes sense that history favored Kolmogorov's theory of

fluid turbulence, which is a mathematically concise description of the energy decay envisioned by Richardson. However, it obscures Onsager's description. It is interesting to note that if one considers the magnitude of velocity differences over separated field points to define an energy spectrum, then Onsager's Hölder exponent yields Kolmogorov's universal scaling relation. Knowing that Onsager's result is consistent with Kolmogorov's prediction, then what does Onsager's statement that a velocity field presenting with the dissipative anomaly can have at most a "third of a derivative" mean?

Colloquially, a continuous function can be drawn without lifting up your writing utensil. Such a function may fail to be differentiable at points and so a stronger condition for continuity is Hölder continuity, where the closeness of the output variables is bounded by a power of the closeness of the input variables. If the Hölder exponent is equal to one, then we say the function is Lipschitz continuous and the implication is that it is differentiable almost everywhere. When the Hölder exponent is reduced, the function is permitted to become rougher. To picture the roughness, consider the absolute value function which is Lipschitz continuous, but lacks a derivative at the cusp. Compare this to the rough paths traced out by Brownian motion. The lower the Hölder exponent, the rougher the curve. As roughness is introduced, one loses control of the derivative and so the most direct consequence of this statement can be seen in the time dynamics of the kinetic energy. Specifically, the time derivative of the global kinetic energy in the fluid is proportional to the integral of the velocity gradients over the fluid. The proportionality constant in this relation is the fluid viscosity. So, one expects that global energy becomes approximately conserved for large Reynolds numbers, which is in contradiction to experimental and simulated data. However, if the velocity gradients are permitted to diverge, then kinetic energy decay can persist even for large Reynolds numbers, and the contradiction is avoided. Another way to think about this is that if the problem could be resolved to an appropriate ordinary differential equation, then the lack of Lipschitz continuity leaves open the possibility of non-unique solution trajectories. In fact, the statistical analysis of direct numerical simulations of turbulence in the inertial

range shows the mean squared distance between initially separated particle paths tends to t^3 in the large time limit. [72] This result was known to Richardson in 1926 and characterizes turbulence as an extremely effective mixer. In light of Onsager's fractional Hölder exponent and its contextualization in terms of differential equations, we see the that mixing through the inertial range induces a particle forgetfulness. Thus the energy cascade is a process where the past configuration of the large-scale eddies, and some of their energy, is forgotten. At this point, we discuss the current status of the theory and conclude with an overview of the role it plays in providing a base for geometric quantum hydrodynamics.

The most current result comes from a 2017 paper of Drivas and Eyink who have recast the conjecture of Onsager in terms of the tools of modern analysis. [73] Specifically, they prove that bounded solutions of Navier-Stokes exhibiting anomalous dissipation limit to distributional or weak solutions of Euler equations that dissipate kinetic energy unless they are above a certain degree of space-time regularity. Their work makes use of the Besov spaces, which generalize the standard Sobolev and Hölder spaces. Suffice it to say that these abstractions reduce to Onsager's original 1/3 Hölder exponent, which was recently proven to be sharp. [74] Their work is part of a trio of papers, with one focused on a generalization to relativistic turbulence and another reporting on how the transition to distributional solutions can be reinterpreted in terms of renormalization group theory. [75, 76] In the latter, the divergence in the velocity gradients is thought of as an ultraviolet catastrophe. Proceeding with a standard Wilson-Kadanoff renormalization they define a scale in the inertial range where the divergence is regularized, and the flow obeys an effective course-grained Euler equation, which is nothing more than a weak Euler equation.

The work of Drivas and Eyink has seen the most progress amongst several lines of research. That said, the notion of a relationship between Navier-Stokes and weak Euler equations is certainly not a unique one. [77, 78] Some intriguing remarks can be found in the works of other researchers. In 1999 Shnirelman states that "The physical meaning of weak solutions of the Euler equations is not quite clear." At the same time in the 2006 Eyink and Sreenivasan

review article of Onsager's turbulence theory, the authors state that they "believe that Onsager's theoretical vision ... is a proper idealization for understanding high Reynolds number flows." Moreover, they conclude with, "The vindication of this belief, if it is true, must come from a set of calculational tools for the zero-viscosity limit, which will make it, in the end, a truly predictive device."

While the recently published results have brought Onsager's perspective of turbulence somewhat out of the shadows, they are still very abstract. A key point in the assertions of Eyink and Sreenivsan is that a deeper understanding of the theory will likely come from inviscid fluids. While the secondary purpose of this section was to review aspects of modern turbulence theory, the primary purpose was to state the connection between Navier-Stokes and Euler evolutions provided by the dissipative anomaly and distributional velocity profiles. In the following section, we derive the Gross-Pitaevskii equation description of mean-field Bose-Einstein condensation from the Euler equations. However, looking forward to Sec. 2.4, we note that the work of Bustamante and Nazarenko [63] defines a singular velocity profile associated with a vortex line and a cutoff length that regularizes small wavelength contributions from the vortex line to the velocity field. These techniques bring the ideas of Onsager closer to the realm of calculation as they are the introductory steps of many simulation techniques. Specifically, when connected to Chapters 3, 4, and 5 of this thesis, we find that corrections to the simplest flows of a vortex line allow for the generation of Kelvin waves, which are the proposed mechanism of decay in quantum turbulence.

2.3 Euler's Equation and the Gross-Pitaevskii Equation

Bernoulli's law is a result saying that the pressure function of an incompressible potential flow can be expressed through the velocity potential, up to an arbitrary time factor. [79] It is derived from Euler's equation where the flow and the time factor arises from an integration of the gradient used to define the velocity field from the potential function. In this derivation, one typically assumes that the fluid has homogeneous density and can be interposed with the gradient without restriction. The vortices of our work have well defined and significant

spatial variation near the core. In a classical fluid, the transition in density to the vortex line is an abrupt one. However, in a Bose-Einstein condensate, the transition is a smooth one. For a rectilinear vortex, the density profile of an arbitrary cross-section looks something like a sigmoid function. [80] Since the mass density is a smooth function decaying to zero on the vortex line, the derivation of Bernoulli's law is no longer straightforward. The consequence is that in situations we would like to consider, the density profile has a spatial dependence and the typical derivation must be altered since the density function cannot be trivially interposed with the gradient. Ultimately, the spatial variation of the density will need to be bounded by changes in the density field as measured by the velocity potential.

The last section tells us that in the inviscid limit, Navier-Stokes equations limit to Euler equations which is defined by Eq. (2.21) in the absence of viscous effects, $\lambda = \mu = 0$,

$$\frac{D\left(\rho\mathbf{v}\right)}{Dt} + \nabla p - \mathbf{f} = 0 \tag{2.22}$$

Knowing that the hydrodynamic description of a Bose-Einstein condensate is predicted to be irrotational and mass conserving, we assume a potential flow $\mathbf{v} = \nabla\phi$ to get,

$$\rho\frac{\partial\nabla\phi}{\partial t} + \rho\left(\nabla\phi\cdot\nabla\right)\nabla\phi + \nabla p - \mathbf{f} = 0. \tag{2.23}$$

If the density profile were constant in space, then the expression could easily be written in terms of the gradient of a single function, which is the route to Bernoulli's law. However, the varying spatial density demands the use of a product rule,

$$\nabla\left(\rho\left\{\frac{\partial\phi}{\partial t} + \frac{1}{2}||\nabla\phi||^2\right\}\right) = \left(\nabla\rho\right)\left(\frac{\partial\phi}{\partial t} + \frac{1}{2}||\nabla\phi||^2\right) + \rho\,\nabla\left(\frac{\partial\phi}{\partial t} + \frac{1}{2}||\nabla\phi||^2\right). \tag{2.24}$$

If the density field were constant then the first term on the right-hand side of the previous equation would vanish. As this is not the case, and since both terms of the previous equation are not present in Eq. (2.23), we will have to assume that the following scaling relation is satisfied,

$$\frac{\nabla\rho}{\rho} \ll \frac{\nabla\left(\frac{\partial\phi}{\partial t} + \frac{1}{2}||\nabla\phi||^2\right)}{\frac{\partial\phi}{\partial t} + \frac{1}{2}||\nabla\phi||^2}, \tag{2.25}$$

where $||\nabla\phi||$ is the magnitude of the vector quantity. We notice that these are logarithmic derivatives and the scaling can be written instead as,

$$\nabla \ln(\rho) \ll \nabla \ln\left(\frac{\partial\phi}{\partial t} + \frac{1}{2}||\nabla\phi||^2\right), \tag{2.26}$$

which implies that spatial variations of the density away from depletions, $\rho \neq 0$, must be well controlled by the spatial variation of the Hamilton-Jacobi equation on the velocity potential. In this case Eq. (2.23) can be approximated as

$$\nabla\left(\rho\frac{\partial\phi}{\partial t} + \rho\frac{1}{2}||\nabla\phi||^2 + p - V\right) = 0. \tag{2.27}$$

where $\mathbf{f} = -\nabla V$. Thus, up to a function of time, which we absorb into V, we have the following equation on the velocity potential

$$\rho\frac{\partial\phi}{\partial t} + \rho\frac{1}{2}||\nabla\phi||^2 + p - V = 0 \tag{2.28}$$

Adding Eq. (2.28) to the conservation of mass equation multiplied by $i = \sqrt{-1}$ yields the following,

$$i\left(\frac{\partial\rho}{\partial t} + \nabla\rho\cdot\nabla\phi + \rho\nabla\cdot\nabla\phi\right) - \rho\frac{\partial\phi}{\partial t} - \rho\frac{1}{2}||\nabla\phi||^2 - p + V = 0 \tag{2.29}$$

Regrouping the terms gives,

$$i\frac{\partial\rho}{\partial t} - \rho\frac{\partial\phi}{\partial t} - p + i\rho\triangle\phi + i\nabla\rho\cdot\nabla\phi - \rho\frac{1}{2}||\nabla\phi||^2 - V = 0 \tag{2.30}$$

If we define the pressure as $p = -\triangle\sqrt{\rho}$ and body potential as $V = 2V_0\rho^2$, after multiplication by $e^{i\phi/2}/2\sqrt{\rho}$ we can re-write Eq. (2.30) as

$$i\psi_t + \frac{1}{2}\triangle\psi - V_0|\psi|^2\psi = 0 \tag{2.31}$$

where $\psi = \sqrt{\rho}\, e^{i\phi/2}$. While we have assumed that $\rho \neq 0$ to arrive at Eq. (2.31), density depletions associated with vortex lines, may be brought back into the solution space at the cost of divergence in Eq. (2.28). In Sec. (2.4) we review recent results [63] showing that divergence in kinetic energy can avoided by tempering the vortex singularity. Up to a space-time scaling and introduction of a single particle energy, this is the Gross-Pitaevskii. That is if we require the density be a function only of pressure (barotropic) and that the average two-particle interactions provide a background potential field, then the Euler equation can be brought into correspondence with the equation of motion for a Bose-Einstein condensate. Summarizing our work up to this point, we now have a formal connection between continuum fluid mechanics and the mean-field theory of dilute ultracold atomic gases. That is, given an Euler equation for an inviscid fluid, which we now see as the equation of motion for a fluid system in the high Reynolds number limit, a potential flow of a mass field can be expressed through a Gross-Pitaevskii wave function whose amplitude defines the density and the phase defines a velocity potential. This connection essentially the inversion of the Madelung transformation. In what follows, we review a recent article that connects Eq. (2.31) to the Biot-Savart integral.

2.4 Gross-Pitaevskii Equation and the Biot-Savart Integral

The Biot-Savart integral is the left inverse of the curl and defines the incompressible, rotational component of a three-dimensional vector field on $\mathbb{R}^3$ from its vorticity. It can be derived from a Green's function analysis on a stream reformulation of a partial differential equation associated with the Helmholtz decomposition of $\mathbf{v} : \mathbb{R}^3 \to \mathbb{R}^3$ and is also sometimes called the fundamental theorem of vector analysis.[2] The Gross-Pitaevskii equation has a Hamiltonian structure, and it is possible to extract the Biot-Savart integral from it. [63]

[2] The generalization of Helmholtz's decomposition theorem is known as the Helmholtz-Hodge decomposition, which applies to differential forms on a Riemannian manifold as opposed to just vector fields on $\mathbb{R}^3$.[81]

The outcome is a Biot-Savart representation of the singular velocity field sourced by a one-dimensional subregion of the fluid consistent with a vortex line in a Bose-Einstein condensate. Moreover, it is also possible to rationally determine a scale at which physics at small wavelengths must be regularized out of the model. In Chapter 5 we start with a distribution of vorticity supported by a Dirac measure on a one-dimensional subregion, to show that approximating this space curve with plane circular arcs leads to a generalization of Hasimoto's transform describing the wave motion through a non-Hamiltonian evolution of the curvature and torsion along the vortex. This theory predicts a mechanism capable of generating Kelvin wave excitations along a vortex line, which is the primitive component of a Kelvin wave cascade. In this context, the discovery of Bustamante and Nazarenko implies that our generation mechanism is consistent with vortex motion in a Bose-Einstein condensate. As the goal of this chapter is define this physical context as a realization of the Navier-Stokes equations in the limit of large Reynolds number, we take a moment to reflect on the details of the connection we establish.

In Sec. 2.2 we reviewed a result asserting that bounded solutions of Navier-Stokes equation exhibiting anomalous dissipation of kinetic energy must do so by inducing a singularity on the velocity profile which is evolved by weak Euler equations. If the velocity field is potential away from the singularity, then Sec. 2.3 defines the evolution of the flow through a Gross-Pitaevskii equation. Results from vector analysis say that this can only be accomplished through a loss of simple connectedness of cross-sections of the fluid domain that when continued form a vortex line consistent with Gross-Pitaevskii vortex profiles and experimental observations. The body of this thesis demonstrates that if the geometric dynamics of the curve are provided by an arclength preserving Biot-Savart induced flow, then the vortex medium responds dispersively and dissipatively to support the generation of helical wave fronts. These Kelvin waves are expected to be the primary form of energy transport for turbulence in ultracold quantum liquids as they couple the vortex substructure to the fluid field through the creation of long wavelength collective excitations known as phonons. The implications of these connections

are briefly discussed in the Chap. 6. This section will summarize the result of Bustamante and Nazarenko. Specifically, when Eq. (2.31) corresponds to the mean-field model of a Bose-Einstein condensate, then the Biot-Savart representation of a velocity field circulating about its singularities reduces to a line integral whose regularization includes non-kinetic information about the vortex core to first order.

The Gross-Pitaevskii equation models the condensation of a dilute preparation of bosonic matter where the individual particles collectively obey an averaged many-body wave function. The evolution is Hamiltonian and given by Bustamante and Nazarenko as

$$H = \int \left(|\nabla \psi|^2 + \frac{1}{2} \left(|\psi|^2 - 1 \right)^2 \right) d\mathbf{x}, \tag{2.32}$$

where $\psi = \sqrt{\rho}\, e^{i\eta}$ and the -1 accounts for their modification of Eq. (2.31) by a constant potential. This wave function defines a Madelung transformation of the Gross-Pitaevskii equation to a hydrodynamic form consistent with an inviscid gas. The Gross-Pitaevskii Hamiltonian also has a hydrodynamic form,

$$H = \frac{1}{2} \int d\mathbf{x} \left(\frac{1}{2} \rho \mathbf{v}^2 + (\rho - 1)^2 + 2 |\nabla \sqrt{\rho}|^2 \right), \tag{2.33}$$

where $\mathbf{v} = 2\nabla\eta$ and $\eta = \phi/2$ for the wavefunction in Eq. (2.31). For vortex lines whose radius of curvature is much larger than the vortex core radius, we have that the kinetic terms dominate over the energies associated with averaging over the two-particle interactions and the quantum pressure. That is, the dynamics of nearly straight vortex lines are dominated by the energy of the background velocity field and the introduction of bending is tantamount to activating features of the vortex core.

Bustamante and Nazarenko specialize the results of Nemirovskii [82] to the case of a vortex line in a Bose-Einstein condensate, which works by restricting the wave function to a space curve prior to studying the Hamiltonian dynamics of the Gross-Pitaevskii equation. Considering a rectilinear vortex, the Hamiltonian structure over the vortex line can be reduced

to a point where vector identities can be used to re-write the wave function in the local frame. When this is compared back to the Hamiltonian structure one can form a relation between an expression of the local frame and the derivative structure of the vortex parameterization. Consequently, the Lagrangian for the vortex line can be expressed as,

$$\mathcal{L} = \frac{\Gamma}{6} \int \boldsymbol{\gamma}_t \cdot (\boldsymbol{\gamma} \times d\boldsymbol{\gamma}) - \mathcal{H}, \tag{2.34}$$

where Γ is the circulation about the vortex and $\mathcal{H}$ is the vortex Hamiltonian as defined below by Eq. (2.36). From this point, the variation of action can be calculated and application of the principle of least action requires that,

$$\frac{\Gamma}{2} (\boldsymbol{\gamma}_t \times \boldsymbol{\gamma}_s) = \frac{\delta \mathcal{H}}{\delta \boldsymbol{\gamma}} \tag{2.35}$$

The body of Bustamante and Nazarenko's work is spent deriving the variational derivative of this Hamiltonian such that the typical ad hoc cutoff is rationally defined in terms of the condensate features.

The derivation of Bustamante and Nazarenko is broken into six steps. In the first step, the Hamiltonian structure associated with a vortex line is defined for the Gross-Pitaevskii equation such that the kinetic terms dominate the first order contribution of the non-kinetic terms. Motion due to the kinetics is assumed to be subsonic and the contributions from the mean-field averaging and quantum pressure are used later to establish the regularization cutoff length. The second step defines a re-scaling of the velocity field and considers a straight line vortex to compute the kinetic and non-kinetic contributions to the Hamiltonian so that an energy density due to the non-kinetic terms can be computed. The third step seeks to localize the vortex cores to the healing length of the vortex. Specifically, the Helmholtz theorem of fluid mechanics is applied to the field where the velocity singularity is assumed to be mild. Furthermore, fluid compressibility is stated to be negligible, which is consistent to working in a regime where curvatures are not large.

It is this step which is key to understanding the Biot-Savart integral, Eq. (2.38). Specifically, their localization procedure avoids the practice of localization of vorticity to a space curve through the use of distributions. That said, key features are maintained. The velocity field is strongly localized to the healing length, which is viewed as the core of the quantized vortex. Additionally, the velocity field still diverges as one approaches the centerline. It is noted that for a Pitaevskii vortex, the velocity singularity is mild enough to avoid a divergence in the kinetic Hamiltonian.

The second half of the derivation starts by introducing an intermediate length scale between the healing length and the radius of curvature used to split the kinetic Hamiltonian into two contributions. One contribution comes from integrating on a domain inside the new length scale and the other from contributions away from this scale. Once this is done the non-kinetic Hamiltonian is added to the near field effects. In the fifth step, an asymptotic approximation yields the effective Hamiltonian,

$$\mathcal{H} = \frac{\Gamma^2}{16\pi} \int_{|\boldsymbol{\gamma}-\boldsymbol{\gamma}'|>c} \frac{d\boldsymbol{\gamma} \cdot d\boldsymbol{\gamma}'}{|\boldsymbol{\gamma}-\boldsymbol{\gamma}'|} \tag{2.36}$$

where the cutoff parameter c is not yet known. To calculate this value the final step relies on numerical quadrature to compute a key intermediate function that acts as a smooth cutoff associated with the Hamiltonian resulting from the localization of vorticity to the quantized vortex core.

The final result is the merger of Eq. (2.36) and Eq. (2.35) and yields

$$\boldsymbol{\gamma}_t \times \boldsymbol{\gamma}_s = \frac{\Gamma}{4\pi} \int_{s_0}^{s_1} \frac{\boldsymbol{\gamma}_s \times [(\boldsymbol{\gamma}' - \boldsymbol{\gamma}) \times d\boldsymbol{\gamma}']}{|\boldsymbol{\gamma}' - \boldsymbol{\gamma}|^3} \tag{2.37}$$

where $s_0 > c$ such that c is their cutoff parameter regularizing the integral over the vortex structure. Through the use of the distributive property of the curl operator with a standard identity [83] one can essentially undo the curl structure in the previous equation to arrive at the Biot-Savart integral for the motion of the vortex line caused by the velocity field induced

by a parametric region of vorticity from s_0 to s_1,

$$\frac{\partial \boldsymbol{\gamma}}{\partial t} = \frac{\Gamma}{4\pi} \int_{s_0}^{s_1} \frac{(\boldsymbol{\gamma}' - \boldsymbol{\gamma}) \times d\boldsymbol{\gamma}'}{|\boldsymbol{\gamma}' - \boldsymbol{\gamma}|^3}, \tag{2.38}$$

where $s_0 > c$. This equation is the starting point for our asymptotic analysis of the autonomous dynamics of a vortex line.

In summary, the work of Bustamante and Nazarenko allows information from the Gross-Pitaevskii evolution of the Bose-Einstein condensate to be provided to the Biot-Savart integral for the purposes of modeling large-scale vortex dominated flows in the superfluid. In particular, by retaining the leading order contributions of non-kinetic terms in the Hamiltonian, as it applies to vortex lines, the mean-field averaging and quantum pressure define a velocity field strongly localized to the vortex core, which is otherwise singular on the vortex line. This inclusion establishes a cutoff parameter for the regularization of the Biot-Savart integral. Using this regularization, it is possible to define a Biot-Savart integral representation of the velocity field induced by an arbitrary parameterization of a vortex line modeling the flow induced by both the geometric properties of the vortex in addition to a non-trivial contribution from its vortex core. The body of this thesis shows that a vortex line seeks to redistribute localized curvature abnormalities into helical Kelvin waves, which are required for the decay of ultracold quantum turbulence and realization of Onsager's conjecture.

CHAPTER 3

GENERALIZED LOCAL INDUCTION EQUATION, ELLIPTIC ASYMPTOTICS, AND SIMULATING SUPERFLUID TURBULENCE

A paper published in the *Journal of Mathematical Physics*, 53, 033102 (2012), doi:10.1063/1.3696689.

Scott A. Strong[*], **Lincoln D. Carr**

Department of Physics, Colorado School of Mines, Golden, CO 80401, USA

[*]Primary researcher and author.

3.1 Abstract

We prove the generalized induction equation and the generalized local induction equation (GLIE), which replaces the commonly used local induction approximation (LIA) to simulate the dynamics of vortex lines and thus superfluid turbulence. We show that the LIA is, without in fact any approximation at all, a general feature of the velocity field induced by any length of a curved vortex filament. Specifically, the LIA states that the velocity field induced by a curved vortex filament is asymmetric in the binormal direction. Up to a potential term, the induced incompressible field is given by the Biot-Savart integral, where we recall that there is a direct analogy between hydrodynamics and magnetostatics. Series approximations to the Biot-Savart integrand indicate a logarithmic divergence of the local field in the binormal direction. While this is qualitatively correct, LIA lacks metrics quantifying its small parameters. Regardless, LIA is used in vortex filament methods simulating the self-induced motion of quantized vortices. With numerics in mind, we represent the binormal field in terms of incomplete elliptic integrals, which is valid for $\mathbb{R}^3$. From this and known expansions we derive the GLIE, asymptotic for local field points. Like the LIA, generalized induction shows a persistent binormal deviation in the local-field but unlike the LIA, the GLIE

provides bounds on the truncated remainder. As an application, we adapt formulae from vortex filament methods to the GLIE for future use in these methods. Other examples we consider include vortex rings, relevant for both superfluid ^{4}He and Bose-Einstein condensates.

3.2 Introduction

The term superfluid denotes a phase of matter whose dynamical flows can be described, at finite non-zero temperature, by a two-component macroscopic field with well-defined properties. [84–86] One component is a purely classical field, while what remains is called the superfluid component. The superfluid is ideal in the sense that it is inviscid and has infinite heat capacity provided by its lack of classical entropy. Rotation enters the superfluid component in quantized vortex filaments[87, 88] that, for example in ^{4}He, transmit thermal information acoustically and are detected by this second-sound. [89] Superfluid dynamics can be generated by the introduction of a small heat flux. [90] Conservation of mass requires that the classical movement away from the heat flux be offset by a counterflow of the superfluid component. If this heat flux is not small, then the quantized vortices tangle, indicating the onset of superfluid turbulence.[91–96] For large heat fluxes, the superfluid transitions into a purely classical phase. In classical turbulence, vorticity can concentrate into complicated geometries. For this reason, large-scale simulation of classical vortex dominated flows is computationally costly.

Vortex line structures are most appropriate to superfluid models of ^{4}He where the quantized filaments have radii of a few angstroms.[89, 97] These quantized vortices provide a coherent structure for aggressive analytical and numerical study unavailable to classical fluids. Vortex line structures can also be used to model atomic Bose-Einstein condensates, where there has recently been a revival of interest in superfluid turbulence due in part to a series of remarkable experiments in the Bagnato group.[98] Our study begins with simplifications to the Biot-Savart representation of the field induced by a vortex line

$$\mathbf{v}(\mathbf{x}) = \frac{\Gamma}{4\pi}\int_{D\subset\mathbb{R}^3}\frac{(\mathbf{x}-\boldsymbol{\omega})\times d\boldsymbol{\omega}}{|\mathbf{x}-\boldsymbol{\omega}|^3} = \frac{\Gamma}{4\pi}\int_{D\subset\mathbb{R}}\frac{(\mathbf{x}-\boldsymbol{\xi})\times d\boldsymbol{\xi}}{|\mathbf{x}-\boldsymbol{\xi}|^3}. \tag{3.1}$$

The associated reduction of dimension aids analytic calculation and reduces numerical cost. When such filaments are considered initial-data to the Navier-Stokes problem, then global well-posedness results. [99, 100] The use of these data to approximate self-induced vortex motion is the backbone of the *vortex filament method*.[101, 102] The question of numerical convergence and accuracy of such vortex filament techniques has been addressed affirmatively in the literature. [103] Vortex filament methods reduce the cost of large-scale simulations by restricting analysis to the local field. Due to the complexity of classical vortical flows, interest in these methods waned during the 1980s.[101, 102, 104–106] However, filament methods are highly appropriate for the constrained vortex structure associated with a superfluid. Although (3.1) provides a straightforward starting point for numerical computations, vortex filament methods avoid numerical integration altogether by replacing (3.1) with a local induction approximation.

The local induction approximation (LIA) is a result from classical fluid dynamics, which states that a space-curve vortex defect of an incompressible fluid field with nontrivial curvature generates a binormal asymmetry in the local velocity field. That is, the field local to a length of curved vortex filament induces a flow, which generates filament dynamics. This result, known by Tullio Levi-Civita and his student Luigi Sante Da Rios in the early 1900's, [107] was rediscovered by various post World-War II groups. [108–111] Together, Ricca [112] and Hama [113] provide an excellent chronology of LIA, a topic now common in vortex dynamics texts.[100, 114, 115] Exploration of LIA occurs in various settings including differential geometry,[116–128] differential equations[108] and limits of matched asymptotic expansions of vortex tubes. [109, 111, 129]

Our derivation avoids the complications of matched asymptotic expansions by treating vorticity concentrated to an arc. Under this geometry Eq. (3.1) can be reduced to a canonical

elliptic representation without the use of power-series approximation to the Biot-Savart integrand.[110, 130] While Taylor approximation quickly reveals binormal flow as a dominant feature of the induced field, it lacks error bounds and is often restricted to a two-dimensional subspace of $\mathbb{R}^3$. This paper resolves both issues by recasting Eq. (3.1), for a vortex-arc, into an elliptic form valid for all field points. Using this form, one can then use a known asymptotic formula to represent the local field. We offer that this should be adopted, instead of LIA, for use in vortex filament methods and Schwarz's description of the Magnus force.[97, 131] Specifically, we will prove the following results:

Theorem 1. ***Generalized Induction Equation***

Let $\boldsymbol{\omega} = \nabla \times \boldsymbol{v}$ be localized to an arbitrary arc with parameterization $\boldsymbol{\xi} = (R\sin(\theta), R - R\cos(\theta), 0)$, where $R \in \mathbb{R}^+$ and $\theta \in D_L = (-L, L]$ for some $L \in (-\pi, \pi]$. Then there exists bounded functions $\boldsymbol{V}_1$, α_1, α_2, $L_\pm$ and k, of $\varepsilon = |\boldsymbol{x}|/R = \kappa|\boldsymbol{x}|$, such that the induced velocity field is given by

$$\boldsymbol{v}(\boldsymbol{x}) = \boldsymbol{V}_1(\varepsilon)\left(\alpha_1(\varepsilon)\left[F(L_+,k) - F(L_-,k)\right] + \alpha_2(\varepsilon)\left[\frac{dF(L_+,k)}{d\varepsilon} - \frac{dF(L_-,k)}{d\varepsilon}\right]\right) \tag{3.2}$$

where F is an incomplete elliptic integral of the first kind. Moreover, there exist constants $\beta_1, \beta_2, \beta_3, \beta_4$ such that $\boldsymbol{V}_1$ can be written as

$$\boldsymbol{V}_1(\varepsilon) = \varepsilon\beta_1\hat{\boldsymbol{t}} - \varepsilon\beta_2\hat{\boldsymbol{n}} + (\varepsilon\beta_2 + \varepsilon\beta_3 + \beta_4)\,\hat{\boldsymbol{b}} \tag{3.3}$$

where $\hat{\boldsymbol{t}}, \hat{\boldsymbol{n}}, \hat{\boldsymbol{b}}$, are the tangent, normal and binormal vectors of the local coordinate system.

Theorem 2. ***Generalized Local Induction Equation***

Under the same hypotheses of theorem 1 and for $\varepsilon \ll 1$ the induced velocity field is dominated by the binormal flow,

$$\boldsymbol{v}_\varepsilon(\boldsymbol{x}) = 4\kappa x_2\left(\alpha_1(\varepsilon)\left[F(L_+,k) - F(L_-,k)\right] + \alpha_2(\varepsilon)\left[\frac{dF(L_+,k)}{d\varepsilon} - \frac{dF(L_-,k)}{d\varepsilon}\right]\right)\hat{\boldsymbol{b}}. \tag{3.4}$$

where x_2 is a dimensionless angular component of the spherical decomposition of $\boldsymbol{x}$ and κ is the curvature of the vortex arc. The limits $\varepsilon \to 0$ and $L \to 0$ imply that $k \to 1$ and $\lambda \to 0$ and in this case the incomplete elliptic integral of the first kind admits the asymptotic relation $F \sim F_1$ where

$$F_1(\lambda, k) = \ln\left(\sqrt{\frac{1+\lambda}{1-\lambda}}\right) + \frac{1}{\lambda}\ln\left(\frac{2}{1+\sqrt{(1-k^2\lambda^2)/(1-\lambda^2)}}\right) + \frac{1-k^2}{8}\ln\left(\frac{1+\lambda}{1-\lambda}\right). \tag{3.5}$$

Using this, along with standard differentiation formula for incomplete elliptic integrals of the first kind, provides a first order asymptotic form for the local field given by

$$\boldsymbol{v}_\varepsilon(\boldsymbol{x}) \sim -8\kappa x_2 \left\{ \frac{9x_2 F_1(\lambda,k)}{2} - \frac{x_2 E(L,k)}{(1-k^2)k} - \frac{k\sin(2L)\left[\sqrt{1+k^2\sin^2(L)} + \sqrt{1-k^2\sin^2(L)}\right]}{2(1-k^2)\sqrt{1-k^4\sin^4(L)}} \right\} \hat{\boldsymbol{b}}, \tag{3.6}$$

where E is an incomplete elliptic integral of the second kind.

In words, the first theorem expresses the velocity field generated by vortex arc in terms of incomplete elliptic integrals of the first kind. Moreover, this field can be decomposed into three fields controlling the tangential, circulatory and binormal flows. Of these fields, the binormal contribution is $O(1)$ while the remaining fields are $O(\varepsilon)$. The second theorem considers the remaining field in the limits of $\varepsilon \to 0$ and $L \to 0$. In this limit the incomplete elliptic integral of the first kind admits an asymptotic form and consequently provides a representation for the velocity field local to the vortex arc. This asymptotic form is comparable to LIA in that the Biot-Savart integral has been 'resolved' and the binormal flow is represented by elementary functions. This form is only valid for filaments of infinitesimal arclength and consequently idealized. However, using the same asymptotic framework, one can construct expansions valid for arcs of finite length. In fact, the remainder terms of such expansions are known and thus the associated approximation error can be controlled. The necessary asymptotic results are quoted in the appendix.

The rest of this document will be organized as follows. In Section II we define the geometry and derive the Biot-Savart representation of the induced velocity field. In Section III we convert this representation into an elliptic form and prove the generalized induction result (3.2)-(3.3). In Section IV we reduce this elliptic form into a sum of incomplete elliptic integrals of the first kind. Lastly, using known asymptotic results, we derive an expression for the local velocity field and prove the generalized local induction equation (GLIE) result (3.6). We conclude with some discussion on adapting this result to vortex filament methods and prospective avenues of future work.

3.3 Biot-Savart and Quantized Vortex Rings

It is well known that a vortex-defect with trivial curvature embedded into an incompressible fluid does not induce autonomous dynamics. This is due to an angular symmetry in the induced velocity field. This symmetry is no longer available for curved vortex elements. Using a vortex ring, it is possible to introduce nontrivial curvature and avoid approximations to the Biot-Savart integral. To be precise, we treat a vortex structure $\boldsymbol{\omega} : \mathbb{R}^3 \to \mathbb{R}^3$ such that

$$\boldsymbol{\omega}(\mathbf{x}) = \begin{cases} 1, & \mathbf{x} \in \boldsymbol{\xi} \\ 0, & \mathbf{x} \notin \boldsymbol{\xi} \end{cases} \tag{3.7}$$

where $\boldsymbol{\xi} : D \to \mathbb{R}^3$, $D \subset \mathbb{R}$, is parameterized by the ring

$$\boldsymbol{\xi} = R\sin(\theta)\hat{\mathbf{i}} + [R - R\cos(\theta)]\,\hat{\mathbf{j}}, \tag{3.8}$$

$$d\boldsymbol{\xi} = \left[R\cos(\theta)\hat{\mathbf{i}} + R\sin(\theta)\hat{\mathbf{j}}\right] d\theta \tag{3.9}$$

for $\kappa^{-1} = R \in \mathbb{R}^+$, $D_L = (-L, L]$ and $L \in [0, \pi]$. Thus, at the point $\mathbf{x} = (\tilde{x}_1, \tilde{x}_2, \tilde{x}_3)$ we get an element level description of the velocity field,

$$v_i(\mathbf{x}) = \int_{D_L} \frac{\epsilon_{ijk}(\tilde{x}_j - \xi_j)d\xi_k}{\left[|\mathbf{x}|^2 + |\boldsymbol{\xi}|^2 - 2(\tilde{x}_1\xi_1 + \tilde{x}_2\xi_2 + \tilde{x}_3\xi_3)\right]^{3/2}} \tag{3.10}$$

where we have used the Levi-Civita symbol, ϵ_{ijk}, and employed Einstein-summation over repeated indices. Noting that $|\boldsymbol{\xi}|^2 = 2R^2 - 2R^2\cos(\theta)$ provides the formulae

$$v_1 = -|\mathbf{x}|\kappa^2 x_3 \int_{D_L} \frac{\sin(\theta)}{D^{3/2}} d\theta, \tag{3.11}$$

$$v_2 = |\mathbf{x}|\kappa^2 x_3 \int_{D_L} \frac{\cos(\theta)}{D^{3/2}} d\theta, \tag{3.12}$$

$$v_3 = \kappa^2 |\mathbf{x}| \int_{D_L} \frac{x_1 \sin(\theta) - x_2 \cos(\theta)}{D^{3/2}} d\theta + \kappa \int_{D_L} \frac{\cos(\theta) - 1}{D^{3/2}} d\theta \tag{3.13}$$

where the denominator is given by

$$D = [c_1 + c_2 \cos(\theta) + c_3 \sin(\theta)] \tag{3.14}$$

and whose coefficients are

$$R^2 c_1 = |\mathbf{x}|^2 + 2R^2 - 2\tilde{x}_2 R, \tag{3.15}$$

$$R^2 c_2 = 2|\mathbf{x}| x_2 R - 2R^2, \tag{3.16}$$

$$R^2 c_3 = -2|\mathbf{x}| x_1 R. \tag{3.17}$$

For future limiting work, we have chosen a radial-representation for $\mathbf{x} = |\mathbf{x}|(x_1, x_2, x_3)$ where x_i is the i^{th} dimensionless angular component of $\mathbf{x}$.

3.4 Conversion to Elliptic Form

The previous integral representations for the velocity field can be cast into elliptic form. To do this, we first reduce each integral into an elliptic integral by taking derivatives with respect to internal parameters. Doing so gives

$$v_1 = 2\kappa x_3 \varepsilon \frac{d}{dc_3} \int_{D_L} \frac{d\theta}{\sqrt{D}}, \tag{3.18}$$

$$v_2 = -2\kappa x_3 \varepsilon \frac{d}{dc_2} \int_{D_L} \frac{d\theta}{\sqrt{D}}, \tag{3.19}$$

$$v_3 = \left[2\kappa\varepsilon x_2 \frac{d}{dc_2} - 2\kappa\varepsilon x_1 \frac{d}{dc_3} + 2\kappa \frac{d}{dc_1} - 2\kappa \frac{d}{dc_2} \right] \int_{D_L} \frac{d\theta}{\sqrt{D}} \tag{3.20}$$

where the parameter $\varepsilon = |\mathbf{x}|/R$ is the ratio of radial distance to the radius of curvature. Application of the chain-rule gives the induced velocity field as

$$\boldsymbol{v}(\mathbf{x}) = \mathbf{V}_1(\varepsilon)\frac{d}{d\varepsilon}\int_{D_L}\frac{d\theta}{\sqrt{D}} \tag{3.21}$$

where the vector $\mathbf{V}_1$ is given by

$$\mathbf{V}_1(\varepsilon) = 2\varepsilon\kappa x_3\frac{dc_3}{d\varepsilon}\hat{\mathbf{i}} - 2\varepsilon\kappa x_2\frac{dc_2}{d\varepsilon}\hat{\mathbf{j}} + \left[2\kappa\varepsilon x_2\frac{dc_2}{d\varepsilon} - 2\kappa\varepsilon x_1\frac{dc_3}{d\varepsilon} + 2\kappa\frac{dc_1}{d\varepsilon} - 2\kappa\frac{dc_2}{d\varepsilon}\right]\hat{\mathbf{k}} \tag{3.22}$$

implying that the velocity field is determined by the derivative of an incomplete elliptic integral. Moreover, this proves Eq. (3.3) from theorem 1 where

$$\beta_1 = 2\kappa x_3\frac{dc_3}{d\varepsilon}, \tag{3.23}$$

$$\beta_2 = 2\kappa x_2\frac{dc_2}{d\varepsilon}, \tag{3.24}$$

$$\beta_3 = -2\kappa x_1\frac{dc_3}{d\varepsilon}, \tag{3.25}$$

$$\beta_4 = 2\kappa\left(\frac{dc_1}{d\varepsilon} - \frac{dc_2}{d\varepsilon}\right). \tag{3.26}$$

For $\varepsilon \ll 1$ we find that the velocity field is dominated by

$$\boldsymbol{v}_\varepsilon(\mathbf{x}) = -8\kappa x_2\frac{d}{d\varepsilon}\int_{D_L}\frac{d\theta}{\sqrt{D}}\hat{\mathbf{k}}. \tag{3.27}$$

In Figure 3.1 we show the vortex configuration as well as the associated field and vortex coordinate geometry. Using the depicted spherical decomposition of $\mathbf{x}$ we find that the previous dimensionless parameter is given by $x_2 = \sin(\gamma_1)\sin(\gamma_2)$. Moreover, we observe that the standard basis vector $\hat{\mathbf{k}}$ corresponds to the binormal vector $\hat{\mathbf{b}}$. These two facts show that the velocity field, asymptotically close to the vortex arc, is asymmetric in the binormal direction and that this effect is extremized for field-points on the normal-axis, which agrees with standard results of induced binormal flow.

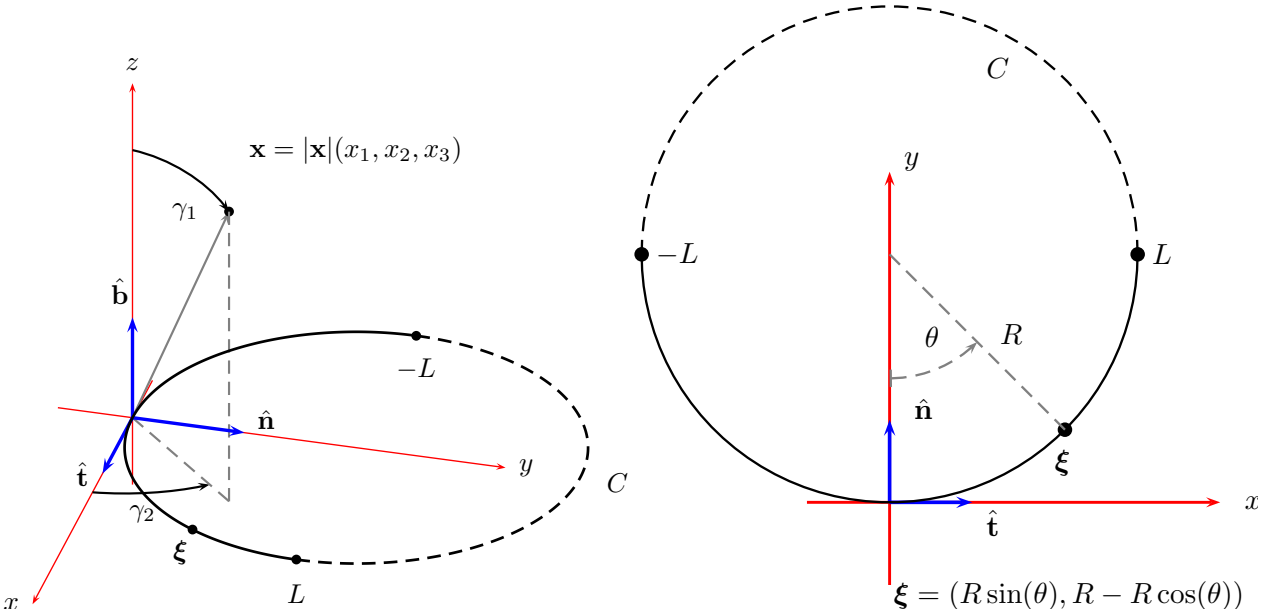

Figure 3.1: Global and Local Coordinate Geometry. In subfigure (a) the vortex arc is depicted in $\mathbb{R}^3$ where the circle parameterization, C, is composed of the solid line representing the vortex filament and a dashed line representing a continuation of the parameterization. These two regions are separated by the cut-off parameter L. This subfigure also shows the spherical decomposition of the field point $\mathbf{x}$ where γ_1 is the azimuthal angle and γ_2 is the polar angle associated with the spherical decomposition of $\mathbf{x}$. Lastly, this subfigure shows the configuration of the Serret-Frenet local basis vectors $\hat{\mathbf{t}}, \hat{\mathbf{n}}, \hat{\mathbf{b}}$, which, for ease of use, are oriented to correspond to the standard global basis vectors for $\mathbb{R}^3$. In subfigure (b) the projection of subfigure (a) onto the x–y plane is given and shows the polar decomposition of the filament point $\boldsymbol{\xi} = (R\sin(\theta), R - R\cos(\theta), 0)$.

3.5 Reduction of Elliptic Form to Canonical Elliptic Integrals

Before we construct the asymptotic representation of the velocity field, the previous integrals are converted into canonical forms. The induced velocity field is controlled by an integral of the form

$$\int_{D_L} \frac{d\theta}{\sqrt{c_1 + c_2\cos(\theta) + c_3\sin(\theta)}}, \tag{3.28}$$

which can be converted to a sum of incomplete integrals of the first kind. First, we introduce a new angle defined by $\tan(\phi) = c_3/c_2$ and hypotenuse $r^2 = c_2^2 + c_3^2$ to get

$$\int_{D_L} \frac{d\theta}{\sqrt{c_1 + c_2\cos(\theta) + c_3\sin(\theta)}} = \int_{-L}^{L} \frac{d\theta}{\sqrt{c_1 + r\cos(\phi - \theta)}}. \tag{3.29}$$

Now, introducing a change of variable $2\psi = \phi - \theta$ and the notation $L_\pm = (\phi \pm L)/2$ we apply trigonometric formulae to get

$$\int_{-L}^{L} \frac{d\theta}{\sqrt{c_1 + r\cos(\phi - \theta)}} = \frac{2}{\sqrt{c_1 + r}} \int_{L_-}^{L_+} \frac{d\psi}{\sqrt{1 - k^2\sin^2(\psi)}} \tag{3.30}$$

where $k^2 = 2r/(c_1 + r)$. Lastly,

$$\int_{D_L} \frac{d\theta}{\sqrt{c_1 + c_2\cos(\theta) + c_3\sin(\theta)}} = \frac{2\left[F(L_+, k) - F(L_-, k)\right]}{\sqrt{c_1 + r}} \tag{3.31}$$

where F is the standard incomplete elliptic integral of the first kind,

$$F(\varphi, k) = \int_0^{\varphi} \frac{d\psi}{\sqrt{1 - k^2\sin^2(\psi)}} = \int_0^{\lambda} \frac{dt}{\sqrt{1 - t^2}\sqrt{1 - k^2t^2}} \tag{3.32}$$

such that $\lambda = \sin(\varphi)$.

3.6 Asymptotics for the Incomplete Elliptic Integral of the First Kind

Having reduced the Biot-Savart representation of the velocity field to a canonical form, we can now make use of the known asymptotic formula of Karp and Sitnik,[132] which permits

the study of (3.32) for all $(\lambda, k) \in [0,1] \times [0,1]$. Specifically, they derive a series representation and remainder term for F, which is asymptotic for $k \to 1$. Their complete theorem is quoted in the appendix, but we only require the first-order approximation

$$F_1(\lambda, k) = \ln\left(\sqrt{\frac{1+\lambda}{1-\lambda}}\right) + \frac{1}{\lambda}\ln\left(\frac{2}{1+\sqrt{(1-k^2\lambda^2)/(1-\lambda^2)}}\right) + \frac{1-k^2}{8}\ln\left(\frac{1+\lambda}{1-\lambda}\right). \tag{3.33}$$

which is asymptotic to F for $\lambda \to 0$ and $k \to 1$. This asymptotic formula is not suited to differentiation. [133–136] Thus, we must first apply the differentiation formula, for the incomplete elliptic integral of the first kind, prior to its asymptotic evaluation. Doing so gives lengthy formulae and for these we introduce the constants

$$A = \frac{x_2 c_2 - x_1 c_3}{r}, \tag{3.34}$$

$$A_1 = \frac{-4}{(c_1+r)^{3/2}}(\varepsilon - x_2 + A), \tag{3.35}$$

$$A_2 = \frac{2}{\sqrt{c_1+r}}, \tag{3.36}$$

$$A_3 = -2\frac{x_2 c_3 + x_1 c_2}{r^2}, \tag{3.37}$$

$$A_4 = \frac{\sqrt{2r}(x_2-\varepsilon)}{(c_1+r)^{3/2}} + \sqrt{\frac{2}{r}}\left(\frac{(c_1+r)^{3/2} - r\sqrt{c_1+r}}{(c_1+r)^2}\right) A. \tag{3.38}$$

Using these constants, find

$$\frac{d}{d\varepsilon}\int_{D_L}\frac{d\theta}{\sqrt{D}} = 2A_1[F(L_+,k) - F(L_-,k)] + A_2\left[\Omega(A_3,A_4,A_5,k,L_+) - \Omega(A_3,A_4,A_5,k,L_-)\right] \tag{3.39}$$

where

$$\Omega(A_3,A_4,A_5,k,L) = \frac{A_3}{\sqrt{1-k^2\sin^2(L)}} + \frac{A_4 E(L,k)}{1(1-k^2)k} - \frac{A_4 F(L,k)}{2k} - \frac{A_4 2k\sin(2L)}{4(1-k^2)\sqrt{1-k^2\sin^2(L)}} \tag{3.40}$$

is given by differentiation formula for incomplete elliptic integrals of the first kind. Together with Eq. (3.21), proves Eq. (3.2) of our first theorem where $\alpha_1 = 2A_1$ and $\alpha_2 = A_2$. From

Eq. (3.27) we find that the local velocity field is given by

$$\boldsymbol{v}_\varepsilon(\mathbf{x}) = -8\kappa x_2 \left(2A_1[F(L_+,k) - F(L_-,k)] + A_2\left[\Omega(A_3,A_4,A_5,k,L_+) - \Omega(A_3,A_4,A_5,k,L_-)\right]\right). \tag{3.41}$$

At this point, the asymptotic formula (3.1) can now be applied to $F(\lambda,k)$ where $\lambda = \sin(L_\pm)$. To compare these results to standard LIA we take $\varepsilon \to 0$ and $L \to 0$. In this case $c_1 = -c_2 = r \sim 2$, $c_3 \sim 0$ and the constants take the asymptotic forms

$$A = \frac{x_2c_2 - x_1c_3}{r} \sim -x_2, \tag{3.42}$$

$$A_1 = \frac{-4}{(c_1+r)^{3/2}}(\varepsilon - x_2 + A) \sim x_2, \tag{3.43}$$

$$A_2 = \frac{2}{\sqrt{c_1+r}} \sim 1, \tag{3.44}$$

$$A_3 = -2\frac{x_2c_3 + x_1c_2}{r^2} \sim x_1, \tag{3.45}$$

$$A_4 = \frac{\sqrt{2r}(x_2-\varepsilon)}{(c_1+r)^{3/2}} + \sqrt{\frac{2}{r}}\left(\frac{(c_1+r)^{3/2} - r\sqrt{c_1+r}}{(c_1+r)^2}\right)A \sim -\frac{x_2}{2}. \tag{3.46}$$

Together this gives the first-order asymptotic representation for the velocity field,

$$\mathbf{v}_\varepsilon(\mathbf{x}) \sim -8\kappa x_2 \left\{ \frac{9x_2F_1(\lambda,k)}{2} - \frac{x_2E(L,k)}{(1-k^2)k} - \frac{k\sin(2L)\left[\sqrt{1+k^2\sin^2(L)} + \sqrt{1-k^2\sin^2(L)}\right]}{2(1-k^2)\sqrt{1-k^4\sin^4(L)}} \right\} \hat{\mathbf{b}} \tag{3.47}$$

for the limits $\varepsilon \to 0$, $k \to 1$ and $L \to 0$, $\lambda \to 0$. This proves Eq. (3.6) of our GLIE. It should be noted that the above formula is nonzero even for the extreme case of $L = 1 - k \to 0$. The physical meaning of this statement is that the local field induced by an infinitesimal segment of a vortex line is nonzero and asymmetric in the binormal direction.

3.7 Discussion and Conclusions

We have derived an asymptotic representation for the local velocity field induced by a curved vortex filament. This derivation generalizes the previously known statements of induced binormal flow, which play an important role in two-component superfluid simulation.

In such simulations one must calculate the superfluid and normal fluid flows as well as their mutual friction interaction. This mutual friction embodies the scattering of rotons and phonons off of the vortex structures.[137–141] It is possible to calculate this interaction in a manner self-consistent with Navier-Stokes and fully coupled to both components.[142] The normal fluid is approximated through Navier-Stokes simulation techniques while the kinematics of the superfluid make use of LIA. Though our focus is LIA dynamics we offer the following references to the computational fluid dynamics literature, which has been used for coupled two-component superfluid simulations. [143–145] While there has been progress in these techniques, [146, 147] the recent growth of the highly adaptable discontinuous Galerkin methods [148] and their application to nonlinear fluid flow and acoustic problems [149] is especially provocative.

Mathematically, the kinematics of a vortex filament, $\boldsymbol{\xi}$, are described by[89]

$$\frac{d\boldsymbol{\xi}}{dt} = \mathbf{V}_S + \mathbf{V}_I + \beta\boldsymbol{\xi}' \times (\mathbf{V}_N - \mathbf{V}_S - \mathbf{V}_I) - \beta'\boldsymbol{\xi}' \times [\boldsymbol{\xi}' \times (\mathbf{V}_N - \mathbf{V}_S - \mathbf{V}_I)]\,. \tag{3.48}$$

In a *filament method*, it is typical to prescribe the normal-fluid flow $\mathbf{V}_N$ and neglect the mutual friction terms involving β and β'. [97] This leaves only a potential flow $\mathbf{V}_S$ and induced flow $\mathbf{V}_I$. Of the remaining quantities, the computationally costly induced flow is managed through the LIA,

$$\mathbf{V}_I(\mathbf{x}) \approx \mathbf{V}_{\text{local}}(\mathbf{x}) = \kappa \ln\left(\frac{2\sqrt{L_+ L_-}}{|\mathbf{x}|}\right)\hat{\mathbf{b}} \tag{3.49}$$

where $L_\pm = (\phi \pm L)/2$ is related to the cutoff length L and angle ϕ. Vortex filament methods avoid integration by application of this approximation to nodal points of the Lagrangian computational mesh attached to the filament centerline. Alternatively, we could simply replace LIA with GLIE (3.4)-(3.5) and write $\mathbf{V}_I \approx \mathbf{V}_\varepsilon$ and prescribe a field point $\mathbf{x}$ and arclength $s = 2RL$. However, if the higher-order circulatory and binormal terms are desired, one could use (3.2)-(3.3) and employ efficient numerical routines for the incomplete elliptic integrals.[150–

152] Either of these changes will then be applied to node points of a computational mesh modeling the filament structure.

The use of piecewise linear interpolants, while prevalent in numerics, cause spurious effects when applied to a vortex centerline. The interpolants themselves have zero local curvature and their connections form cusps with undefined local curvature. Typically, local induction is applied to higher-order interpolations. While one can use the generalized induction equation or GLIE on this mesh, the natural vortex-arc construct has been adapted to efficient meshing techniques. [153] Consequently, computational cusps are avoided and local curvature is always well-defined when GLIE is applied to such vortex-arc meshes. Lastly, what remains is re-meshing to allow for the experimentally witnessed vortex nucleation.[154, 155]

Meshing is the most difficult aspect of vortex filament implementations. Not only must the mesh adapt to the vortex dynamics, it must be made to reconnect filament elements that are not predicted by the Eurelian theory. [156] The most elementary reconnection algorithms appeal to nonlinear Schödinger theory and force reconnection of filaments passing within a few core widths of each other.[131, 157] The current theory of the reconnection process is not satisfactory and efforts to avoid ad hoc simulated reconnection continue.[158–163]

Superfluid turbulence dominated by quantized vortex flows is an active area of analytic, numerical and experimental research.[98, 164–174] Though local induction techniques will play a part in continued numerical investigations, understanding geometric and topological quantification of a tangled state is as important and still a work in progress. [175–178] Lastly, the vortex line approximation, while useful and appropriate, must eventually be discarded in favor of nontrivial core-structure. It is likely that the methods developed within this paper can be adapted to current arguments used to study fields induced by vortex tubes. [109, 109, 129]

That being said, this work makes it clear that binormal flow proportional to curvature is a general feature of vortex filament dynamics. This means that the well-celebrated transformation of Hasimoto[8], which connects the filament's curvature and torsion variables

to a wavefunction controlled by nonlinear Schrödinger evolution, is fundamental to vortex filament dynamics. Consequently, even geometrically complicated filament dynamics are rooted in integrable systems theory. This connection underpins efforts to predict allowed filament geometrics from the associated integrable systems. [179–183]

The authors thank Paul Martin for useful discussions. This material is based in part upon work supported by the National Science Foundation under grant numbers PHY-0547845 and PHY-1067973. LDC acknowledges support from the Alexander von Humboldt foundation.

A.1 Appendix - Asymptotic Representation for Incomplete Elliptic Integrals of the First Kind

The following theorem is one of the two major results proven in Karp and Sitnik. [132] The second result gives a simpler expression but is not valid on the leftmost edge of the unit square and therefore not used in our calculations.

Theorem 3. *For all* $(\lambda, k) \in [0,1] \times [0,1]$ *and an integer* $N \geq 1$*, the previous elliptic integral admits the representation*

$$\begin{aligned} F(\lambda,k) = \frac{1}{2}\ln\left(\frac{1+\lambda}{1-\lambda}\right)\sum_{j=0}^{N}\frac{(1/2)_j(1/2)_j}{(j!)^2}(1-k^2)^j + \\ + \frac{1}{2\lambda}\sum_{n=0}^{N-1}\left(\frac{1-\lambda^2}{-\lambda^2}\right)^n s_n\left(\frac{(1-k^2)\lambda^2}{1-\lambda^2}\right) + R_N(\lambda,k), \end{aligned} \tag{3.1}$$

where $s_n(\cdot)$ *is given by the recurrence formulae*

$$s_{n+3} = \frac{a_n s_{n+2}(x), + b_n s_{n+1}(x) + c_n s_n(x) + h_n}{4(n+3)^2}, \tag{3.2}$$

$$a_n(x) = 8n^2 + 36n + 42 - x(2n+5)^2, \tag{3.3}$$

$$b_n(x) = 2x(4n^2 + 14n + 13) - (2n+3)^2, \tag{3.4}$$

$$c_n(x) = -4x(n+1)^2, \tag{3.5}$$

$$h_n(x) = \frac{x(2n+5)(2n+4)^2 + (n+3)(8n^2+24n+17)}{8(n+3)[(n+2)!]^2}[(3/2)_n]^2(-x)^{n+2}, \tag{3.6}$$

$$s_0(x) = -2\ln\left(\frac{1+\sqrt{1+x}}{2}\right), \tag{3.7}$$

$$s_1(x) = \left(\frac{x}{2} - 1\right)\ln\left(\frac{1+\sqrt{1+x}}{2}\right) - \frac{1}{2}\sqrt{1+x} + \frac{1}{2} + \frac{x}{2}, \tag{3.8}$$

$$s_2(x) = \left(-\frac{9}{32}x^2 + \frac{x}{4} - \frac{3}{4}\right)\ln\left(\frac{1+\sqrt{1+x}}{2}\right) + \left(\frac{9}{32}x - \frac{7}{16}\right)\sqrt{1+x} + \frac{7}{16} + \frac{1}{8}x - \frac{21}{64}x^2 \tag{3.9}$$

and the remainder term is negative and satisfies,

$$\frac{[(1/2)_{N+1}]^2(1-k^2)^N}{2[(N+1)!]^2} f_{N+1}(\lambda,k) \leq -R_N(\lambda,k) \leq \frac{[(1/2)_{N+1}]^2(1-k^2)^N}{2[(N+1)!]^2} f_N(\lambda,k), \tag{3.10}$$

where the positive function

$$f_N(\lambda,k) = \frac{1}{1-\alpha(1-k^2)} \cdot \left\{ \frac{\ln\left(\frac{\sqrt{1+(1-\lambda^2)/[\alpha\lambda^2(1-k^2)]}+1}{\sqrt{1+(1-\lambda^2)/[\alpha\lambda^2(1-k^2)]}-1}\right)}{\alpha\lambda\sqrt{1+(1-\lambda^2)/[\alpha\lambda^2(1-k^2)]}} - (1-k^2)\ln\left(\frac{1+\lambda}{1-\lambda}\right) \right\}_{|\alpha=(N+1/2)^2/(N+1)^2} \tag{3.11}$$

is bounded on every subset of E of the unit square, where

$$\sup_{k,\lambda\in E} \frac{1-k}{1-\lambda} < \infty \tag{3.12}$$

and is monotonically decreasing in N.

From this theorem we denote its first-order approximation as

$$F_1(\lambda, k) = \ln\left(\sqrt{\frac{1+\lambda}{1-\lambda}}\right) + \frac{1}{\lambda}\ln\left(\frac{2}{1+\sqrt{(1-k^2\lambda^2)/(1-\lambda^2)}}\right) + \frac{1-k^2}{8}\ln\left(\frac{1+\lambda}{1-\lambda}\right), \tag{3.13}$$

and note that this expression is asymptotic in the λ variable.

CHAPTER 4

NON-HAMILTONIAN DYNAMICS OF QUANTIZED VORTICES IN BOSE-EINSTEIN CONDENSATES

A paper submitted to *Physical Review Letters*, arXiv:1712.05885

Scott A. Strong*, **Lincoln D. Carr**

Department of Physics, Colorado School of Mines, Golden, CO 80401, USA

*Primary researcher and author.

.

4.1 Abstract

The dynamics of quantized vortices in weakly interacting superfluids are often modeled by a nonlinear Schrödinger equation. In contrast, we show that quantized vortices in fact obey a non-Hamiltonian evolution equation, which enhances dispersion along the vortex line while introducing a gain mechanism. This allows the vortex medium to support a helical shock front propagating ahead of a dissipative soliton. This dynamic relaxes localized curvature events into Kelvin wave packets. Consequently, a beyond local induction model provides a pathway for decay in low-temperature quantum turbulence.

4.2 Paper Body

Quantized vortices are slender, non-diffusive regions of low density about which the superfluid bulk circulates at strengths defined by multiples of Planck's constant scaled by a characteristic mass [184]. A vortex line is modeled as a one-dimensional region of the quantum liquid about which the irrotational fluid circulates. A quantum tangle is a randomized configuration of quantized vortex lines that supports various cascade processes which transfer energy between the spatial scales [185]. Unique to quantum fluids is the Kelvin

wave cascade which relaxes high curvature cusps, formed through vortex interactions, to small wavelength helical excitations along the vortex. These waves transport turbulent energy to the boundaries [186]. In this Letter, we derive a relatively simple, but non-Hamiltonian evolution of the geometric properties of a vortex defect under local induction models. This evolution predicts that the vortex medium transforms a curvature soliton into a helical shock wave where a dissipative soliton travels behind helical excitations. Gain mechanisms introduced by the non-Hamiltonian structure result in an increase of mean curvature and signify the emergence of the small-scale structures necessary for stimulating acoustic emission.

The Biot-Savart integral provides a representation of the velocity field by "un-curling" the vorticity field. Locally induced evolutions are given by asymptotic approximations to regularizations of this singular integral. There are several regularization techniques available and all yield a lowest order local induction approximation (LIA). The LIA states that a vortex flows at a speed proportional to its local curvature and in a direction defined by its local binormal vector [6]. The Hasimoto transformation is a scalar version of Madelung's hydrodynamic transformation of the Schrödinger equation [3]. When applied to the LIA, curvature and torsion of the vortex are found to obey a cubic focusing nonlinear Schrödinger equation [8]. This theory predicts a bright curvature soliton defining a traveling kink on the vortex line, which we call a Hasimoto vortex soliton, see Figure 4.1. This integrability obstructs the transfer of energy between Kelvin waves and prohibits the cascade process [59]. Our non-Hamiltonian description overcomes the restrictions imposed by the integrable theory by introducing a curvature gain/loss mechanism while enhancing dispersion on the vortex medium. We call a cascade soliton the non-Hamiltonian evolution of Hasimoto's vortex soliton, which deforms a bright curvature soliton into a log-normal distribution. Represented on the vortex line, the soliton kink decreases its amplitude while the curvature of the straight background increases ahead of the disturbance. Furthermore, our non-Hamiltonian dynamic predicts the existence of two qualitatively different dynamical regimes. For small perturbations, the kink maintains its structure for longer times, a robustness that is indicative

of a dissipative soliton. Increasing dispersion erodes the previously robust kink into a packet of Kelvin waves generating a profile similar to a dispersive shock wave. This Letter introduces a nonlinear integro-differential equation and uses it to approximate the non-Hamiltonian dynamics of the Hasimoto vortex soliton from the integrable theory. Prior to simulations, we consider the dynamics predicted by the emergent gain/loss mechanism in conjunction with the changes to plane wave dispersion to understand the short-time behavior of a soliton.

Vortex filament methods simulate a quantum fluid by evolving its vortical skeleton according to the Biot-Savart integral and are significantly more efficient than mean-field methods for vortex dominated flows [55]. Recent simulations by Salman demonstrate that evolutions given by the mean-field, Biot-Savart and induction models are consistent up to the point where the smallest length scales dominate the physics, a known limitation of filament methods [187]. Specifically, the LIA and Eulerian evolution of vortex lines conserves their total length, preventing reconnection from occurring. At the same time, Bustamante and Nazarenko have shown that the Biot-Savart integral manifests from Gross-Pitaevskii mean–field dynamics and provides a self-consistent regularization procedure [63]. This allows us to derive a non-Hamiltonian evolution consistent with a locally induced flow generated by a region of vortex whose arc-length is on the order of the condensate healing length. Our prediction of helical waves generated from a localized curvature event is consistent with current models of energy transfer in the highly quantum turbulent regime [188].

As shown in Figure 4.1, we define $\vec{\gamma} \in \mathbb{R}^3$ as the set of points in three-space corresponding to a Hasimoto vortex soliton, i.e., a bright curvature soliton shown in the inset of Figure 4.1. The vortex is parameterized by an arc-length, s, and changes with time, t, so that $\vec{\gamma} = \vec{\gamma}(s,t)$. Beginning with the Biot-Savart integral, our previous work derives the velocity field induced by $\vec{\gamma}$ in terms of elliptic integrals [60]. The LIA is the first term in an asymptotic approximation of this representation, where circulatory and axial velocities are neglected. Symbolically, we have that this component of the velocity field generates a flow satisfying the vector evolution law,

$$\frac{\partial \vec{\gamma}}{\partial t} = \alpha \left(\frac{\partial \vec{\gamma}}{\partial s} \times \frac{\partial^2 \vec{\gamma}}{\partial s^2} \right), \tag{4.1}$$

where the cross-product $\vec{\gamma}_s \times \vec{\gamma}_{ss} = \kappa \hat{\boldsymbol{b}}$ is defined using the binormal vector of the Frenet-Serret basis and $\kappa = \kappa(s,t)$ is the local curvature. The Hasimoto vortex soliton is a prediction of the LIA, given by Eq. (4.1) where $\alpha = 1$, and forms a propagating curvature disturbance, $\kappa(s,t) = 2\,\mathrm{sech}(s-t)$, with constant torsion, $\tau = 1$. To understand the transition to a cascade soliton, we consider the case of non-constant α.

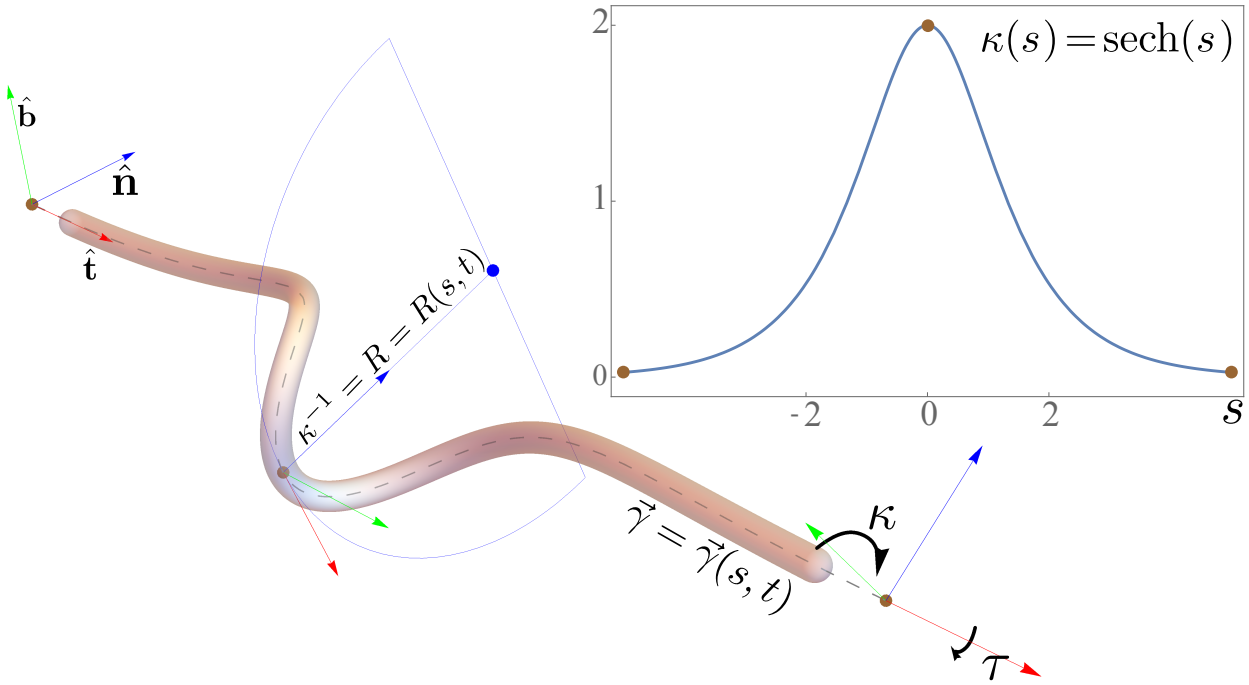

Figure 4.1: Hasimoto's Vortex Soliton. We depict the Frenet basis, $\hat{\mathbf{t}}, \hat{\mathbf{n}}, \hat{\mathbf{b}}$, for a hyperbolic secant (inset) bright soliton, $\kappa, \tau = 1$, from the integrable theory, $2i\psi_t + 2\psi_{ss} + |\psi|^2\psi = 0$, corresponding to Hasimoto's map applied to the LIA, $\vec{\gamma}_t = \kappa \hat{\mathbf{b}}$.

The condensate healing length, ξ, defines the vortex core size and its product with the characteristic curvature, κ, yields the small parameter $\epsilon = \xi\kappa \ll 1$. The healing length, in ratio with the characteristic system size, d, defines the parameter $\delta = d/\xi$ and is large when the characteristic system size is taken to be the condensate width. The proportionality constant in Eq. (4.1) is a function of the dimensionless parameters, $\alpha = \alpha(\delta, \epsilon)$, and has a

tidy representation given by the matched asymptotic expansion [189],

$$\alpha(\delta,\epsilon)=\frac{\Gamma}{4\pi}\left[\ln\left(\frac{1}{\delta}\right)+\ln\left(\sqrt{1+\frac{\epsilon^2\delta^2}{8}}\right)\right], \tag{4.2}$$

where Γ measures the strength of the condensate circulation about the vortex line. The LIA retains only the curvature-independent logarithmic singularity and is defined as Eq. (4.1), where $\alpha=\alpha(\delta,\epsilon=0)$. If we assume that ϵ is not formally zero, then the scale separation $\epsilon\ll\epsilon\delta\ll\delta$ defines a regime where the linearization of Eq. (4.2), i.e. the LIA, is accurate. If a parameterization is given, then the characteristic length, d, can be associated with the domain of Biot-Savart integration. Parameterizing an arbitrary vortex element by a plane circular arc gives a wide range for the non-dimensional parameter, $\delta\in(a,100)$, where $a=0.3416293$. The lower bound of this interval is the Bustamante-Nazarenko regularization, while the upper bound corresponds to an integration domain up to two orders of magnitude larger than the healing length, $d=100\xi$. While this approach maintains the scale separation of LIA, it is less restrictive and permits the study of flows induced by arcs of vorticity with small central angle such that $\epsilon\delta=O(\epsilon)$.

Hasimoto's transformation rotates the Frenet basis into $\mathbb{C}^3$ where the geometric wave function, $\psi(s,t)=\kappa(s,t)\ \mathrm{Exp}\left[i\int_0^s ds'\tau(s',t)\right]$, carries the curvature and torsion variables of a vortex line satisfying LIA [8]. This transformation is robust and can be used to map more general flows, often leading to complicated integro-differential equations [190, 191]. Restricting ourselves to binormal flows defined by Eq. (4.1) and applying an asymptotic representation of α, we recast the corresponding integro-differential equation as a nonlinear differential equation. The predicted state is a cascade soliton, which is a solitary wave accompanied by helical excitations, and is depicted in Figure 4.2.

Throughout the following, t will refer to a non-dimensional time. If we scale this time by $\tilde{t}=4\pi\tilde{\gamma}/(\tilde{\kappa}\Gamma a_0(\delta))$, to define a laboratory time, then $\alpha(\delta,0)=1$. Application of the Hasimoto transformation to the general case, $\alpha=\alpha(\delta,\epsilon)$ yields a nonlinear integro-differential evolution of the geometric variables,

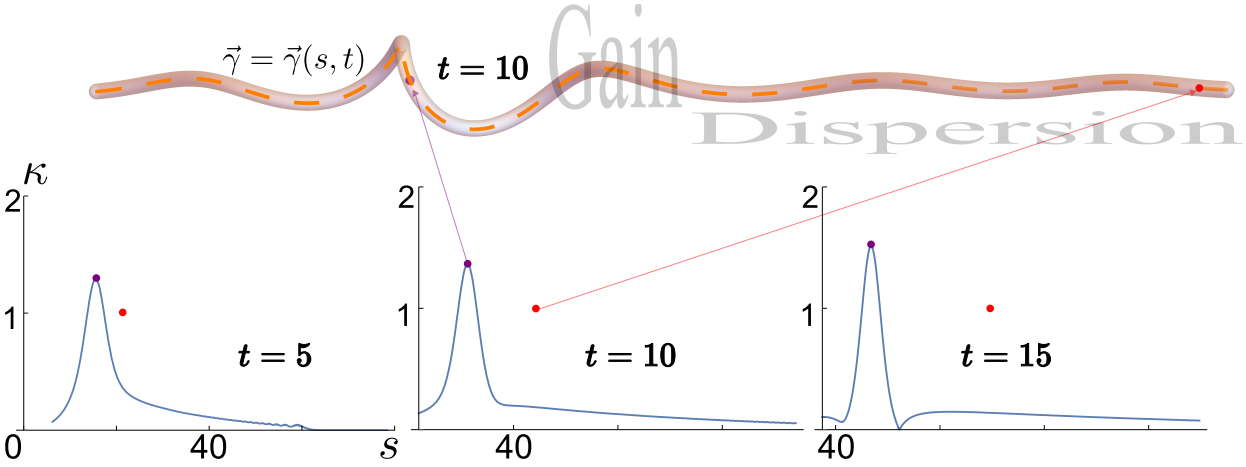

Figure 4.2: Non-Hamiltonian Cascade Soliton. An initial Hasimoto vortex soliton experiences dispersion producing helical waves propagating ahead of the soliton kink. The non-Hamiltonian gain mechanism supports both the kink and the helical excitations as the localized curvature event is transitioned to a cascade process.

$$i\psi_t + [\alpha\psi]_{ss} + \frac{\alpha}{2}|\psi|^2\psi + \frac{\psi}{2}\int^s |\psi|^2\alpha_{s'}\, ds' = 0. \tag{4.3}$$

This evolution maintains the Schrödinger structure seen for $\alpha = 1$. However, it is difficult to derive useful information from it. The small parameter $\epsilon \ll 1$ provides an expansion of α in powers of κ. From Eq. (4.2), we find that $\alpha(-\kappa) = \alpha(\kappa)$. After truncating quartic and higher terms we arrive at the simpler evolution,

$$i\psi_t + \psi_{ss} + \frac{1}{2}|\psi|^2\psi + \lambda\left(\left[|\psi|^2\psi\right]_{ss} + \frac{3}{4}|\psi|^4\psi\right) = 0, \tag{4.4}$$

which we call the *non-Hamiltonian vortex cascade equation* (NVC). The correction parameter, λ, depends on our dimensionless constants and is the ratio of the second and first coefficients in the expansion of α. In the LIA $\lambda = 0$ and we have an integrable theory. If $\lambda \neq 0$, then integrability is compromised so severely that nearly all underlying symmetries are broken. With the exception of arc-length, a quantity conserved by the LIA, nothing typical, like energy or momentum, is conserved by the NVC.

To understand this loss of mathematical structure we inspect the fully nonlinear term $[|\psi|^2\psi]_{ss}$. One can show that there does not exist a functional whose variational derivative satisfies the necessary self-adjoint conditions and therefore the evolution cannot be written as an infinite-dimensional Hamiltonian system [192, 193]. The system is invariant with respect to arbitrary time and space translations. However, as the system is not Hamiltonian, Noether's theorem does not apply and our continuous symmetries need not correspond to conserved densities. Application of the SYM symmetry software package [194] to Eq. (4.4) found no additional continuous symmetries. Additionally, a Mathematica package that symbolically calculates conservation laws found no low-order conserved densities [195]. While the system does possess discrete parity and time symmetries, we consider non-symmetric, time-irreversible dynamics of the nonlinear evolution.

Without $[|\psi|^2\psi]_{ss}$, the NVC is a complex quintic Ginzburg-Landau equation used in the study of dissipative solitons [196]. Our real coefficients imply a Hamiltonian structure and a nonlinear gain/loss mechanism must enter through other means. Madelung's transformation decomposes Schrödinger evolutions into real and imaginary parts [9]. Transforming the NVC yields a system of first-order evolutions on the bending density, $\rho = \kappa^2 = |\psi|^2$ and torsion. We find that the total bending across the vortex,

$$\frac{d}{dt}\int_a^b \kappa^2\, ds = -2\lambda \int_a^b \rho_s \rho\tau\, ds, \tag{4.5}$$

is no longer conserved in time. The density, $\rho\tau$, corresponds to the momentum density in the condensate picture, and is also not conserved by the NCV. This non-Hamiltonian geometric gain/loss mechanism provides a pathway for dissipative soliton dynamics. For example, if the torsion is positive, then bending energy grows/decays over regions where curvature is decreasing/increasing. Simulations indicate that this feature is robust against distortions manifesting from plane wave dispersion.

A plane wave solution of the form $\psi = Ae^{i(ks-\omega t)}$ defines a single mode helix. According to the NVC, plane waves obey the corrected nonlinear dispersion relation [197],

$$\omega(k, A, \lambda) = k^2(1 + \lambda A^2) - \frac{A^2}{2} - \frac{3\lambda}{4}A^4. \tag{4.6}$$

The initial state, $\psi = 2\text{sech}(s)e^{is}$, corresponds to a Hasimoto soliton, and defines a narrow-band curvature packet with over 99% of its total initial bending captured between wave numbers $k \in [0, 5]$. Relating the wave amplitude, A, to wavenumber via Fourier transform allows us to plot the group velocity for the initial data, which is given in Figure 5.3. These data show that increasing λ enhances the propagation speed of long wavelength curvature modes. Enhancing dispersion of these modes causes the curvature function to distort. Simulations indicate that the peak jettisons curvature, which causes the first moment of the distribution to propagate faster, distorting the distribution into a log-normal form. Additionally, the simulations depict a localized curvature peak that stays discernible under considerable dispersion because of the support provided by the emergent gain/loss mechanism. If total bending were conserved, then the dynamic would cause the peak amplitude to erode completely into the vortex.

Our non-Hamiltonian vortex dynamics can be simulated through the vector evolution equation, Eq. (4.1), on a mesh of points representing the vortex in $\mathbb{R}^3$, or by scalar evolution of the geometric variables through the NVC. In this way the Hasimoto transformation effectively separates the geometric evolution from its Frenet-Serret representation and is significantly more efficient if vortex visualization is not required. It should be noted that the boundary conditions for each problem are physically different. Specifically, for an arc-length variable $s \in [a, b]$, Dirichlet boundary conditions, $\psi(a, t) = \psi(b, t) = 0$, allow for moving endpoints with zero curvature. In contrast, Dirichlet conditions on the vector evolution fix the endpoints, $\vec{\gamma}(a, t) = \vec{\gamma}_a$ and $\vec{\gamma}(b, t) = \vec{\gamma}_b$ where $\vec{\gamma}_a, \vec{\gamma}_b \in \mathbb{R}^3$. To suppresses differences manifesting from the endpoint behavior, we simulate Hasimoto's soliton under both the vector and scalar evolutions on an arc-length domain an order of magnitude larger than the characteristic

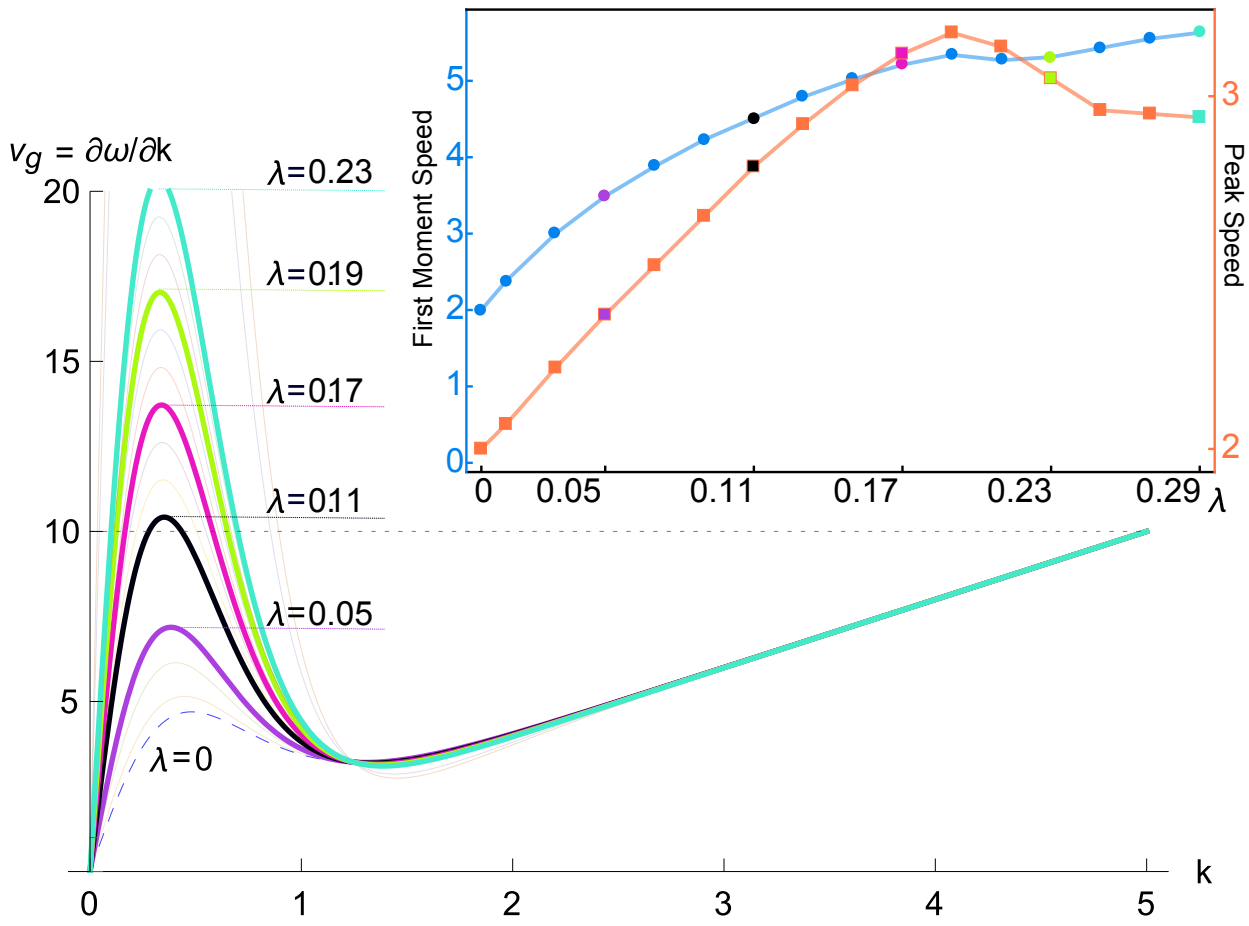

Figure 4.3: Dispersion of Hasimoto's Soliton. The non-Hamiltonian evolution enhances to group velocity of the long wavelength modes in an initial soliton state. The speed of the curvature peak and first moment (inset) are increasing functions of λ until roughly $\lambda = 0.19$ where a majority of shape defining Fourier modes leave an eroding peak to bolster the first moment.

width of this curvature disturbance.[3] This is consistent with the modeling context which assumes a fluid of infinite extent implying that the geometric dynamics are isolated from the physical boundary. The total bending was calculated for both methods and found to have less than 1% squared relative error in the curvature across the lifetime of the simulation. Our focus is on simulations where $\lambda = 0.17$, which displays both the dissipative soliton dynamic and dispersive cascade of Kelvin waves predicted by the NVC.

The NVC predicts two qualitatively different dynamical regimes, one characterized by the cascade soliton and the other by strong dispersion of this dissipative soliton. In Figure 4.4 we plot curvature as a density for $\lambda = 0.17$ and we see that the maximum amplitude is strongly localized while the bending energy disperses in the direction of peak propagation. In Figure 4.4a we plot the maximum value, first moment (red) and wave front (yellow), i.e., the furthest point ahead of the peak were $\kappa \approx 2\%$ of the initial peak value are fitted to linear models with square residuals, 0.99999, 0.999198, 0.998574, respectively. Simulations also show the presence of breathing oscillations, seen by the dark side bands to the peak appearing twice. In Figure 4.4c the middle of a one breathing period can be seen as pinch in the curvature function occurring at $t = 15$ and is plotted along with curvatures at $t = 0, 5, 10, 25$, in the co–moving frame. Simulations omitting the $[|\psi|^2\psi]_{ss}$ term exhibit a similar dynamic and indicates that breathing is, in part, a consequence of the quintic nonlinearity. The completion of two breathing oscillations was corroborated with a power–spectrum analysis of the time data. In addition to this breathing, the gain/loss mechanism creates an asymmetry in the curvature profile that when coupled to dispersion leads to a trailing helical wake of low wavenumber curvature modes. The dissipative/cascade soliton corresponds to the peak amplitude following the helical excitations. Additional simulations show that for $\lambda < 0.17$, we see a similar dynamic but the peak is strongly maintained and less curvature is dispersed. For $\lambda > 0.17$, the peak speed begins to decrease as low wavenumber modes shift the curvature

[3] Our simulations utilize the `NDSolve` routine of Mathematica, set to work at 10 digits of internal precision and interpolating at the order of the underlying method chosen to numerically integrate the system of ordinary differential equations arrived at by application of the method of lines.

distribution to a log-normal form. While the curvature peak is discernible, it is difficult to spot immersed in a sea of Kelvin waves. Additionally, the breathing is abated on the simulated time scale. If a condensate is punctured by a vortex defect with circulation $997 \times 10^{-4} \mu\text{m} \cdot \text{cm}$, length 100μm and core size of 0.67μm, then for an vortex element whose radius of curvature is 12μm, a reasonable size for a vortex ring, Eq. (4.2) yields a characteristic time scale on the order of milliseconds, which is with the range of times considered in reconnection studies [198, 199].

Understanding that the Biot-Savart integral is a manifestation of the mean-field Gross-Pitaevskii dynamics of the condensate, our beyond local induction model self-consistently describes the dynamics of isolated quantized vortices whose flow is induced at length scales nearing the healing length. While this non-integrable and computationally inexpensive result can be easily added to current filament models [200], it is also a useful symbolic tool for investigation of post-reconnection dynamics where simulations of randomized initial curvature configurations can provide statistical properties associated with the energy spectra of Kelvin wave cascade. While deformations to the vortex profile, resulting in reconnection, are not modeled by Eq. (4.1), one expects that reconnection generates regions of localized curvature where NVC dynamics dominate. Such events are now witnessed in experimental condensates with a few vortex defects [48]. Perhaps through minimally defected flows we can gain greater insight into Onsager's conjectured mechanism of anomalous dissipation, which asserts that weak solutions of inviscid fluid dynamics are not necessarily conservative and that the geometry itself is capable of relaxation by radiating turbulent energy toward the fluid boundaries [67].

In conclusion, we derive a non-Hamiltonian evolution for the curvature and torsion of a quantized vortex that breaks the integrability of the LIA and introduces a helical shock wave on the vortex medium. Such a dynamic is necessary to support the cascade process associated with low temperature quantum turbulence. The shock consists of a leading packet of Kelvin waves dispersed from a dissipative vortex soliton, i.e., a non-Hamiltonian cascade

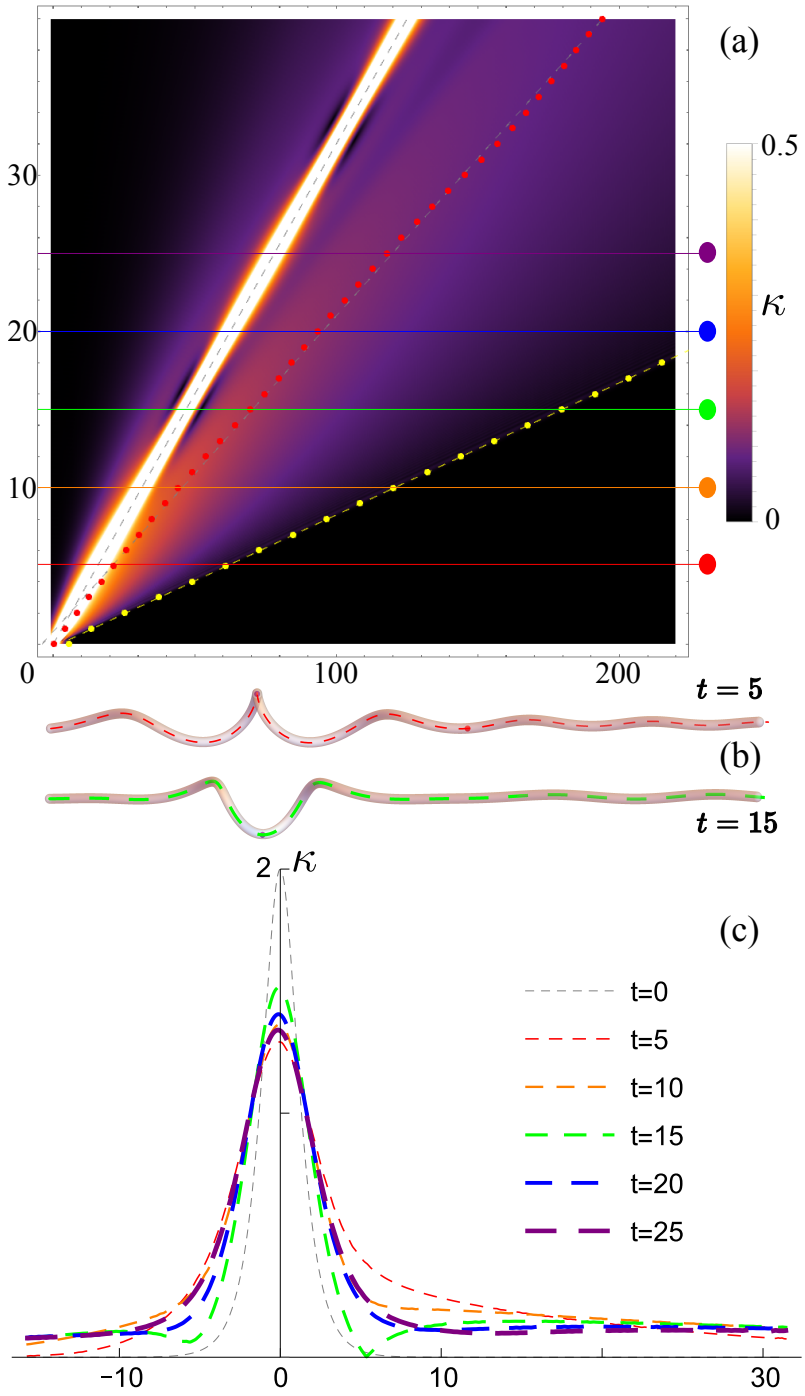

Figure 4.4: Cascade Dynamics. (a) For moderate dispersion the cascade soliton has a well defined peak as it breaths and disperses. The clearly defined peak is tracked along with the first moment (red) and wave front (yellow) on a density plot of curvature. (b) Additionally, we depict vortex configurations at $t = 5$ (orange), $t = 15$ (green) which illustrates the breathing dynamic. (c) Lastly, a sequence of curvatures at five-second intervals are plotted against the initial state, adjusted for translations, and show a clear asymmetry in the profile in addition to the breathing.

soliton.

The authors acknowledge support from the US National Science Foundation under grant numbers PHY-1306638, PHY-1520915, OAC-1740130, and the US Air Force Office of Scientific Research grant number FA9550-14-1-0287. This work was performed in part at the Aspen Center for Physics, which is supported by the US National Science Foundation grant PHY-1607611.

CHAPTER 5

NON-HAMILTONIAN KELVIN WAVE GENERATION ON VORTICES IN BOSE-EINSTEIN CONDENSATES

A paper submitted to *Physical Review Fluids*, arXiv:1803.00147

Scott A. Strong[*], **Lincoln D. Carr**

Department of Physics, Colorado School of Mines, Golden, CO 80401, USA

[*]Primary researcher and author.

.

5.1 Abstract

Ultra-cold quantum turbulence is expected to decay through a cascade of Kelvin waves. These helical excitations couple vorticity to the quantum fluid causing long wavelength phonon fluctuations in a Bose-Einstein condensate. This interaction is hypothesized to be the route to relaxation for turbulent tangles in quantum hydrodynamics. The local induction approximation is the lowest order approximation to the Biot-Savart velocity field induced by a vortex line and, because of its integrability, is thought to prohibit energy transfer by Kelvin waves. Using the Biot-Savart description, we derive a generalization to the local induction approximation which predicts that regions of large curvature can reconfigure themselves as Kelvin wave packets. While this generalization preserves the arclength metric, a quantity conserved under the Eulerian flow of vortex lines, it also introduces a non-Hamiltonian structure on the geometric properties of the vortex line. It is this non-Hamiltonian evolution of curvature and torsion which provides a resolution to the missing Kelvin wave motion. In this work, we derive corrections to the local induction approximation in powers of curvature and state them for utilization in vortex filament methods. Using the Hasimoto transformation, we arrive at a nonlinear integro-differential equation which reduces to a modified nonlinear

Schrödinger type evolution of the curvature and torsion on the vortex line. We show that this modification seeks to disperse localized curvature profiles. At the same time, the non-Hamiltonian break in integrability bolsters the deforming curvature profile and simulations show that this dynamic results in Kelvin wave propagation along the dispersive vortex medium.

5.2 Introduction

Quantized vortex lines provide the simplest scaffolding for three-dimensional fluid turbulence. While vortex lines and filaments are fundamental to quantum fluids, they also appear as the geometric primitives in a variety of hydrodynamic settings including atmospheric, aerodynamic, oceanographic phenomenon and astrophysical plasmas. [201] Through an analogy with the Euler elastica, the twist and writhe of filament structures appear in models of biological soft-matter and are used to explain the dynamics of DNA supercoiling and self-assembly of bacterial fibers. [202–204] Recent research utilizes filaments in less exotic settings where a turbulent un-mixing provides motility to phytoplankton that simultaneously protects them from predation and enhances their seasonal survival. [205, 206] In quantum liquids, turbulent tangles of vorticity are known to undergo various changes of state. Transition to the ultra-cold regime is marked by a subsiding Richardson cascade resulting in a randomized tangle with no discernible large-scale structure. In this state, turbulent energy is driven by vortex-vortex interactions where reconnection events trigger a cascade of wave motion along the lines. When these interactions become infrequent, the turbulence begins to relax to a configuration where the mobile vortices spend most of their time in isolation. In this paper, we show that vortex lines in perfect barotropic fluids seek to transport bending along their length in an effort to disperse localized regions of curvature. In mean-field Bose-Einstein condensates, this dynamic predicts the generation of Kelvin waves which are capable of insonifying the Bose gas, providing a pathway to relaxation of ultra-cold quantum turbulence. [186, 207]

Our result derives from the Hasimoto transformation of the Biot-Savart description of the flow induced by a vortex line. We begin with a natural parameterization of the vortex about

an arbitrary reference point. In this setting, the Biot-Savart integral (BSI) can be calculated exactly, and asymptotic formulae may be applied to get an accurate description of the velocity field in terms of elementary functions. In the analogous setting of electromagnetism, a steady line current plays the role of vorticity and literally induces a field, in this case magnetic, which has a representation given by the BSI. Our analysis yields an induced velocity field generating a vortex dynamic that preserves the Hamiltonian structure associated with the Eulerian flow of vortex lines. Additionally, the velocity field admits a Hasimoto transformation which describes the evolution of vorticity through its curvature and torsion. The geometric dynamics are provided by a nonlinear, non-local integro-differential equation of Schrödinger type that can be reduced to a local differential equation, which is fully nonlinear in powers of curvature. An analytic analysis assisted by symbolic computational tools indicates that higher order contributions reinforce the changes described by the first correction to the lowest order integrable structure. When simulated, we find that regions of localized curvature disperse, causing the production of traveling Kelvin waves. In addition, a gain mechanism emerges to support the dispersion process keeping the helical waves from being absorbed into an otherwise straight vortex line.

The local induction approximation (LIA) is the lowest order truncation of BSI representations of the velocity field induced by a vortex line and is used to describe the local flow about vortex points. The Hasimoto transformation (HT) shows that this is an integrable theory of the curvature and torsion dynamics and, it is argued, incapable of modeling energy transfer through Kelvin waves. It is expected that to elicit Kelvin waves models must undermine or, at least, reallocate the conserved quantities of the flow. There are currently two distinct ways to adapt the LIA to accommodate the study of Kelvin waves. One option is to consider perturbations of the Hasimoto transformation which are known to introduce non-locality and non-integrability into the geometric evolution. [191] This technique can study wave motion on wavelengths much smaller than the radius of curvature and much larger than the core thickness. Here the focus is on kink and hairpin formations in classical vortices capable of

self-stretching. [208, 209] The second method is to consider approximations of the Hamiltonian structure within the LIA and is capable of modeling resonant interactions between Kelvin waves. Currently, there are two derivations of this result which predict cascade features and time scalings arising from the kinetics of Kelvin waves. [59, 210, 211] While the exact source of driven Kelvin wave motion is an open topic [212–214], there is little doubt that vortex plucking through reconnection generates helical wave motion. [215] Our results do not seek to model the inception of localized regions of curvature and are instead focused on how the fluid responds to curved abnormalities on the vortex. Where LIA asserts that the curvature, κ, and torsion, τ, obey a cubic focusing nonlinear Schrödinger equation, both Hamiltonian and integrable, our generalization predicts that the function $\psi = \kappa \mathrm{Exp}[\int_0^s ds' \tau]$ obeys the non-Hamiltonian evolution $i\psi_t + \psi_{ss} + |\psi|^2\psi/2 + [\tilde{\alpha}\psi]_{ss} + f(|\psi|)|\psi|^2\psi = 0$ where $\tilde{\alpha}$ and f are even functions of curvature with related coefficient structures. An evolution is Hamiltonian if it corresponds to a flow induced by a highly structured vector field. For a completely integrable evolution, one has the ability to utilize linearizations throughout the phase space of solutions associated with a Hamiltonian evolution. The relationship between the flow and the vector field inducing it demands that the operator of the Hamiltonian evolution be self-adjoint. Our modified evolution is incapable of supporting such a structure and is, consequently, non-Hamiltonian. Moreover, its fully nonlinear correction allows for energy transfer between helical modes of the vortex line, which significantly alters the evolution of the solitons predicted by the LIA.

The body of this paper is organized into three sections. First, in Sec. (5.3), we derive an exact expression for the BSI representation of the velocity field induced by a vortex line which requires the use of incomplete elliptic integrals. Application of asymptotic formulae makes accessible an expansion of the field in powers of curvature. The coefficients in this expansion depend on the characteristic arclength in ratio with the vortex core size and can be tuned to numerical meshes used in vortex filament methods. Second, in Sec. (5.4), we apply the Hasimoto transform to describe the effect of the vector evolution in terms of the

curvature and torsion. We show that the corrected dynamic is non-Hamiltonian and allows for helical wave dispersion supported by a gain mechanism. Lastly, we simulate the evolution of soliton, breathing, and ring dynamics. Specifically, we consider the bright curvature soliton that produces Hasimoto's vortex soliton and find that at various degrees of non-Hamiltonian correction the corrective terms seek to disperse bending in the form of helical wave generation along the vortex line. After this we consider breathing and ring states to find that the intuition given by changes to Hasimoto's soliton carries over and that both cases breakdown into helical wave motions. A notable example is that of a helically perturbed vortex ring which experiences far less dispersive deformation and, in this way, appears stable under simulation.

5.3 The Biot-Savart Integral and Local Induction Models

The special orthogonal group acts to transform real three-dimensional space by committing rigid rotations about a specific axis which is given by the curl operator. [64] If we define the instantaneous velocity of a fluid continuum over this spatial domain, then curl represents the axis about which a fluid element rotates. Curves that are parallel to the vorticity vector are called vortex lines. [83] A vortex filament is the idealization of a vortex tube whose dynamics are characterized by the behavior of the vortex line. The Biot-Savart integral (BSI) is frequently used to model line and filament dynamics which ignore transverse variations to the vortex core. The BSI provides the unique velocity field such that $\nabla \times \boldsymbol{v} = \boldsymbol{\omega}$ defines the vorticity [216, 217] and can be thought of as the unique left-inverse of the curl operator. [218, 219] In accordance with Helmholtz decomposition of $\mathbb{R}^3$, the BSI treats the velocity field as being sourced by vortical elements convolved with Poisson's formula for the Green's function of a stream reformulation of the hydrodynamic problem. [201, 220] If the evolution of the vortex is given by the Euler equations, then it is known to be arclength conserving Hamiltonian flow and, in this case, the Biot-Savart volume integral reduces to an integral over the vortex line. [221] An isolated vortex line is depicted in Figure 5.1a and can be defined distributionally for a vortex with homogeneous vorticity density, Ω,

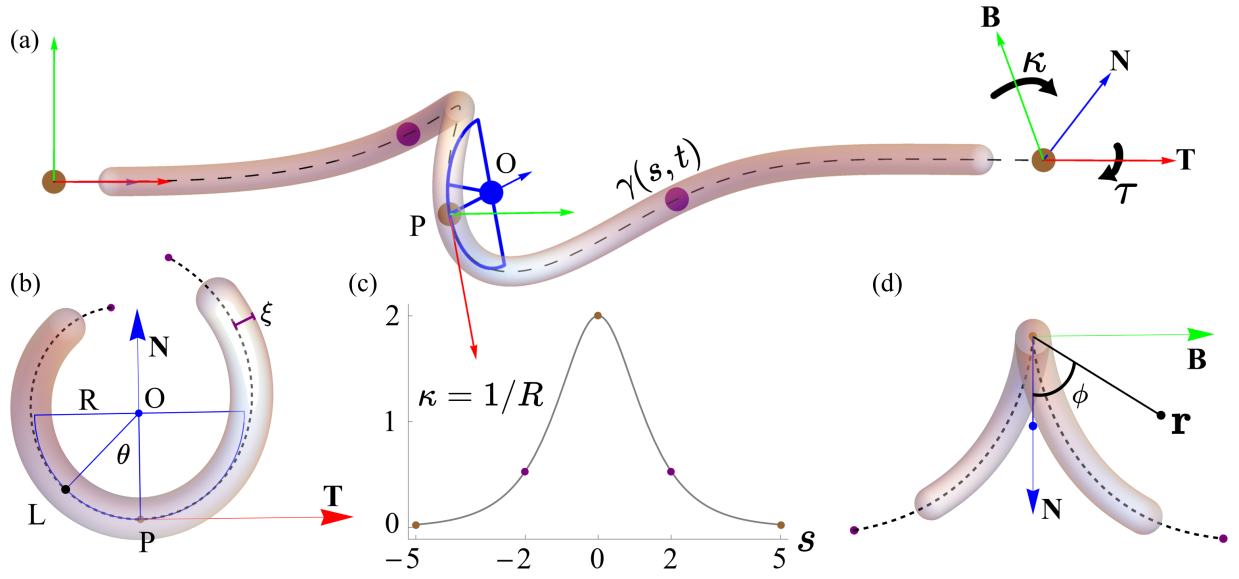

Figure 5.1: Vortex Line Geometry. (a) The local orthogonal frame, tangent (red, $\mathbf{T}$), normal (blue, $\mathbf{N}$) and binormal (green, $\mathbf{B}$) vectors, at the initial, middle and terminal points (brown) of the vortex line, $\boldsymbol{\gamma}(s,t)$, with embellished width. At the reference point P we have a local description of the vortex given by a blue semi-circle. Changes to the Frenet frame from point to point are described by the curvature, κ, and torsion, τ. (b) View down the long axis of $\boldsymbol{\gamma}$ where we see the osculating plane spanned by the tangent and normal vectors. The local geometry at P is defined by the radius of curvature R, which is related to the curvature by $\kappa = R^{-1}$. The angle θ sweeps out an arclength from 0 to L providing a local parameterization to $\boldsymbol{\gamma}$ about P. The core scale is defined as ξ; in Bose-Einstein condensates taken as the superfluid healing length. (c) The curvature distribution associated with the vortex line in (a) with unit torsion. (d) The normal plane is spanned by $\mathbf{N}$ and $\mathbf{B}$, with observation point, $\mathbf{r} = (0, x_2, x_3)$, placed in this plane and defined by the polar angle ϕ.

$$\boldsymbol{\omega}(\mathbf{r},t) = \Omega \int_0^L \delta(\mathbf{r} - \boldsymbol{\gamma})\, d\boldsymbol{\gamma}, \tag{5.1}$$

where $\boldsymbol{\gamma} : (0, L) \times \mathbb{R}^+ \to \mathbb{R}$, is the dynamic parametric representation of the one-dimensional sub-region on which the vorticity is supported. [201] Additionally, if $\boldsymbol{\gamma} = \boldsymbol{\gamma}(s,t)$ is parameterized in the natural gauge, then $\mathbf{T} = \boldsymbol{\gamma}_s$ is the unit-tangent vector. [222] Such a distribution of vorticity reduces the BSI to an integral over the vortex line,

$$\boldsymbol{v}(\mathbf{r},t)=\frac{1}{4\pi}\iiint_{\mathbb{R}^3}\frac{\boldsymbol{\omega}(\boldsymbol{y},t)\times(\mathbf{r}-\boldsymbol{y})}{|\mathbf{r}-\boldsymbol{y}|^3}d\boldsymbol{y}=-\frac{\Gamma}{4\pi}\int_0^L\frac{(\mathbf{r}-\boldsymbol{\gamma})\times d\boldsymbol{\gamma}}{|\mathbf{r}-\boldsymbol{\gamma}^3|}, \tag{5.2}$$

where the circulation/strength Γ is the product of Ω and the characteristic volume resulting from the ideal concentration of vorticity to $\boldsymbol{\gamma}$, and $\mathbf{r}$ is the location at which the velocity field is observed in the normal plane,Figure 5.1d. In the context of electromagnetism, the velocity field plays the role of the magnetic field induced by a steady charge concentrated on the line, $\boldsymbol{\gamma}$. Analogous to problems in electromagnetism, the BSI diverges on the vortex line which is an ideally localized source of the ambient velocity field. We seek to characterize the flow predicted by Eq. (5.2). To arrive at a beyond leading order asymptotic representation of the flow induced by the vortex, multiple layers of analytic work will be needed. To assist the reader we provide an overview of the process.

The analysis which we apply to Eq. (5.2) is as follows. After stating a parameterization for $\boldsymbol{\gamma}$ one must consider field points asymptotically close to the vortex line with $|\mathbf{r}|$ on the order of vortex core size defined by ξ, see Figure 5.1b. Since the field diverges at the vortex source, we must regularize the BSI which is tantamount to eliminating high frequency oscillations along the vortex. The local induction approximation (LIA) is the reduction of BSI to its logarithmic singularity. A classic treatment can be found in Batchelor [220] who derives the result by formally setting the ratio of the observation point magnitude, $|\mathbf{r}|$, with the local radius of curvature, R, to zero. While this is the most expedient route to the lowest order kinematics, it quickly loses accuracy at moments where the local curvature becomes large, see Figure 5.2a. While our exact elliptic representation of the regularized BSI can certainly resolve the field at moments of large curvature, they obstruct our understanding of primitive wave motions along the vortex understood through Hasimoto's transform. Thus, we apply asymptotic approximations to the exact field to get simpler representations in powers of curvature. Moments of large curvature are a consequence of vortex-vortex interactions leading to tent/cusp like formations and, when pushed far enough, reconnection. In LIA

the ratio of arclength to vortex core radius is required to be large, $L \gg |\mathbf{r}| \sim \xi$, which is incompatible with reconnection where the vorticity local to the event drives the dynamics. We now correct LIA so that we can describe the dynamics in this regime of interest.

The dynamics nearing reconnection remain unresolved by LIA, and we seek to rectify this issue by retaining curvature dependence in the BSI integrand. While our approximation recovers LIA in the standard limit, it also allows for an interplay between the characteristic length scales of curvature, arclength and core size that is forbidden by LIA and allows for accuracy in scenarios applicable to modeling wave motions post-reconnection. The end result will be that the speed of the local velocity field is given by $|\boldsymbol{v}| \propto \alpha(\kappa)$, where

$$\alpha(\kappa) = \sum_{n=0}^{\infty} a_{2n}\kappa^{2n}, \tag{5.3}$$

such that restricting the series to a_0 results in the LIA. Prior to regularization and asymptotic approximation we extract the divergent component of BSI. First, we restrict the parameterization of the vortex line at an arbitrary point, P, in the osculating plane, see Figure 5.1b, and consider only the binormal component of the local velocity field to get

$$v_3(\mathbf{r}) \propto \int_0^L \frac{\epsilon_{3jk}(x_j - \gamma_j)d\boldsymbol{\gamma}_k}{|\mathbf{r}-\boldsymbol{\gamma}|^3} = -x_2\int_0^L \frac{\gamma_1'}{|\mathbf{r}-\boldsymbol{\gamma}|^3}\,ds + \int_0^L \frac{\gamma_2\gamma_1' - \gamma_1\gamma_2'}{|\mathbf{r}-\boldsymbol{\gamma}|^3}\,ds, \tag{5.4}$$

where we have made use of the Levi-Civita permutation tensor, ϵ_{ijk}, in conjunction with the Einstein summation convention to compute the cross-product integrand in terms of the components of the parameterization, $\boldsymbol{\gamma} = (\gamma_1, \gamma_2, 0)$ and their first partials with respect to arclength, $\partial_s\boldsymbol{\gamma} = (\gamma_1', \gamma_2', 0)$. Additionally, we may omit the first component in the location of the observer, $\mathbf{r} = (0, x_2, x_3)$, who is restricted to the normal plane, see Figure 5.1d. A quick computation of v_2 reveals the circulatory counterpart to the x_2 term of the velocity field. Thus, the last term in Eq. (5.4) defines a non-circulatory binormal flow, which is understood as a non-stretching dynamic capable of producing geometric alterations to the vortex line.

To derive a locally induced flow from Eq. (5.4) one must consider field points asymptotically close to the vortex line and also regularize the divergence by excising a portion of the vortex line neighboring the reference point. The length of the excised domain of integration in Eq. (5.4) is often decided in an ad hoc manner. [223] However, the recent work of Bustamante and Nazarenko provides a regularization cutoff consistent with the mean field vortices of a Bose-Einstein condensate. [63] To make use of this we specify a parameterization of the vortex line local to the reference point and explicitly process the binormal flow in Eq. (5.4). In generalization to Batchelor's work [220], we consider a dynamic element of vorticity given by $\boldsymbol{\gamma}(s,t) = (R\sin(\kappa s), R - R\cos(\kappa s), 0)$ where $\kappa^{-1} = R = R(s,t)$ and $\kappa s = \theta \in (-\pi, \pi)$, see Figure 5.1b, whose quadratic approximation is consistent with the parameterization given in [220]. In either case, the exact representation of the induced field is given in terms of incomplete elliptic integrals. Since our derivation relies on differentiation of the integral with respect to an internal parameter, elliptic integrals of both first and second kind appear. [60] Integrating the final term in Eq. (5.4) over the angle θ, which is related to arclength by $s = R\theta$, gives the following representation for the binormal flow induced by a plane circular arc,

$$\boldsymbol{v}_{\mathbf{B}} = -\frac{\Gamma\kappa}{4\pi}\int_0^L \frac{\cos(\theta)-1}{(c_1 + c_2\cos(\theta))^{3/2}}\,d\theta, \quad c_1 = \epsilon^2 - 2\epsilon\cos(\phi) + 2, \quad c_2 = 2\epsilon\cos(\phi) - 2, \quad (5.5)$$

where ϕ is the polar angle of the field point in the normal plane, see Figure 5.1d, and $\epsilon = |\boldsymbol{r}|\kappa$ is the product of the distance of the field point and the local curvature. Except at moments of reconnection where cusps form on the vortex line, this parameter is small, though not formally zero as in Batchelor's derivation. As was perhaps first witnessed with the theory of boundary layers, the predictions in the asymptotic regime of $\epsilon \to 0$ differ significantly from those stemming from $\epsilon = 0$, which prohibits the existence of large curvatures. The corresponding indefinite integral can be evaluated to the form

$$\int \frac{\cos(\theta)-1}{(c_1+c_2\cos(\theta))^{3/2}}\,d\theta = F\,C_- - E\,C_+ + \frac{c_2\sin(\theta)}{c_2(c_1-c_2)\sqrt{c_1+c_2\cos(\theta)}} \tag{5.6}$$

where

$$F = F\left(\frac{\theta}{2}\middle|\,\frac{2c_2}{c_1+c_2}\right), \tag{5.7}$$

$$E = E\left(\frac{\theta}{2}\middle|\,\frac{2c_2}{c_1+c_2}\right), \tag{5.8}$$

$$C_\mp = \frac{2(c_1\mp c_2)\sqrt{\dfrac{c_1+c_2\cos(\theta)}{c_1+c_2}}}{c_2(c_1-c_2)\sqrt{c_1+c_2\cos(\theta)}}. \tag{5.9}$$

Here we have used the traditional notation for the elliptic integrals native to Mathematica, which are related to the standard notations by $F(z,m) = F(z|m^2)$ and $E(z,m) = E(z|m^2) = \int_0^z \sqrt{1-m^2\sin^2(t)}dt$. Of the terms in Eq. (5.6), only the first is divergent as $\epsilon \to 0$. There are various asymptotic formulae for elliptic integrals. [224] The result of Karp and Sitnik was found to be more accurate than the prior result of Carlson and Gustafson, in the sense of average absolute and relative errors, over a wider range of parameters. [225, 226] As $\epsilon \to 0$, the Karp and Sitnik representation of the divergent term in Eq. (5.6) is given by

$$F\left(\frac{\theta}{2}\middle|\,\frac{2c_2}{c_1+c_2}\right)C_- \sim \mathcal{A}\left[\ln\left(\frac{\epsilon\sin(\theta/2)}{\sin(\theta/2)\sqrt{A_3}+\sqrt{A_2}}\right) - \frac{2A_3}{\sqrt{A_2}\sin(\theta/2)}\ln\left(\frac{\sqrt{4A_1}}{\sqrt{A_1}+2}\right)\right], \tag{5.10}$$

where

$$A_1 = \cos(\theta)+1, \tag{5.11}$$

$$A_2 = c_2\cos(\theta) - c_1, \tag{5.12}$$

$$A_3 = 2c_1 - \epsilon^2, \tag{5.13}$$

$$D_1 = A_3(A_3-c_1)/2, \tag{5.14}$$

$$\mathcal{A} = \frac{A_2}{2D_1A_3^{3/2}}. \tag{5.15}$$

Comparing this approximation to the elliptic form gives an average absolute and relative error of less than 1.5% over the parameter domain $(\epsilon, \theta) \in (0, 1) \times (10^{-9}, \pi)$, which gets significantly better away from the boundaries in θ and away from the upper bound in ϵ. Noting that as $\epsilon \to 0$, $c_1 \sim 2$, $c_2 \sim -2$, $A_2 \sim -2A_1$ and $A_3 \sim 4$, implies the divergence manifests from the $\ln(\epsilon)$ term in Eq. (5.10). However, discarding the remaining terms in Eq. (5.10) raises both error measures to roughly 30%. Thus, our interest is in how terms other than $\ln(\epsilon)$ temper the divergence away from the singularityand how we can incorporate their effects into our expansion of the field strength as a function of curvature given by Eq. (5.3). However, before we proceed, we must regularize the integral by omitting a portion of vortex neighboring the reference point.

Previously, regularization of the BSI for a vortex line were conducted ad hoc with cutoffs tuned to experimental observation. [227] However, a recent derivation of BSI from the Gross-Pitaevskii (GP) equation, which models mean–field Bose–Einstein condensates, provides an a priori regularization of high-frequency spatial modes. [63] Adapting the results to our parameterization defines a domain of integration, $D = (a\epsilon, \epsilon\delta)$, such that $\pi > \epsilon\delta = \kappa L$ where $a \approx 0.3416293$ and L is the length of half of the symmetric vortex arc. It is important to note that the cutoff parameter, a, of Bustamante and Nazarenko is not phenomenological as in prior regularization techniques. Instead, by reformulating the Hamiltonian structure of the Gross-Pitaevskii equation to be consistent with vortex lines, the authors were able to numerically approximate a cutoff value under the assumption that density fluctuations ceased far from the vortex. Interestingly, their derivation of a self-consistent cutoff relies on incorporating the leading order contributions of quantum pressure and the mean-field potential, in addition to the kinetic term of the Bose-Einstein condensate Hamiltonian. Thus, our generated Kelvin waves arise from a regularization procedure that takes into account a non-trivial portion of vortex core dynamics.

Assisted by Mathematica, we compute the coefficients of a power-series expansion of Eq. (5.10) up through the first twenty terms. Due to the complicated dependence on ϵ,

computation of higher order coefficients requires more sophisticated handling of system memory. Restricting our field observation to the normal plane and averaging over ϕ, we find that the first ten odd coefficients vanish, which is consistent with the symmetry properties of known matched asymptotic expansion. [228] The two-parameter regime, $0 < \epsilon < 0.35$ and $a < \delta < 10$, corresponds to vortex lines whose radius of curvature is up to 35% of the core radius that is integrated from the Bustamante-Nazerenko cutoff through an order of magnitude greater than the core radius. The following regularized two-term approximation has an average absolute error that is roughly 3.1% different than the exact elliptic form,

$$\alpha^* = \int_{a\epsilon}^{\delta\epsilon} \frac{\cos(\theta) - 1}{(c_1 + c_2\cos(\theta))^{3/2}} d\theta \sim a_0 + a_2\epsilon^2, \tag{5.16}$$

$$a_0(\delta, a) = g(a) - g(\delta), \tag{5.17}$$

$$a_2(\delta, a) = \frac{h(a)}{48} - \frac{h(\delta)}{48} + \left(\frac{3}{4}\right)^2 a_0, \tag{5.18}$$

where $g(\eta) = \text{arcsinh}(\eta)$ and $h(\eta) = (\eta^5 - 12\eta^3 - 11\eta)(1+\eta^2)^{-3/2}$. We define α, from Eq. (5.3), by normalizing all coefficients of Eq. (5.16) by a_0. That is, $\alpha = \alpha^*/a_0$.

Prior to taking Hasimoto's transformation, we would like to make sure that our expansion recovers LIA. Also, we would like to understand how well the beyond lowest order LIA terms in Eq. (5.3) approximate the BSI defined by Eq. (5.5). Neglecting the quadratic term and noting that $\text{arcsinh}(\delta) \sim \ln(\delta)$ as $\delta \to \infty$ yields $\alpha^* \sim -\ln(\delta) + O(1)$ That is, from Eq. (5.16) we recover the standard LIA with $\delta = L/|\mathbf{r}|$. In Figure 5.2a we depict the absolute percent error, averaged over $0.1 < \delta < 10$ for the first, second and third corrections as a function of ϵ. Specifically, $\alpha^* \approx a_0$ gives the LIA, while the higher order corrections correspond to $\alpha^* \approx a_0 + a_2\epsilon^2$ (First correction), $\alpha^* \approx a_0 + a_2\epsilon^2 + a_4\epsilon^4$ (Second), and $\alpha^* \approx a_0 + a_2\epsilon^2 + a_4\epsilon^4 + a_6\epsilon^6$ (Third). We see that the terms in Eq. (5.10) tempering the logarithmic singularity significantly improves the lowest order approximation for regions with larger curvature. In Figure 5.2b we provide a logarithmic plot of this error now as a function of δ and averaged over $0.05 < \epsilon < 1$. We see that LIA is an inaccurate approximation of

the binormal speed of the vortex when curvature is large. In Figure 5.2c and Figure 5.2d we plot information about the coefficients in our expansion of the asymptotic representation of the local velocity field. The Domb-Sykes plot [229, 230] in Figure 5.2d shows that we expect a mean radius of convergence for the series of approximately $\epsilon = 0.94$, which is consistent with the assumptions of our approximation. Altogether, we find that the LIA demands the lowest order term dominates the representation and requires the scale separation, $\epsilon \ll \epsilon\delta \ll \delta = L/|\boldsymbol{r}|$ In contrast, our generalized local induction equation permits the study of flows where the scale separation is much less restrictive. Specifically, it requires that the vortex arc has a small central angle, θ, and a radius of curvature bounded by vortex core size,

$$\epsilon\delta < \pi, \tag{5.19}$$

$$\epsilon < 1. \tag{5.20}$$

For a barotropic inviscid fluid, Kelvin's circulation theorem tells us that a vortex line flows as if frozen into the ambient fluid flow. Thus, the contortions it undergoes result from the flow which it induces. Furthermore, if the fluid is incompressible and of infinite extent, then its autonomous dynamics are completely determined by the Biot-Savart integral, which provides a representation of the ambient flow. Since the vortex line inherits the velocity of the fluid background, we have the following evolution law for the vortex,

$$\frac{\partial \boldsymbol{\gamma}}{\partial t} = \frac{\Gamma a_0}{4\pi}\alpha(\kappa)\frac{\partial \boldsymbol{\gamma}}{\partial s} \times \frac{\partial^2 \boldsymbol{\gamma}}{\partial s^2}, \tag{5.21}$$

where $\alpha = \alpha^*/a_0$, given by Eq. (5.16), is even in the curvature variable and $\boldsymbol{\gamma}_s \times \boldsymbol{\gamma}_{ss} = \mathbf{B}$. The local induction approximation is then the linear approximation to α, in κ, where $a_0 = \ln(\delta)$ and the starting point of Hasimoto's mapping. In the next section, we apply this transformation to a generalization of Eq. (5.21) and show that higher order curvature effects break the fragile integrability and allow the vortex medium to support a wider array of nonlinear waves.

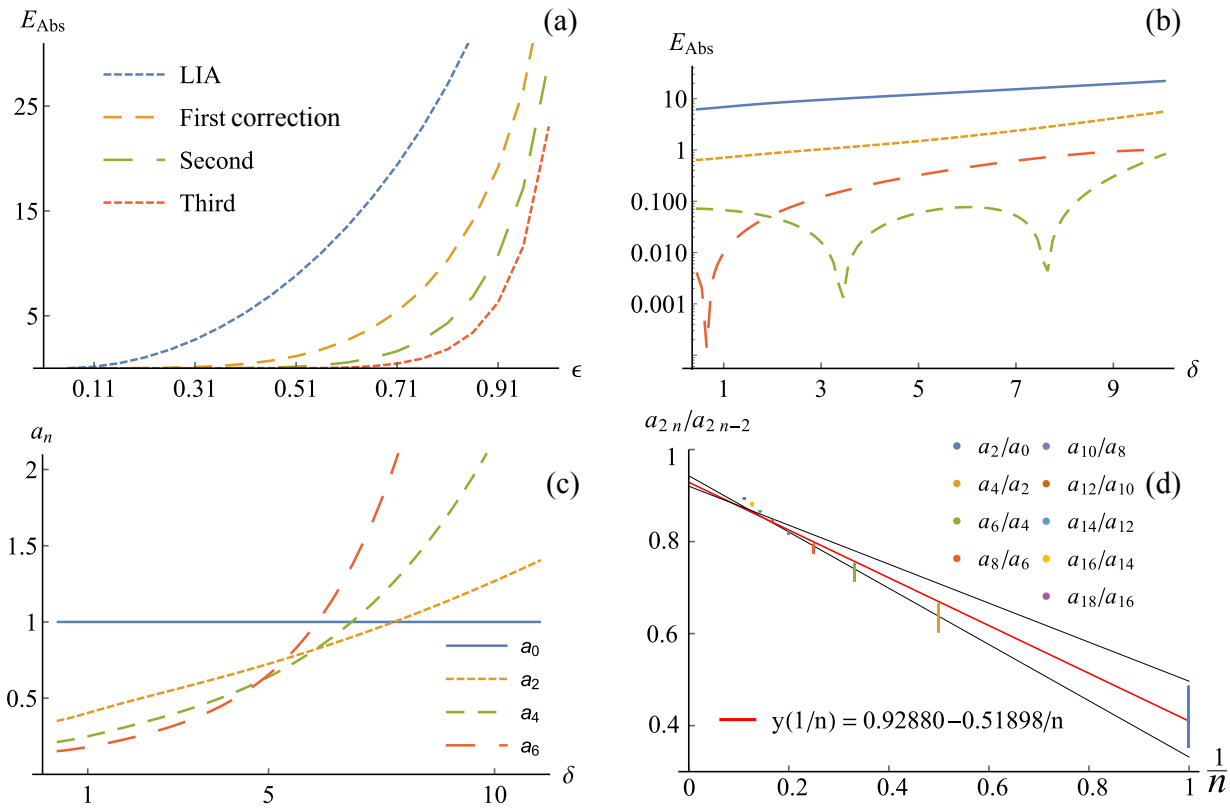

Figure 5.2: Absolute errors and convergence analysis. (a) The average absolute error, E_{Abs}, of LIA and the first, second, and third corrections given by expanding the asymptotic representation of the Biot-Savart integral in powers of curvature. The error is calculated against numerical quadrature converged to six digits of accuracy. While the accuracy improves with higher order corrections, what is noteworthy is how quickly LIA loses its accuracy for large curvature. (b) The error as a function of δ shows that LIA is a generally inaccurate approximation. (c) The first four non-trivial coefficients in our expansion correcting LIA as a function of δ. (d) A Domb-Sykes plot where the data are given by a uniform sampling of the coefficients over $a + 0.01 < \delta < 2$ where a is the Bustamante-Nazarenko cutoff. We see that a_2/a_1 varies the most over this sampling. The data for each δ in the sampling are fitted to linear models with an average square residual of 0.98. The red curve depicts a line whose vertical intercept and slope are given by averaging over the system of linear fits. The resulting vertical intercept predicts a radius of convergence in ϵ of roughly 0.94.

5.4 Hasimoto's Transformation of Binormal Flows

A space curve is defined by how the local tangent, normal and binormal frame, $(\mathbf{T}, \mathbf{N}, \mathbf{B})$, changes between points, see Figure 5.1. The Frenet-Serret equations, in the natural arclength parameterization, is a system of first-order skew-symmetric ordinary differential equations that recovers the local frame based on how a curve fails to be straight (curvature, κ) and planar (torsion, τ) along its arclength. [231] How Eq. (5.21) affects the global geometry is described by the Hasimoto transformation. [8] The Hasimoto transform is a coordinate change which decouples the evolution of the extrinsic shape defined by the parametric curve from its intrinsic curvature and torsion, with the Frenet-Serret equations acting as the intermediary. The modern perspective is that the Hasimoto transform is a scalar manifestation of the Madelung transformation, which is the inversion of volume preserving mappings from the Euler equation phase space to the projective space of non-vanishing complex functions. [3] In light of Bustamante and Nazarenko's work, the geometric analysis provided by Hasimoto transform applied to BSI flows is formally a study of isolated vortex lines in Bose-Einstein condensates. This analysis also describes Eulerian fluids whose phase space is made topologically distinct from the isotropic state with trivial vorticity through the presence of vortex lines.

The Euler evolution of vortex lines is known to be a Hamiltonian flow of the arclength metric. Shortly after Hasimoto's discovery, it was recognized that the velocity fields defined by LIA were Killing, or arclength preserving, on $\mathbb{R}^3$ and that Hasimoto transform connects them to the sequence of commuting Hamiltonian flows of the integrable cubic focusing nonlinear Schrödinger equation. [232, 233] The Hasimoto evolution complicates itself substantially when perturbing off the Killing structure, leading to a quasilinear integro-differential equation of Schrödinger type, it also produces other mixtures of Schrödinger and Korteweg-de Vries hierarchies. [190, 191, 234] Generalizing LIA in powers of curvature maintains the Killing structure and, consequently, the Hamiltonian of the Euler equations. The cost, however, is that it introduces a non-Hamiltonian evolution to the geometric variables of curvature and torsion. In other words, nonlinear curvature dependent binormal flow is an arclength

preserving non-Hamiltonian flow on the vortex geometry that gives rise to the dispersive bending generation along the vortex.

If the Madelung transformation [9] describes a mean-field Gross-Pitaevskii Bose-Einstein condensate as a perfect and incompressible fluid in which rotation must manifest through circulation about a topological defect known as a vortex line, then the Biot-Savart integral provides its evolution, in the absence of boundary effects. We consider the Hasimoto transformation on a perturbation of our Biot-Savart derived binormal flow, Eq. (5.21),

$$\frac{\partial \boldsymbol{\gamma}}{\partial t} = A\alpha(\kappa)\kappa\mathbf{B} + \mu\boldsymbol{\nu} \tag{5.22}$$

where $A = \Gamma a_0/4\pi$, $\boldsymbol{\nu} \in \mathbb{R}^3$ and $\mu \ll 1$. Perturbations of this form were first considered by Klein and Majda and will be a useful contrast to our result. [191] Specifically, we see that arclength metric preserving modifications of LIA generally result in gain/loss mechanisms. First, however, we express two key quantities in Hasimoto's work that track the frame changes from point to point and through time,

$$\boldsymbol{\aleph}(s,t) = (\mathbf{N}(s,t) + i\mathbf{B}(s,t))e^{i\phi(s,t)}, \tag{5.23}$$
$$\psi(s,t) = \kappa(s,t)\, e^{i\phi(s,t)}, \tag{5.24}$$

which are written in in terms of the dimensionless phase, $\phi(s,t) = \int_0^s ds'\tau(s',t)$. The Hasimoto frame, $(\mathbf{T}, \boldsymbol{\aleph}, \bar{\boldsymbol{\aleph}})$, constitutes an orthogonal coordinate system for $\mathbb{R} \times \mathbb{C}^2$ with respect to the Hermitian inner-product. Our derivation is greatly simplified by using the following modifications of the standard commutator and anti-commutator operators, $[A, B] = A\bar{B} - \bar{A}B$ and $\{A, B\} = A\bar{B} + B\bar{A}$, which takes into account the way complex conjugation, $\bar{\boldsymbol{\aleph}} = (\mathbf{N} - i\mathbf{B})e^{-i\phi}$, appears in our adaptation of Hasimoto's transformation. Additionally, we will use subscript notation to denote partial differentiation, $\partial_s\psi = \psi_s$. The first notable change to Hasimoto's process occurs when trying to express the derivative of Eq. (5.22) in terms of $\boldsymbol{\aleph}$. In Sec. (5.5) we introduce the Frenet-Serret equations, Eq. (5.39). For now, we note that $\mathbf{B}_s = -\tau\mathbf{N}$ which, in conjunction with Eq. (5.22) and the relation $(\boldsymbol{\gamma}_t)_s = \mathbf{T}_t$, gives

$$\mathbf{T}_t = \frac{iA}{2}\left[\eta, \boldsymbol{\aleph}\right] + \mu\boldsymbol{\nu}_s, \quad \eta = \frac{\partial}{\partial s}\left(\alpha\psi\right) = \left(\alpha\psi\right)_s, \tag{5.25}$$

where we have assumed continuity of the second order mixed space-time partial derivatives so that $\partial_{st} = \partial_{ts}$. This alteration affects a critical step in the transformation where two definitions of the mixed partial derivative of $\boldsymbol{\aleph}$ are equated. Specifically, we have the two equations

$$\boldsymbol{\aleph}_{st} = -\psi_t\mathbf{T} - \psi\mathbf{T}_t, \tag{5.26}$$

$$\boldsymbol{\aleph}_{ts} = iR_s\boldsymbol{\aleph} - i\left(R\psi + A\eta_s\right)\mathbf{T} - \frac{iA\eta}{2}\left\{\psi, \boldsymbol{\aleph}\right\}, \tag{5.27}$$

where the first expression derives from the definition of the frame coupled to Eq. (5.25) and the second from the orthogonal decomposition of $\boldsymbol{\aleph}_t$. Projecting out the coefficients using the local tangent gives,

$$i\psi_t + A(\alpha\psi)_{ss} + R\psi + i\psi\mu(\boldsymbol{\nu}\cdot\mathbf{T}) = 0, \tag{5.28}$$

while using the Hasimoto normal vector gives

$$R_s = \frac{A}{2}\left\{\psi, \eta\right\} + \frac{i\mu}{2}\left[\psi, \boldsymbol{\aleph}\right]\cdot\boldsymbol{\nu}_s. \tag{5.29}$$

Letting $\alpha = 1$ implies that $\eta = \psi_s$ and if $\mu = 0$, we have Hasimoto's original transformation where the first-term becomes the exact derivative of $A|\psi|^2/2$. However, after integrating by parts to find R we have that, up to constants of integration, Eq. (5.28) is generally given bythe integro-differential equation,

$$i\psi_t + A(\alpha\psi)_{ss} + \frac{A\psi}{2}\int_0^s \alpha_{s'}|\psi|^2 ds' + \mu\left\{i[(\boldsymbol{\aleph}\cdot\boldsymbol{\nu}_s)_s - \psi\nu_s\cdot\mathbf{T}] + \psi\int_0^s \mathrm{Im}[\psi\bar{\boldsymbol{\aleph}}]\cdot\boldsymbol{\nu}_{s'}\, ds'\right\} = 0. \tag{5.30}$$

As this evolution contains nonlinearities in the highest order derivative, it is fully nonlinear. Additionally, we say that it is of Schrödinger type since $\alpha \to 1$ and $\mu \to 0$ produces the

cubic focusing nonlinear Schrödinger equation consistent with LIA. The terms associated with μ were found to model perturbations whose wavelength was small with respect to the radius of curvature, but long compared to core thickness. Letting $\alpha = 1$ and $\boldsymbol{\nu} = \mu\mathbf{B}$ reduces Eq. (5.30) to a complex Ginzburg-Landau type equation with a torsion driven gain/loss term and shows that even the simplest arclength preserving alteration to LIA is capable of breaking its fragile integrability. Focusing now on ambient flows completely characterized by Eq. (5.21), we let $\mu = 0$ and expand α in powers of curvature to calculate the first integral in Eq. (5.30) explicitly. Doing so, under an appropriate time rescaling, reduces Eq. (5.30) to the fully nonlinear differential equation,

$$i\psi_t + \psi_{ss} + \frac{1}{2}|\psi|^2\psi + (\tilde{\alpha}\psi)_{ss} + f(|\psi|)|\psi|^2\psi = 0, \tag{5.31}$$

such that $\alpha = 1 + \tilde{\alpha}$ and

$$f(|\psi|) = \sum_{n=1}^{\infty} a_{2n}\frac{2n+1}{2n+2}|\psi|^{2n}, \tag{5.32}$$

where a_n are the coefficients in the series Eq. (5.3) defined by the Taylor expansion of Eq. (5.16). Thus, when $\tilde{\alpha} = 0$ we have the LIA, which is an integrable theory on the geometric variables from the Frenet frame. As we will see, any amount of curvature correction to the integrable theory yields a non-Hamiltonian evolution.

Our even expansions of α correct the cubic focusing nonlinear Schrödinger equation of LIA, to fourth order in κ, in the following way

$$i\psi_t + \psi_{ss} + \frac{1}{2}|\psi|^2\psi + a_2\left(\left[|\psi|^2\psi\right]_{ss} + \frac{3}{4}|\psi|^4\psi\right) + a_4\left(\left[|\psi|^4\psi\right]_{ss} + \frac{5}{6}|\psi|^6\psi\right) = 0. \tag{5.33}$$

While the nonlinearities due to powers of $|\psi|$ can adapt to the typical Hamiltonian structure of the integrable theory, the fully nonlinear derivative terms cannot. Specifically, the question of whether the Hermitian inner-product on the Hilbert space of complex-valued square integrable functions on the real line induces a symplectic form such that one can identify

a self-adjoint Hamiltonian whose variational derivative defines a Hamiltonian vector field consistent with Eq. (5.33) has a negative answer. [235] Consequently, Noether's theorem is inapplicable and known symmetries need not generate conserved quantities. [236] Our inability to formulate Eq. (5.33) as an infinite-dimensional Hamiltonian flow is rooted to the fully nonlinear derivative terms . Considering a smooth compactly supported perturbation, $\varepsilon\xi$, of the fully nonlinear derivative term, $(|\psi|^2\psi)_{ss}$ we find the linearization,

$$\left(|\psi+\varepsilon\xi|^2(\psi+\varepsilon\xi)\right)_{ss} = \left(|\psi|^2\psi\right)_{ss} + \varepsilon\left(2|\psi|^2\xi+\bar{\xi}\psi^2\right)_{ss} + O(\varepsilon^2). \tag{5.34}$$

Assuming a smooth compactly supported perturbation and test function u the functional given by the induced symplectic form yields [237]

$$\int \bar{u}\left[2|\psi|^2\xi+\bar{\xi}\psi^2\right]_{ss} ds = \int \bar{\xi}\left[2|\psi|^2 u_{ss}+\bar{u}_{ss}\psi^2\right] ds \neq \int \bar{\xi}\left[2|\psi|^2 u+\bar{u}\psi^2\right]_{ss} ds, \tag{5.35}$$

implying that a formal self-adjointness condition cannot be satisfied. [192] It can be verified that the linear derivative term and higher order power terms obey a Hamiltonian structure. Thus, our break from Hamiltonian structure is due to the full nonlinearity. Though our existing space-time symmetries do not yield the "total energy" and "total momentum" conservation typically associated with Schrödinger evolutions, this does not preclude the existence of conserved quantities nor additional non-obvious symmetries. However, application of the SYM symmetry software package [194] to the a_2 correction of Eq. (5.33) found no additional continuous symmetries. Also, a Mathematica package that symbolically calculates conservation laws found no low-order conserved densities. [195]

While this result speaks to the wholesale loss of Hamiltonian structure that appears as we move away from LIA, it tells us nothing about the wave motions of the vortex line. A useful perspective is given by decomposing the system into its real and imaginary components via Madelung's transformation to get,

$$\frac{\partial}{\partial t}\begin{bmatrix}\rho\\ \tau\end{bmatrix}+\frac{\partial}{\partial s}\begin{bmatrix}2\alpha\rho\tau\\ \left(\alpha\sqrt{\rho}\right)_{ss}/\sqrt{\rho}+f(\rho)\rho+\rho/2-\alpha\tau^2\end{bmatrix}=\begin{bmatrix}-2\alpha_s\rho\tau\\ 0\end{bmatrix}, \tag{5.36}$$

where $\rho=\kappa^2=|\psi|^2$, which we call the bending density. If $\alpha=1$, then $a_2=0$ and we recover the standard hydrodynamic reformulation of cubic focusing NLS, which asserts that ρ is conserved and τ obeys an Euler equation. Furthermore, curves of constant torsion define a Jacobian matrix whose spectrum reveals a single traveling wave solution which is the Hasimoto soliton or its generalization to elliptic representations of soliton trains. [238] The Jabcobian matrix in the general case, or for systems with non-constant torsion, are too complicated to analyze directly and we cannot make an assertion of hyperbolicity for the system. However, this reformulation does highlight the emergence of a source term in the bending density for non-constant α. For compactly supported functions or those with suitable decay, we can integrate the first equation to find that for a segment of vortex line, parameterized by the arclength $s_0<s<s_1$, the total bending obeys

$$\frac{d}{dt}\int_{s_0}^{s_1}\kappa^2 ds=-2\int_{s_0}^{s_1}\alpha_s\rho\tau ds=-2\int_{s_0}^{s_1}(a_2+2a_4\rho+3a_6\rho^2+\cdots)\rho_s\rho\tau ds. \tag{5.37}$$

Given that this non-conservation of the total norm can be traced back to the fully nonlinear term in Eq. (5.33), the previous loss of Hamiltonian structure is, perhaps, not surprising. It is interesting to note that if the coefficients a_n are non-negative, then higher order corrections enter this formula additively and reinforce the gain/loss mechanism supplied by the first correction to LIA. Hasimoto originally considered a class of solitons defined by traveling curvature waves with constant torsion given by, $\kappa=2\tau\text{sech}(\tau(s-ct))$ with $\tau=c/2$, which we refer to Hasimoto vortex solitons. Setting $\tau=1$, we calculate the parenthesis of the last integrand, α_ρ, in Eq. (5.37) and find it to be non-negative, see Figure 5.3a. This implies that, at least initially, the higher order contributions reinforce the gain/loss emergent in the first correction to LIA. Additionally, we plot the integrand, $\alpha_s\rho\tau$, in Fig. (Figure 5.3a) and see that the vortex line should experience curvature gain ahead and loss behind the soliton peak which

is propagating in the positive s direction. If we consider the system as a scalar conservation equation on ρ, for fixed τ, then one can state the approximate characteristic speed as $c = [2\alpha\rho\tau]_\rho = 2\alpha_\rho\rho\tau + 2\alpha\tau$. [239] For $\alpha = 1$, we have the LIA and a predicted speed of $c = 2$ for the Hasimoto vortex soliton. Using our expansion for α provides the new approximate speed, $c = 2\tau(1 + 2a_2\rho + 3a_4\rho^2 + 4a_6\rho^3 + \dots)$. As with Eq. (5.37), we see an additive influence of higher order corrections. In Sec. (5.5) we consider simulations of Hasimoto's vortex soliton under a first correction to LIA. We find that the curvature peak, $\kappa_{\max}$, has a strong linear relationship with the first correction, $\kappa_{\max}(a_2) = 2.02810 - 4.42020a_2$, with a square residual of 0.9929. Using this and a first correction of c we find that the approximation quickly loses its accuracy with greater than a 3% underestimation of the simulated peak speed for a 1% correction strength. The implication is that the dynamics of gain/loss and torsion non-trivially affect the speed of the peak. Additionally, we see that if $\kappa \propto \mathrm{sech}(s)$, then the approximate speed has a Gaussian-like profile which defines a non-convex/concave flux. That is, if the speed of a point on the traveling curvature wave is dependent on the value of curvature at that point, then the associated flux given by the first derivative of the speed with respect to ρ shows that the speeds of points on the curvature distribution are neither strictly increasing nor decreasing functions of curvature. If, for example, the waves were strictly increasing with respect to curvature, then we would expect the soliton profile to undergo a wave steepening dynamic but this is not our case. The simplest analog here is the Buckley-Leverett equation [240] which predicts a shock front followed by a rarefaction wave. In our simulations, one can see a wake of helicity behind the propagating curvature profile. This structure is supported by the gain/loss mechanism which acts to evolve the soliton curvature profile to a step. However, this shock formation is tempered by other dynamics. In particular, there is a gross deformation of the curvature profile due to the nonlinear dispersion of helical/Fourier modes.

A single mode helix, $\psi = \mathcal{A}e^{i(ks-\omega t)}$, which is a Fourier mode of the soliton state, initially obeys the nonlinear dispersion relation [197] associated with Eq. (5.33),

$$\omega(k,\mathcal{A},\lambda) = k^2(1 + a_2\mathcal{A}^2 + a_4\mathcal{A}^4 + a_6\mathcal{A}^6) - \frac{\mathcal{A}^2}{2} - \frac{3}{4}a_2\mathcal{A}^4 - \frac{5}{6}a_4\mathcal{A}^6 - \frac{7}{8}a_6\mathcal{A}^8, \qquad (5.38)$$

where again we see the corrections alter the LIA dispersion relation additively. The Hasimoto vortex soliton given by $\psi = 2\text{sech}(s)e^{is}$ contains 95% of its total Fourier energy contained between wave numbers $k \in [-2, 2]$. In Figure 5.3b we plot the group velocity, where wave amplitude, $\mathcal{A}$, is related to wavenumber k via Fourier transform, for the second correction to LIA. We find that these corrective terms seek to enhance the propagation speed of long wavelength modes, which will cause the initial curvature profile to distort. Thus, together with Eq. (5.37), the a_4 and a_6 corrections reinforce the gain/loss and dispersion mechanisms seen in the a_2 correction, a pattern which we checked holds for the first 10 nontrivial corrections. As we reported in a previous work [61] for a perturbative correction, the original peak can maintain localization even under the enhanced dispersion. Thus, when the kink is discernible, it is reasonable to consider it a dissipative soliton. [196]

5.5 Simulating Binormal Vortex Motion

Together, continuum mechanics, vector analysis,and Helmholtz's and Kelvin's theorems from fluid mechanics assert that the motion of a vortex line is prescribed by the flow of the ambient field in which it is embedded. Past the lowest order approximation, the dynamics are sufficiently complicated to necessitates the use of numerical tools. The previous sections imply two distinct simulation procedures. The first is clear cut and relies on the approximation of solutions to initial-boundary value problems evolved according to an approximation to the vector evolution, Eq. (5.2). With the existence of efficient routines to evaluate incomplete elliptic integrals [241] it appears possible to simulate the binormal evolution outright without approximation, however, such an investigation has never been attempted. Instead people work through the full BSI over an interpolated mesh or approximations via LIA at mesh points. We call simulations stemming from Eq. (5.5), vector simulations and consider first and second corrections to LIA given by Eq. (5.21).

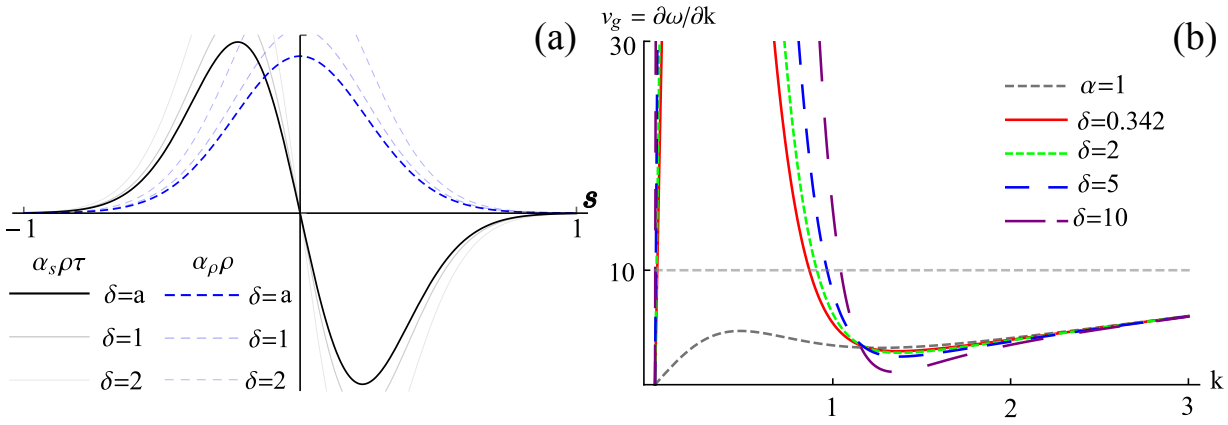

Figure 5.3: Non-Hamiltonian gain/loss and dispersion of helical modes. Corrections to LIA increase/decrease line bending to right/left of a hyperbolic secant curvature profile with higher order corrections reinforcing this effect additively. Also, long wavelength modes propagate faster under correction causing a deformation of the initial curvature profile. (a) The integrand of Eq. (5.37), up through the first ten coefficients, for Hasimoto's vortex soliton (black.) The thinner and lighter black curves indicate how the integrand changes as we increase δ. As we accumulate more vorticity with the Biot-Savart integral, the amplitude of the integrand increases while not distorting the basic shape. In addition, we plot the contribution due to the $\alpha_\rho\rho$ expansion of the integrand and see that the quantity is strictly positive. (b) The dispersion relation for helical modes of the initial state for the second correction. We see that the low wavenumber modes experience an enhanced dispersion, which grows as δ increases.

On the other hand, the Hasimoto transform works by separating the parameterization of the vortex line from the evolution of its intrinsic geometric description given by the curvature and torsion variables. We will call a simulation of the vortex through the geometric variables a Hasimoto simulation. Naturally, this procedure introduces a post-processing step, which reconstructs the curve through the Frenet-Serret equations. [242] Specifically, we must find the tangent vector by solving the following non-autonomous linear system of equations

$$\frac{d}{ds}\begin{bmatrix}\mathbf{T}\\ \mathbf{N}\\ \mathbf{B}\end{bmatrix} = \begin{bmatrix}0 & \kappa & 0\\ -\kappa & 0 & \tau\\ 0 & -\tau & 0\end{bmatrix}\begin{bmatrix}\mathbf{T}\\ \mathbf{N}\\ \mathbf{B}.\end{bmatrix} \tag{5.39}$$

From the tangent vector the curve's parameterization is found. The coefficient matrix in Eq. (5.39) is skew-symmetric and thus an infinitesimal generator of the rotations mapping

the Frenet frame from one point on the vortex line to the next. More importantly, these group elements of $SO(3)$ have spinor representations in the general linear group of two-by-two complex valued matrices under the isometric mapping, $-2x_k = \mathrm{Tr}(X\sigma_k),\ k = 1, 2, 3$, where $X = i(x_1\sigma_z - x_2\sigma_y - x_3\sigma_x)$ are defined through the standard Pauli spin matrices. In this representation, the Frenet-Serret equations are implicitly defined by the lower dimensional form,

$$\frac{dU}{ds} = F(s)U, \quad 2F(s) = \begin{bmatrix} 0 & i\psi/2 \\ i\bar{\psi}/2 & 0 \end{bmatrix}, \tag{5.40}$$

where $\psi = \kappa\,\mathrm{Exp}\left[\int_0^s ds'\tau\right]$ and $U \in \mathbb{C}^{2\times 2}$ such that $\bar{U}^{\mathrm{T}}U = I$, which defines the spinor tangent vector $E_1 = iU^{-1}\sigma_z U$. [222, 243] Interestingly, the spinor representation yields a Frenet-Serret coefficient matrix where the curvature and torsion are cast into the form of Hasimoto's wave function. Thus, the second process is to simulate the evolution of vortex line configurations through Eq. (5.33) and then recover the curve geometry by the application of quadrature to the traced out tangent vector created by the numerical approximation of Eq. (5.40). It is also possible to numerically differentiate rectified phase data to recover the torsion, which can then be used in Eq. (5.39).

We consider the a_2 correction to the evolution of a Hasimoto vortex soliton given by the initial state $\psi(s, 0) = 2\mathrm{sech}(s)e^{is}$. To gain intuition over how a perturbation affects the solitonic evolution, we consider three cases, $a_2 \in \{0.11, 0.19, 0.23\}$. When $a_2 = 0.11$ a small number of low wavenumber curvature modes, 13.40% of the total Fourier energy, begin to propagate faster than those modes responsible for 95% of the total initial bending. At $a_2 = 0.19$, 38.55% of the total Fourier energy is contained in the low wavenumber modes propagating faster than the remaining modes. The final value is chosen so that 47.73% of the initial bending is propagating faster than the remaining modes. Density plots of these three cases are given in Figure 5.4. In each case, we see an asymmetric evolution consistent with the gain/loss mechanism described in Sec. 5.4. We also see that dispersion of low wavenumber modes smears the distribution out. Additionally, the non-Hamiltonian gain mechanism keeps

the peak from being completely eroded by dispersion. For smaller corrections, there is a breathing feature, which causes pockets of small curvature to form tightening the localization of the curvature peak. This feature, which was confirmed with an analysis of the power spectrum, is short-lived under strong dispersion. In Figure 5.5 we depict vortex lines produced from this correction to LIA at $t = 10$. In Figure 5.5a through Figure 5.5c we depict vortex lines corresponding to the density plots in Figure 5.4. The remaining two are the result of higher order correction and we see that the Hasimoto vortex soliton decomposes itself into helical excitations of the vortex line. In light of the way corrections appear additively in speed, bending and dispersion calculations, it is reasonable that the evolution to a Kelvin wave cascade is more profound at higher order.

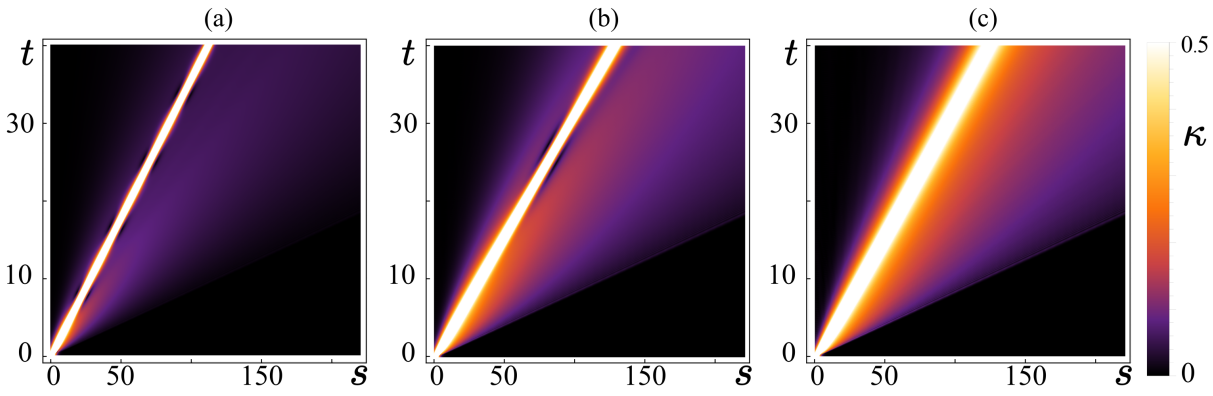

Figure 5.4: Density plots of Hasimoto vortex soliton under first correction. The non-Hamiltonian binormal evolution of the bright soliton state maintains the kink feature despite dispersive deformations to the curvature distribution. (a) Evolution of the initial soliton state for $a_2 = 0.11$ produces a tightly confined peak with limited dispersion to the right. A slight breathing fluctuation is present. (b) The first correction is now $a_2 = 0.19$, and we see increased dispersion and a less frequent but more pronounced breathing dynamic. (c) Lastly, we have $a_2 = 0.23$ and see that under strong dispersion the breathing abates but a propagating peak, supported by the non-Hamiltonian gain mechanism, remains.

Prior to Hayder's work of 2014 [187], a comparison between Hasimoto, vector, and mean-field simulations had not been conducted. His work showed a qualitative agreement between the methods, except at points of reconnection which the mean-field model handled natively. In Figure 5.6) we depict the a_2 correction to LIA, at various strengths, applied to

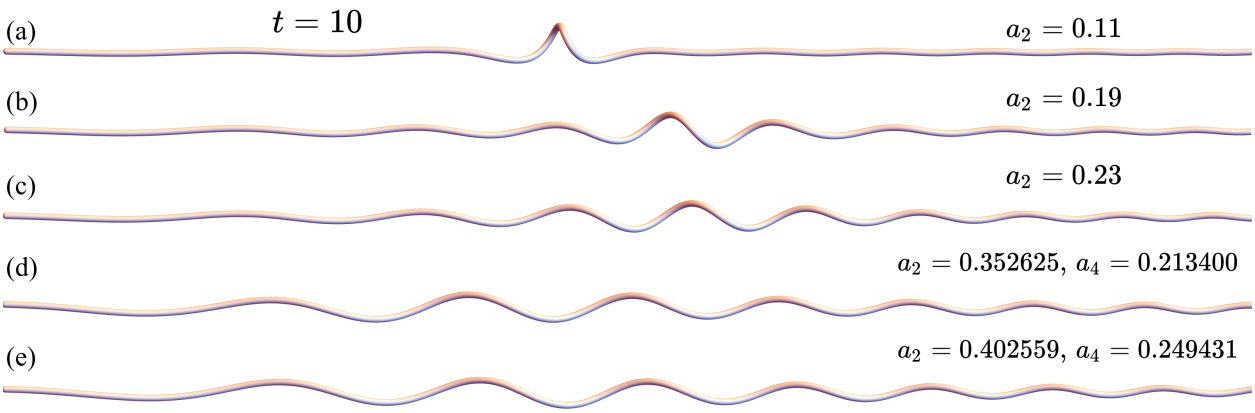

Figure 5.5: Vortex configurations. Subplots (a)-(c) correspond to the evolutions in Figure 5.4 at $t = 10$. We see that the increased dispersion corresponds to Kelvin wave generation, the largest in amplitude of which is an artifact of the original kink. (d) A Hasimoto soliton under the second correction where the coefficients, $a_2 = 0.352625$ and $a_4 = 0.213401$, are chosen so that $\delta \to a$, which represents the smallest length of regularized vortex permitted under the Bustamante-Nazarenko cutoff. The quick decomposition of the soliton into a Kelvin wave cascade pronounced. (e) Hasimoto soliton evolved with $a_2 = 0.402559$ and $a_4 = 0.249431$ which corresponds to $\delta = 1$. We see a minimal change to the dynamics even though $\delta \approx 3a$ indicating the corrections to LIA imply a rapid cascade dynamic.

the Akhmediev breather considered in [187]. We see that the correction not only increases the frequency of breathing, but the dispersion retards the relaxation to a non-peaked state. That the peaks are still maintained through several cycles is due to the non-Hamiltonian gain/loss mechanism. The appearance of small-scale structures, caused by wave interference across the periodic boundary, resulted in inefficient simulations for larger corrections. Using the spinor representation of the Frenet-Serret equations we were able to reconstruct the vortex line and found results consistent with the Hasimoto vortex solitons applied to each loop formed by the twisting and bending of the breathing dynamic. Specifically, the traveling curvature events, emerging from one period of the breathing, jettison helical excitations cascading Kelvin waves away from the regions of highly localized curvature making it impossible to achieve a full exhalation, see Figure 5.6b.

Lastly, we conducted simulations on vortex rings perturbed by Kelvin waves and vortex rings with initially localized out of plane perturbation to a vortex ring, similar to those seen

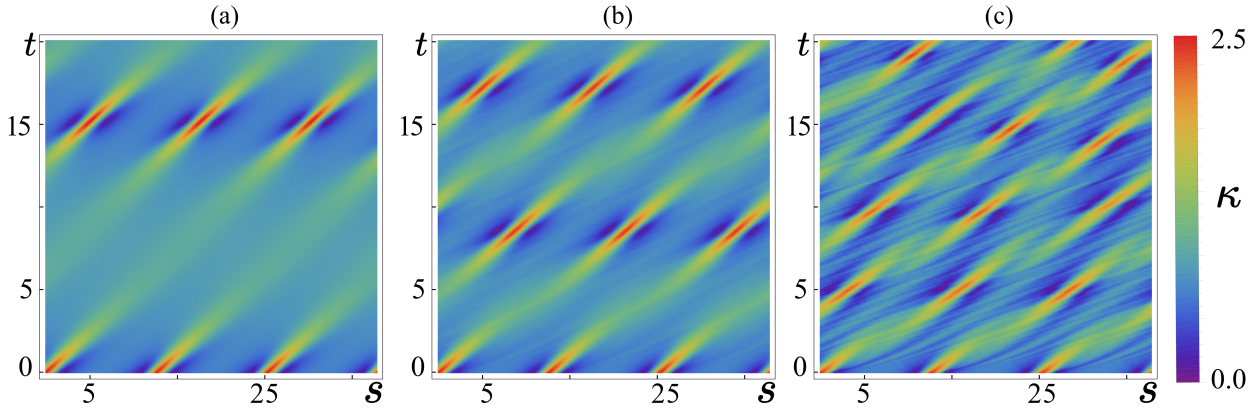

Figure 5.6: Evolution of space-time periodic Akhmediev breather. (a) We plot the LIA evolution of the breather first considered in [187]. (b) The first correction to LIA, where $a_2 = 0.01$, increases the frequency of breathing. (c) Increasing the strength of correction to $a_2 = 0.05$ sees two major changes. First, the frequency of breathing continues to increase with correction strength. Second, the dispersion tends to erode the relatively flat period occurring during one period of breathing.

after reconnection in classical hydrodynamics. Under LIA, perturbed rings oscillated about the plane normal to their direction of motion as the perturbation releases its bending into the ring in the form of smaller amplitude traveling helical waves. Initial testing indicates that the perturbation creates two curvature disturbances that are similar to a Hasimoto soliton traveling around the ring. However, these features were not true soltions and lost their shape as they traveled, even under LIA. A first correction to LIA increased the speed of propagation of the ring and helical decomposition of any kinks formed on the ring, see Figure 5.7. On the other hand, the Kelvin rings which were tested appeared stable under LIA and corrected LIA. Specifically, while the speed of rotation and propagation was enhanced, the shape was relatively un-deformed when compared against LIA. While further testing is necessary, the possible decomposition of perturbations into Kelvin rings may provide stability to closed vortex structures propagating through mean-field simulated BEC.

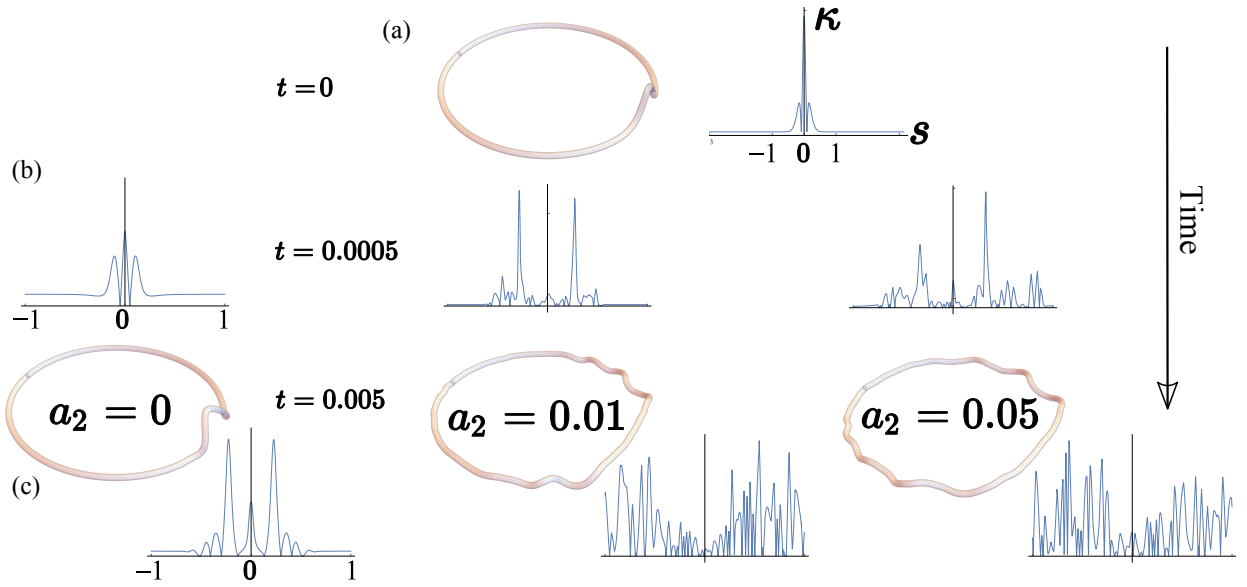

Figure 5.7: Perturbed Rings. (a) A non-planar perturbation on a vortex ring, whose height is one-third of the ring radius, and its curvature profile. (b) Curvature profiles for the three evolutions, LIA where $a_2 = 0$, $a_2 = 0.01$, and $a_2 = 0.05$ at $t = 0.0005$ shows that the perturbation jettisons curved regions away from the initial deformation. (c) Plots of the initial vortex state under LIA and corrections. We see that the corrections greatly increases the speed of the dynamic. For LIA we see the emergence of two curvature peaks propagating away from the initial peak. The corrections produce a similar state in shorter time. Fast moving waves vibrate the ring and cause noise in the curvature distributions. That said, in the vortex shows the existence of two counter propagating kink formations. All of these dynamics seek to distribute the bending along the vortex in a way similar to that which is seen in interacting bubble rings in classical hydrodynamic settings.

5.6 Conclusions

In this paper we presented an integrability breaking modification to the local induction approximation that maintains the arclength preserving Hamiltonian structure of the Eulerian flow induced by a vortex line while enhancing dispersion and introducing a non-Hamiltonian gain/loss mechanism affecting the geometric properties of the vortex medium. This correction allows localized curvature distributions to decompose into Kelvin wave packets. In fact, we derive a hierarchy of non-Hamiltonian vortex cascade evolutions, which limit to an integro-differential equation resulting from the Hasimoto transformation of arbitrary curvature dependent binormal flows defined by the Biot-Savart representation of the velocity field

induced by a vortex line. While we are unable to prove positivity in the coefficient structure of our expansion, which is an open and hard mathematical problem, the first ten non-trivial coefficients do not contradict this conjecture and a Domb-Sykes analysis predicts a radius of curvature for our expansion which is consistent with the assumptions of our derivation. If the coefficients are positive to all orders, then the higher order terms in the asymptotic expansion of the local field additively reinforce the emergent non-Hamiltonian dynamics given by the first correction to the lowest order integrable theory. In other words, all curvature driven non-stretching Eulerian evolutions of vortex lines seek to disperse locally bent regions by the generation of helical waves.

The coefficient formulae depend on the characteristic length scales defined by arclength, vortex core size and local curvature and are ready for integration into established vortex filament methods. [200] These methods are used to simulate quantum fluids with a dense arrangement of quantized vortices and gain efficiency by approximation of the Biot-Savart integral with locally induced flows. They result in qualitatively similar dynamics for systems where vortex-vortex and self-interaction is weak. [187] When these dynamics dominate the flow, mean-field models that take into account additional physics of the vortex core must be included. That said, our analysis is appropriate for flows induced by lengths of vorticity nearing these scales and may represent as far a regulated Biot-Savart line integral can take the model into a core structure. With the emergence of experiments at both larger[4] and small scales, focused on tangle behavior and primitive vortex interactions [48], the importance of efficient multi-scale models for quantum turbulence is clear. [200]

Preliminary analysis and simulations show that local but non-integrable induction models permit the excitation of Kelvin waves and indicate that a vortex line may attempt to find stability by storing bending in helical coils arrived at by a curvature cascade. It is expected that this energy transfer process couples to the fluid so that the bending can be relaxed through long wavelength acoustic fluctuations of the mass density. Incorporation of this

[4]Mark Raizen, UT Austin, private communication (2017)

effect into the geometric picture supports a connection between geometric hydrodynamics and the analysis of anomalous dissipation conjectured by Onsager. [67, 244, 245] The current understanding is that classical Navier-Stokes solutions exhibiting anomalous kinetic energy dissipation in the inviscid limit correspond to weak Euler solutions, the singular fields defined by vortex lines being one such example. [246] Furthermore, this mechanism is expected to be non-existent above a certain degree of solution regularity. The Biot-Savart perspective may be compatible with the regularity analysis associated with Onsager's conjecture and provide a geometric connection between anomalous dissipation and the relaxation of ultracold quantum turbulence observable through the wave motion of the vortical substructure.

A less theoretical application can be found in the recent high-resolution imaging of vortex ring breakdown where a self-similar decomposition of toroidal rings into vortex filaments occurs and is very much in the spirit of the predictions of Richardson and da Vinci. High-speed and high-resolution imagery [247] shows that interactions leading to tent formations [248, 249] and the flattening of tubes leads to filament generation at fine scales. In other words, the smoke we see as classical rings collide hides a discernible vortical skeleton comprised of bent filaments. At the finest scales, vortex lines should be the most appropriate model for the dynamics of the bent classical filaments and offer an opportunity to provide experimental corroboration of line models. In a similar thread, recent experiments seek to induce vortex line interactions in Bose-Einstein condensates whose vortical structure is not dense. [48] This offers the clearest picture of vortex line dynamics, post tent formation and will certainly be an important apparatus in understanding primitive vortex dynamics. As our understanding of Kelvin wave generation on vortex lines and filaments is still in its early stages, such theoretical/experimental crossovers will be important for the continued development of future theories.

CHAPTER 6

CONCLUSIONS AND OUTLOOK

In this thesis, we develop the geometric quantum hydrodynamic theory of vortex line motion in a Bose-Einstein condensate. In particular, we model the dynamics of an isolated vortex line capable of dispersing localized regions of curvature across the vortex in the form of helical waves. This vortex line is an appropriate model for vortices in superfluid states of matter where helical Kelvin waves are expected to be the generator of long wavelength phonon fluctuations of the density field. For an ultracold turbulent superfluid state, the vorticity forms a tangle of lines whose interactions eventually abate. Kelvin waves coupling the vortex structure to the density field is the proposed agent of energy decay in the quantum tangle. Before this work, the only analytic model for the wave motion on a vortex line was an integrable model that restricted the behavior of helical modes through a rich structure of conservation laws. In this thesis, we have derived a model that supports the transfer of energy between helical modes. Additionally, we connect this geometric analysis into the theoretical context of continuum fluid mechanics. In this way, the desire of a vortex to relax curvature abnormalities into helical structures is seen as a clear and direct realization of Onsager's conjectured dissipation of kinetic energy in the absence of viscosity.

In a quantum tangle, regions of localized curvature manifest through vortex-vortex interactions leading to reconnection which leaves the vortex line with a tented formation and a cusp in the local curvature function. Our new model predicts that perturbations of the simplest flows of a vortex line introduce a non-Hamiltonian gain mechanism working in concert with dispersion to transfer curvature along the line. This mechanism generates helical wavefronts traveling away from the curvature abnormality on the vortex line. Our non-Hamiltonian model derives from a quadratic correction, in the curvature variable, to the well known local induction approximation. This correction can be directly applied to

vortex filament methods. Currently, one way to understand the energy spectrum associated with decay in a quantum tangle is through simulations based on simplified local flows of vortex lines. Another way is to study the statistical properties of Kelvin waves generated by ensembles of random curvature abnormalities on straight vortex lines. The form of the universal power law for a Kelvin wave cascade, similar to the Kolmogorov 5/3 law for the inertial range of a Richardson's cascade, is a topic of recent debate. Our new model is capable of Kelvin wave generation sourced by curvature abnormalities resulting from vortex reconnection and may shed some light on these issues.

In addition to our discovery of a Kelvin wave generation mechanism, we provide a sketch of the connection between vortex line models and continuum fluid mechanics. Specifically, we outline a sequence of results that connects the Navier-Stokes equations to the three-dimensional Gross-Pitaevskii equation, modeling a fully condensed Bose gas, and the Biot-Savart integral representing the velocity induced by a vortex line. To do this, we leverage two recent results. The first stems from mathematical analysts who continue the study of Onsager's conjectured dissipation anomaly. Briefly, in the limit of large Reynolds number, solutions to the Navier-Stokes equation limit to distributional solutions of Euler's equation so that velocity gradients may diverge allowing for dissipation of kinetic energy without the assistance of viscosity. We then derive an inverse Madelung transformation of the Euler equation, resulting in the Gross-Pitaevskii equation for fluids whose mass density spatial variation can be controlled by the corresponding Hamilton-Jacobi equation on the velocity potential. When the body forces and pressure are chosen to be consistent with mean-field averaging and barotropic quantum pressure, then this Gross-Pitaevskii equation corresponds to the evolution of a dilute Bose-Einstein condensate. Lastly, a recent result shows that a vortex line can be mapped onto the Hamiltonian structure of the Gross-Pitaevskii equation resulting in the Biot-Savart integral. The key result of this connection is that the Biot-Savart integral from vector analysis provides the appropriate representation for a vortex line manifesting from a singular velocity field. The velocity field is strongly localized to a core region and defined

single-term approximations to the potential energies associated with the quantum pressure and the effective mean-field potential. Consequently, the generation of Kelvin waves should be thought of as a connection between Onsager's dissipative anomaly and phonon emission in Bose-Einstein condensates.

In the next section, we provide a chapter by chapter overview of the details that lead to this conclusion. The final section is devoted to four possible applications of the techniques in geometric quantum hydrodynamics outlined in this thesis.

6.1 Conclusions

Chapter 1 began with a simple overview of laminar versus turbulent fluid flow and its relationship to Reynolds number through the classic parachute problem modeled as an ordinary differential equation. The mass-spring problem is then introduced in a Lagrangian context leading to Feynman's derivation of Schrödinger's equation. Bose-Einstein condensation is covered and related back to hydrodynamic phenomenon. A direct analogy with electromagnetism is leveraged to conceptualize the geometric principles central to the study of vorticity in this thesis. Before ending with a discussion of the contents of this thesis, we review experimental Bose-Einstein condensates exhibiting vortex motion and conclude with a description of a turbulent quantum tangle.

Chapter 2 provided a basis for geometric quantum hydrodynamics, which is the study of the geometric evolution of the vortex line structures in a quantum fluid. In this chapter, we derived the Navier-Stokes equations. After this we reviewed modern results in turbulence research focused on Onsager's 1949 work on the dissipative anomaly. Currently, the mathematical analysis indicates that solutions to the Navier-Stokes equations limit to distributional solutions to the Euler equations in the large Reynolds number limit. A scaling argument is then used to derive what is essentially the inverse of Madelung's transformation mapping the Euler equations onto the Gross-Pitaevskii equation. Recent results [63] describing how the Gross-Pitaevskii equation can be used to derive the Biot-Savart integral from a vortex solution are outlined and discussed prior to our concluding statements. The remaining chapters described

a derivation of the geometric evolution of isolated vortex lines consistent with an asymptotic analysis of the Biot-Savart integral.

Chapter 3 reprints a paper published in the Journal of Mathematical Physics [60] presenting a derivation of an exact representation of the velocity field induced by a plane circular arc of vorticity in terms of the incomplete elliptic integrals. Additionally, we derived an asymptotic formula for this velocity field for scalings where the core size is small relative to the radius of curvature of the vortex at an arbitrary reference point. This result reduces to the standard local induction approximation when truncated to lowest order, and manifests from the logarithmic singularity present in the incomplete elliptic integral of the first kind. This local representation of the velocity field associated with our Bose-Einstein condensate provides a basis for the geometric analysis covered in the remaining chapters of the thesis body.

Chapter 4 reprints a manuscript under review in Physical Review Letters [61], which outlined the key results associated with an asymptotic analysis of the Biot-Savart integral and its subsequent transformation into a scalar evolution of the intrinsic geometric variables of curvature and torsion on the vortex line. This chapter discussed the emergence of a non-Hamiltonian gain/loss mechanism coupled to an enhanced dispersion relation from corrections to the local induction approximation. Under correction, the evolution of the curvature and torsion allows initially localized curvature distributions to decompose themselves into helical waves along the vortex line. In addition to these analytic predictions, the results of simulations are reported. The derivation of the analytic details and further results from simulations are discussed in the following chapter.

Chapter 5 reprints a manuscript under review in Physical Review Fluids [62], which reported on key details supporting the results of Chapter 4. Specifically, the elliptic forms of Chapter 3 are reintroduced and an asymptotic analysis, aided by symbolic computational tools, is conducted so that the local induction approximation can be corrected in powers of curvature. This representation is then transformed into a scalar evolution of the vortex geometry. The general result is a nonlinear integro-differential equation that reduces to a

fully nonlinear non-Hamiltonian partial differential equation when corrections past local induction are considered. Simulations of vortex solitons, breathing modes, and perturbed vortex rings are considered and it is hypothesized that a vortex line seeks to reallocated localized curvature disturbance into helical waves.

Chapter 6 concludes the thesis by summarizing its contents and reviewing several directions for future work. First, we reintroduce the concept of anomalous dissipation and how the results of this thesis may move what is currently a discussion of mathematical analysis to a more differential geometric flavor. Additionally, we discuss a less technical question about the nature of the helical wave motion. Then, we discuss how our results can be ported over to preexisting vortex filament methods at minimal cost and avenues of understanding the relationship between Kelvin waves and phonon excitations of the gas. Next, we discuss a pathway to study relativistic superfluids that can be found in astrophysical settings such as neutron stars. Lastly, we discuss a relation between the geometric evolution of vortex filaments and the theory of thin elastic rods which appear in biological contexts.

6.2 Outlook

Geometric quantum hydrodynamics provides the basis for understanding the dynamics of vortex lines and connects continuum hydrodynamics to the differential geometry of curves. Consequently, it has a variety of future applications. We would like to briefly touch on four.

We have shown that in the limit of large Reynolds number, the Navier-Stokes equations appear connected to a non-Hamiltonian Kelvin wave generation mechanism. If one were to formalize the connections we have outlined here with the relevant function spaces, then geometric principles could be included in the mathematical analysis of Onsager's conjecture. With this in place, quantum turbulence in a Bose-Einstein condensate could be seen as a realization of Terence Tao's belief in the existence of carefully prepared configurations of Navier-Stokes equations leading to finite time blow up. [250–252] More importantly, this scenario allows for a loss in regularity that would not require the introduction of additional physics external to the models from continuum mechanics.

When viewing the helical decomposition of a region of localized curvature on an otherwise straight vortex, e.g., Figure 5.5, we see a structure akin to a dispersive shock wave which is a region of transition in a nonlinear wave that is bookended by a harmonic oscillation and a solitary wave. The mathematical structure of the wave is described through Whitham's nonlinear averaging principle, which assumes the existence of an asymptotic representation of a traveling wave whose amplitude, frequency and mean experience a slow modulation over a region encompassing many oscillations. [253] Even though there is numerical evidence to support the existence of dispersive shock waves in non-integrable systems, the theory can only guarantee the evolution of discontinuous data into a shock when leveraging the heightened structure found in integrable systems. Our structure is a helical wavefront followed by a dissipative soliton predicted by a non-Hamiltonian evolution of the geometric properties of the vortex line. As the Gross-Pitaevskii equation is known to admit dispersive shock waves, there is a reason to think a vortex line manifestation is possible. However, to understand whether the Kelvin wave decomposition of a region of localized curvature constitutes a dispersive shock wave requires the application of Whitman's theory to our geometric quantum hydrodynamic formalism. Here there are two significant hurdles. The first is associated with whether a curvature abnormality can be thought of as a Riemann step, which is the starting point for discussions of shock waves in hyperbolic systems. The second is how Whitman's theory will adapt to the non-Hamiltonian terms latent in the generalized local induction evolution. Connecting geometric quantum hydrodynamics to these concepts will provide further characterization of the nonlinear wave motion of vortex lines in Bose-Einstein condensates.

Simulations built on our non-Hamiltonian correction to the local induction approximation allows for Kelvin wave motion and can be used to study the statistical properties of a quantum tangle. Additionally, there is a second way to relate our model back to turbulence theory. Specifically, one could consider statistical properties associated with the evolution of a random configuration of curvature disturbances on an ensemble of vortex lines. Both

analyses seek to understand the Kelvin wave cascade whose energy spectrum is a recently debated topic. Additionally, it may be possible to use the connections of geometric quantum hydrodynamics to explore the length scales where the Gross-Pitaevskii equation must be employed to handle reconnection dynamics. Such knowledge would inform future multiscale simulations involving vortex filament methods [200] with mean-field methods defined when core structure dominates. Quantifying these terms through the hydrodynamic theory would define regimes where the Gross-Pitaevskii equation must be employed to handle vortex core dynamics that are central to reconnection processes.

Another avenue of understanding Kelvin wave cascades lies with the Bustamante and Nazarenko connection. Specifically, quantization of the hydrodynamic Hamiltonian manifesting from the Gross-Pitaevskii equations is a route to describing the phonon excitations of the Bose-Einstein condensate. [254] The Biot-Savart integral is the result of deriving an effective Hamiltonian for a vortex line consistent with the mean-field evolution. Thus, the first step in connecting our geometric quantum hydrodynamic description to excitations of the Bose gas is to determine a relationship between the Hamiltonian structure and our expansion of the Biot-Savart integral in powers of curvature. This step, by itself, is compelling as a relationship between vortex geometry and the potential terms given by quantum pressure and mean-field averaging may be found and leveraged to understand vortex core structure. After this, one could calculate the quantization of the effective Hamiltonian and attempt to find a direct relationship between the Kelvin waves on the vortex line and phonon oscillations of the condensate. Ultimately, such an extension of the theory would make clearer the role geometric non-Hamiltonian gain/loss plays in the setting of the condensate properties.

Glitches in the periodic rotation in neutron stars are expected to occur when the quantized vortices connecting the outer core to the crust undergo a catastrophic unpinning. This leads to the generation of Kelvin waves exciting phonons supporting a rapid transfer of angular momentum between the two layers. [255, 256] Since the neutron star is so dense, a Euclidean space-time should not be assumed. The Biot-Savart integral has been applied to electro-

magnetic problems in non-Euclidean settings [219], and it is reasonable to expect that local flow approximations for fluid problems can be generalized as well. Understanding relaxation dynamics of non-relativistic quantum tangles, if generalized to the relativistic settings, will further our understanding of post-glitch recovery. Thus the relativistic generalization of the approach used in this thesis is worth pursuing as a step toward understanding neutron star dynamics.

Due to their geometric nature, the tools of Chapter 3 through 5 find application in a variety of fields. In a 1999 work, Shi and Hearst derived a nonlinear Schrödinger equation describing the static configurations of a Kirchhoff elastic rod that was then used to model the supercoiling of DNA. [204] Such models also exist for actin filaments, cell flagella, polymeric liquid crystals and, generally, stiff polymers where the nonlinear response is expected to be a significant contribution to the dynamics. [202, 257–260] Our new non-Hamiltonian evolution of bent vortex lines may prove useful in these settings as well.

REFERENCES CITED

[1] V. Arnold. Sur la géométrie différentielle des groupes de Lie de dimension infinie et ses applications à l'hydrodynamique des fluides parfaits. *Annales de l'institut Fourier*, 16(1): 319–361, 1966.

[2] T. Tao. *Compactness and Contradiction*. American Mathematical Society, 2013.

[3] G. Misiolek, K. Modin and B. Khesin. Geometric Hydrodynamics via Madelung Transform. arXiv:1711.00321, 2017.

[4] C. Trahan and R. Wyatt. *Quantum Dynamics with Trajectories: Introduction to Quantum Hydrodynamics*. Interdisciplinary Applied Mathematics. Springer New York, 2005.

[5] L. S Da Rios. *Sul moto d'un liquido indefinito con un filetto vorticoso di forma qualunque: memoria*. 1910.

[6] R. L. Ricca. The contributions of Da Rios and Levi-Civita to asymptotic potential theory and vortex filament dynamics. *Fluid Dynamics Research*, 18(5):245–268, 1996.

[7] F. R. Hama. Genesis of the LIA. *Fluid Dynamics Research*, 3(1-4):149–150, 9 1988.

[8] H. Hasimoto. A soliton on a vortex filament. *Journal of Fluid Mechanics*, 51:477–485, 1972.

[9] E Madelung. Eine anschauliche Deutung der Gleichung von Schrödinger. *Naturwissenschaften*, 14:1004, 1926.

[10] L. Onsager. Statistical hydrodynamics. *Il Nuovo Cimento (1943-1954)*, 6(2):279–287, 1949.

[11] A. Einstein. Zur Elektrodynamik bewegter Körper. *Annalen der Physik*, 322:891–921, 1905.

[12] Lord Rayleigh. On the flow of viscous liquids, especially in two dimensions. *The London, Edinburgh, and Dublin Philosophical Magazine and Journal of Science*, 36(221):354–372, 1893.

[13] D. B. Meade and A. A. Struthers. Differential Equations in the New Millennium: the Parachute Problem. doi:10.1.1.34.9555, 2007.

[14] S. N. Bose. Plancks Gesetz und Lichtquantenhypothese. *Zeitschrift für Physik*, 26(1): 178–181, 1924.

[15] A. Einstein. Quantentheorie des einatomigen idealen Gases. *Albert Einstein: Akademie-Vorträge*, pages 237–244. Wiley-VCH Verlag GmbH & Co. KGaA, 2006.

[16] B. G. Levi. Cornell, Ketterle, and Wieman share Nobel Prize for Bose-Einstein condensates. *Physics Today*, 54(12):14–16, 2001.

[17] D. Derbes. Feynmans derivation of the Schrödinger equation. *American Journal of Physics*, 64(7):881–884, 1996.

[18] D. J. Griffiths. *Introduction to Quantum Mechanics*. Cambridge University Press, 2016.

[19] L. I. Schiff. *Quantum Mechanics*. International series in pure and applied physics. McGraw-Hill, 1955.

[20] C. J. Pethick and H. Smith. *Bose-Einstein Condensation in Dilute Gases*. Cambridge University Press, 2002.

[21] M. Ueda. *Fundamentals and New Frontiers of Bose-Einstein Condensation*. World Scientific, 2010.

[22] S. Childress. *An Introduction to Theoretical Fluid Mechanics*. American Mathematical Soc., 2009.

[23] A. M. Kuethe and C. Y. Chow. *Foundations of aerodynamics: bases of aerodynamic design*. Wiley, 1986.

[24] J. Katz and A. Plotkin. *Low-Speed Aerodynamics*. Cambridge Aerospace Series. Cambridge University Press, 2001.

[25] D. J. Griffiths. *Introduction to Electrodynamics*. Prentice Hall, 1999.

[26] G. Krstulovic. Kelvin-wave cascade and dissipation in low-temperature superfluid vortices. *Phys. Rev. E*, 86(5):55301, 2012.

[27] E. Kozik and B. Svistunov. Kelvin-Wave Cascade and Decay of Superfluid Turbulence. *Phys. Rev. Lett.*, 92(3):35301, 2004.

[28] J. A. Biello and T. Dimofte. Why do earth's equatorial waves head east? *Science*, 358 (6366):990–991, 2017.

[29] N. J. Higham and M. R. Dennis. *Princeton Companion to Applied Mathematics*. Princeton University Press, 2015.

[30] A. A. Simon, L. Li, and D. C. Reuter. Smallscale waves on jupiter: A reanalysis of new horizons, voyager, and galileo data. *Geophysical Research Letters*, 42(8):2612–2618, 2015.

[31] Sir William Thomson. Vibrations of a columnar vortex. *The London, Edinburgh, and Dublin Philosophical Magazine and Journal of Science*, 10(61):155–168, 1880.

[32] T. Von Kármán. *Aerodynamics*. McGraw-Hill, 1963.

[33] L. F. Richardson. *Weather Prediction by Numerical Process*. Cambridge University Press, 2007.

[34] N. Proukakis, S. Gardiner, and M. Davis. *Quantum Gases: Finite Temperature and Non-equilibrium Dynamics*. Cold atoms. Imperial College Press, 2013.

[35] R. Huebener, N. Schopohl, and G. E. Volovik. *Vortices in Unconventional Superconductors and Superfluids*. Physics and astronomy online library. Springer, 2002.

[36] R. M. Price, D. Trypogeorgos, D. L. Campbell, A. Putra, A. Valdés-Curiel, and I. B. Spielman. Vortex nucleation in a Bose-Einstein condensate: from the inside out. *New Journal of Physics*, 18(11):113009, 2016.

[37] Y. J. Lin, R L Compton, K. Jiménez-García, J. V. Porto, and I. B. Spielman. Synthetic magnetic fields for ultracold neutral atoms. *Nature*, 462:628, 2009.

[38] C. Raman, J. R. Abo-Shaeer, J. M. Vogels, K. Xu, and W. Ketterle. Vortex Nucleation in a Stirred Bose-Einstein Condensate. *Phys. Rev. Lett.*, 87(21):210402, 2001.

[39] I. Coddington, P. Engels, V. Schweikhard, and E. A. Cornell. Observation of Tkachenko Oscillations in Rapidly Rotating Bose-Einstein Condensates. *Phys. Rev. Lett.*, 91(10): 100402, 2003.

[40] P. Engels, I. Coddington, P. C. Haljan, V. Schweikhard, and E. A. Cornell. Observation of Long-Lived Vortex Aggregates in Rapidly Rotating Bose-Einstein Condensates. *Phys. Rev. Lett.*, 90(17):170405, 2003.

[41] S. Serafini, M. Barbiero, M. Debortoli, S. Donadello, F. Larcher, F. Dalfovo, G. Lamporesi, and G. Ferrari. Dynamics and Interaction of Vortex Lines in an Elongated Bose-Einstein Condensate. *Phys. Rev. Lett.*, 115(17):170402, 2015.

[42] M. R. Andrews, C. G. Townsend, H.-J. Miesner, D. S. Durfee, D. M. Kurn, and W. Ketterle. Observation of Interference Between Two Bose Condensates. *Science*, 275 (5300):637, 1997.

[43] S. Donadello, S. Serafini, M. Tylutki, L. P. Pitaevskii, F. Dalfovo, G. Lamporesi, and G. Ferrari. Observation of Solitonic Vortices in Bose-Einstein Condensates. *Phys. Rev. Lett.*, 113(6):65302, 2014.

[44] D. V. Freilich, D. M. Bianchi, A. M. Kaufman, T. K. Langin, and D. S. Hall. Real-Time Dynamics of Single Vortex Lines and Vortex Dipoles in a Bose-Einstein Condensate. *Science*, 329(5996):1182, 2010.

[45] K. M. Mertes, J. W. Merrill, R. Carretero-González, D J Frantzeskakis, P. G. Kevrekidis, and D. S. Hall. Nonequilibrium Dynamics and Superfluid Ring Excitations in Binary Bose-Einstein Condensates. *Phys. Rev. Lett.*, 99(19):190402, 2007.

[46] G. Lamporesi, S. Donadello, S. Serafini, F. Dalfovo, and G. Ferrari. Spontaneous creation of Kibble-Zurek solitons in a Bose-Einstein condensate. *Nature Physics*, 9:656, 2013.

[47] C. N. Weiler, T. W. Neely, D. R. Scherer, A. S. Bradley, M. J. Davis, and B. P. Anderson. Spontaneous vortices in the formation of BoseEinstein condensates. *Nature*, 455:948, 2008.

[48] S. Serafini, L. Galantucci, E. Iseni, T. Bienaimé, R. N. Bisset, C. F. Barenghi, F. Dalfovo, G. Lamporesi, and G. Ferrari. Vortex Reconnections and Rebounds in Trapped Atomic Bose-Einstein Condensates. *Phys. Rev. X*, 7(2):21031, 2017.

[49] E. A. L. Henn, J. A. Seman, E. R. F. Ramos, M. Caracanhas, P. Castilho, E. P. Olimpio, G. Roati, D. V. Magalhães, K. M. F. Magalhães, and V. S. Bagnato. Observation of vortex formation in an oscillating trapped Bose-Einstein condensate. *Phys. Rev. A*, 79(4): 43618, 2009.

[50] E. A. L. Henn, J. A. Seman, G. Roati, K. M. F. Magalhães, and V. S. Bagnato. Emergence of Turbulence in an Oscillating Bose-Einstein Condensate. *Phys. Rev. Lett.*, 103(4):45301, 2009.

[51] E. A. L. Henn, J. A. Seman, G. Roati, K. M. F. Magalhães, and V. S. Bagnato. Generation of Vortices and Observation of Quantum Turbulence in an Oscillating Bose-Einstein Condensate. *Journal of Low Temperature Physics*, 158(3):435, 2009.

[52] A. J. Allen, N. G. Parker, N. P. Proukakis, and C. F. Barenghi. Quantum turbulence in atomic Bose-Einstein condensates. *Journal of Physics: Conference Series*, 544:012023, 2014.

[53] A. J. Allen, N. G. Parker, N. P. Proukakis, and C. F. Barenghi. Isotropic vortex tangles in trapped atomic Bose-Einstein condensates via laser stirring. *Phys. Rev. A*, 89(2):25602, 2014.

[54] R. Lopes, C. Eigen, N. Navon, D. Clément, R. P. Smith, and Z. Hadzibabic. Quantum Depletion of a Homogeneous Bose-Einstein Condensate. *Phys. Rev. Lett.*, 119(19):190404, 2017.

[55] M. Tsubota, K. Fujimoto, and S. Yui. Numerical Studies of Quantum Turbulence. *Journal of Low Temperature Physics*, 188(5):119–189, 2017.

[56] A. W. Baggaley. The importance of vortex bundles in quantum turbulence at absolute zero. *Physics of Fluids*, 24(5):055109, 2012.

[57] N. Sasa, T. Kano, M. Machida, V. S. L'vov, O. Rudenko, and M. Tsubota. Energy spectra of quantum turbulence: Large-scale simulation and modeling. *Phys. Rev. B*, 84 (5):54525, 2011.

[58] P. Walmsley, D. Zmeev, F. Pakpour, and A. Golov. Dynamics of quantum turbulence of different spectra. *Proceedings of the National Academy of Sciences of the United States of America*, 111 Suppl 1(Supplement 1):4691–8, 2014.

[59] R. A. Van Gorder. Motion of isolated open vortex filaments evolving under the truncated local induction approximation. *Physics of Fluids*, 29(11):115105, 2017.

[60] S. A. Strong and L. D. Carr. Generalized local induction equation, elliptic asymptotics, and simulating superfluid turbulence. *Journal of Mathematical Physics*, 53(3), 2012.

[61] S. A. Strong and L. D. Carr. Non-Hamiltonian Dynamics of Quantized Vortices in Bose-Einstein Condensates. arXiv:1712.05885, 2017.

[62] S. A. Strong and L. D. Carr. Non-Hamiltonian Kelvin wave generation on vortices in Bose-Einstein condensates. arXiv:1803.00147, 2018.

[63] M. .D. Bustamante and S. Nazarenko. Derivation of the Biot-Savart equation from the nonlinear Schrödinger equation. *Phys. Rev. E*, 92(5):53019, 2015.

[64] P. D. Lax. *Linear Algebra and Its Applications*. Wiley, 2007.

[65] L. Onsager. The Distribution of Energy in Turbulence. In *Minutes of the Meeting of the Metropolitan Section held at Columbia University*, New York, 1945. Physical Review.

[66] G. L. Eyink and K. R. Sreenivasan. Onsager and the theory of hydrodynamic turbulence. *Rev. Mod. Phys.*, 78(1):87–135, 2006.

[67] Gregory L Eyink and Katepalli R Sreenivasan. Onsager and the theory of hydrodynamic turbulence. *Rev. Mod. Phys.*, 78(1):87–135, 1 2006.

[68] A. Kolmogorov. Dissipation of energy in the locally isotropic turbulence. *Proceedings of the Royal Society of London A: Mathematical, Physical and Engineering Sciences*, 434 (1890):15–17, 1991.

[69] A. Kolmogorov. The local structure of turbulence in incompressible viscous fluid for very large Reynolds numbers. *Proceedings of the Royal Society of London A: Mathematical, Physical and Engineering Sciences*, 434(1890):9–13, 1991.

[70] U. Frisch. *Turbulence: The Legacy of A. N. Kolmogorov*. Cambridge University Press, 1995.

[71] Y. Kaneda, T. Ishihara, M. Yokokawa, K. Itakura, and A. Uno. Energy dissipation rate and energy spectrum in high resolution direct numerical simulations of turbulence in a periodic box. *Physics of Fluids*, 15(2):L21–L24, 2003.

[72] R. Bitane, H. Homann, and J. Bec. Geometry and violent events in turbulent pair dispersion. *Journal of Turbulence*, 14(2):23–45, 2013.

[73] T. Drivas and G. Eyink. An Onsager Singularity Theorem for Turbulent Solutions of Compressible Euler Equations. *Communications in Mathematical Physics*, 359, 2, 733–763, 2017.

[74] P. Isett. A Proof of Onsager's Conjecture. arXiv:1608.08301, 2016.

[75] G. Eyink and T. Drivas. Cascades and Dissipative Anomalies in Relativistic Fluid Turbulence. *Phys. Rev. X*, 8(1):11023, 2018.

[76] G. Eyink and T. Drivas. Cascades and Dissipative Anomalies in Compressible Fluid Turbulence. *Phys. Rev. X*, 8(1):11022, 2 2018.

[77] J. Duchon and R. Robert. Inertial energy dissipation for weak solutions of incompressible Euler and Navier-Stokes equations. *Nonlinearity*, 13(1):249–255, 2000.

[78] A. Shnirelman. Weak Solutions with Decreasing Energy of Incompressible Euler Equations. *Communications in Mathematical Physics*, 210(3):541–603, 2000.

[79] John Hunter. An Introduction to the Incompressible Euler Equations. math.ucdavis.edu/ hunter/notes/euler.pdf, 2006.

[80] N. G. Berloff, M. Brachet, and N. P. Proukakis. Modeling quantum fluid dynamics at nonzero temperatures. *Proceedings of the National Academy of Sciences*, 111: 4675–4682, 2014.

[81] J. Cantarella, D. DeTurck, and H. Gluck. Vector Calculus and the Topology of Domains in 3-Space. *The American Mathematical Monthly*, 109(5):409–442, 2002.

[82] M. Tsubota, T. Araki, and S. K. Nemirovskii. Dynamics of vortex tangle without mutual friction in superfluid ˆ4He. *Phys. Rev. B*, 62(17):11751–11762, 2000.

[83] P. G. Saffman. *Vortex Dynamics*. Cambridge Monographs on Mechanics. Cambridge University Press, 1993.

[84] L. Landau. Theory of the superfluidity of helium II. *Phys. Rev.*, 60(4):356–358, Aug 1941.

[85] L. D. Landau and E. M. Lifshitz. *Course of Fluid Mechanics*. Oxford: Pergamon Press, 1959.

[86] A. Griffin. New light on the intriguing history of superfluidity in liquid ^{4}He. *Journal of Physics Condensed Matter*, 21(16), 2009.

[87] R.P. Feynman. Chapter II: Application of quantum mechanics to liquid helium. volume 1 of *Progress in Low Temperature Physics*, Elsevier, 1955.

[88] L. Onsager. Statistical hydrodynamics. *Il Nuovo Cimento (1943-1954)*, 6:279–287, 1949.

[89] R. J. Donnelly. *Quantized Vortices in Helium II*. Cambridge University Press, 2005.

[90] C. F. Barenghi. Introduction to Superfluid Vortices and Turbulence. In C. F. Barenghi, R. J. Donnelly, & W. F. Vinen, editor, *Quantized Vortex Dynamics and Superfluid Turbulence*, volume 571 of *Lecture Notes in Physics, Berlin Springer Verlag*, 2001.

[91] W. F. Vinen. Mutual friction in a heat current in liquid helium II: I. Experiments on steady heat currents. *Royal Society of London Proceedings Series A*, 240:114–127, 1957.

[92] W. F. Vinen. Mutual friction in a heat current in liquid helium II: II. Experiments on transient effects. *Royal Society of London Proceedings Series A*, 240:128–143, 1957.

[93] W. F. Vinen. Mutual friction in a heat current in liquid helium II: III. Theory of the mutual friction. *Royal Society of London Proceedings Series A*, 242:493–515, 1957.

[94] W. F. Vinen. Mutual friction in a heat current in liquid helium II: IV. Critical heat currents in wide channels. *Royal Society of London Proceedings Series A*, 243:400–413, 1958.

[95] K. W. Schwarz. Theory of turbulence in superfluid ^{4}He. *Physical Review Letters*, 38: 551–554, 1977.

[96] K. W. Schwarz. Three-dimensional vortex dynamics in superfluid ^{4}He: Homogeneous superfluid turbulence. *Physical Review B*, 38:2398–2417, 1988.

[97] D. C. Samuels. Vortex Filament Methods for Superfluids. In C. F. Barenghi, R. J. Donnelly, & W. F. Vinen, editor, *Quantized Vortex Dynamics and Superfluid Turbulence*, volume 571 of *Lecture Notes in Physics, Berlin Springer Verlag*, 2001.

[98] E. A. L. Henn, J. A. Seman, G. Roati, K. M. F. Magalhães, and V. S. Bagnato. Emergence of turbulence in an oscillating bose-einstein condensate. *Phys. Rev. Lett.*, 103(4):045301, Jul 2009.

[99] G. H. Cottet and J. Soler. Three-dimensional navier-stokes equations for singular filament initial data. *Journal of Differential Equations*, 74(2):234 – 253, 1988.

[100] P. K. Newton. *The N-Vortex Problem*, *Applied Mathematical Sciences*. Springer, 2001.

[101] A. Leonard. Vortex methods for flow simulation. *Journal of Computational Physics*, 37:289–335, 1980.

[102] A. Leonard. Computing three-dimensional incompressible flows with vortex elements. *Annual Review of Fluid Mechanics*, 17:523–559, 1985.

[103] J. T. Beale and A. Majda. Vortex methods. I - Convergence in three dimensions. II - Higher order accuracy in two and three dimensions. *Mathematics of Computation*, 39: 1–52, July 1982.

[104] A. J. Chorin. Vortex models and boundary layer instability. *SIAM Journal on Scientific and Statistical Computing*, 1(1):1–21, 1980.

[105] B. Couët, O Buneman, and A Leonard. Simulation of three-dimensional incompressible flows with a vortex-in-cell method. *Journal of Computational Physics*, 39(2):305 – 328, 1981.

[106] W. T. Ashurst and E. Meiburg. Three-dimensional shear layers via vortex dynamics. *Journal of Fluid Mechanics*, 189:pp 87–116, (1988).

[107] R. L. Ricca. Rediscovery of Da Rios equations. *Nature*, 352:561–562, August 1991.

[108] R. Betchov. On the curvature and torsion of an isolated vortex filament. *Journal of Fluid Mechanics*, 22:471–479, 1965.

[109] R. J. Arms and F. R. Hama. Localized-Induction Concept on a Curved Vortex and Motion of an Elliptic Vortex Ring. *Physics of Fluids*, 8:553–559, April 1965.

[110] G. K. Batchelor. *An Introduction to Fluid Dynamics*. Cambridge University Press, February 2000.

[111] A. J. Callegari and L. Ting. Motion of a curved vortex filament with decaying vortical core and axial velocity. *SIAM Journal of Applied Mathematics*, 35:148–175, July 1978.

[112] R. L. Ricca. The contributions of Da Rios and Levi-Civita to asymptotic potential theory and vortex filament dynamics. *Fluid Dynamics Research*, 18:245–268, 1996.

[113] F. R. Hama. Genesis of the LIA. *Fluid Dynamics Research*, 3:149–150, 1988.

[114] M. J. P. Cullen. Vortex dynamics. Edited by P. G. Saffman. Cambridge University Press. *Quarterly Journal of the Royal Meteorological Society*, 122:1015–1015, 1996.

[115] A. J. Majda and A. L. Bertozzi. *Vorticity and Incompressible Flow*. Cambridge University Press, 2001.

[116] L.S. Da Rios. Sul moto d'un liquido indefinito con un filetto vorticoso di forma qualunque (on the motion of an unbounded liquid with a vortex filament of any shape). *Rend. Circ. Mat. Palermo*, 22:117135, 1906.

[117] L.S. Da Rios. Sul moto dei filetti vorticosi di forma qualunque (on the motion of vortex filaments of any shape). *Rend. R. Acc. Lincei*, 18:7579, 1909.

[118] L.S. Da Rios. Sul moto dei filetti vorticosi di forma qualunque (on the motion of vortex filaments of any shape). *Rend. Circ. Mat. Palermo*, 29:354368, 1910.

[119] L.S. Da Rios. Sul moto intestino dei filetti vorticosi (on the interior motion of vortex filaments). *Giornale di Matematiche del Battaglini*, 49:300308, 1911.

[120] L.S. Da Rios. Sezioni trasversali stabili dei filetti vorticosi (stable cross-sections of vortex filaments). *Atti R. Ist. Veneto Sci. Lett. Arti*, 75:299308, 1916.

[121] L.S. Da Rios. Sui tubi vorticosi rettilinei posti a raffronto (comparative study of rectilinear vortex tubes). *Atti R. Acc. Sci. Lett. Arti Padova*, 32:343350, 1916.

[122] L.S. Da Rios. Vortici ad elica (helical vortices). *II Nuovo Cimento*, 11:419431, 1916.

[123] L.S. Da Rios. Sur la thorie des tourbillons. *Comptes Rendus Acad. Sci. Paris*, 191: 399–401, 1930.

[124] L.S. Da Rios. Sui vortici piani indeformabili (on planar vortices of invariant shape. *Atti Pontificia Acc. Sci. Nuovi Lincei*, 84:720–731, 1931.

[125] L.S. Da Rios. Sui vortici piani indeformabili (on planar vortices of invariant shape). *Atti Soc. Ital. Progresso Scienze*, 2:7–8, 1931.

[126] L.S. Da Rios. Anelli vorticosi ruotanti (rotating vortex rings). *Rend. Sem. Matem. Univ. Padova*, 9:142–151, 1931.

[127] L.S. Da Rios. Ancora sugli anelli vorticosi ruotanti (again on rotating vortex rings). *Rend. R. Acc. Lincei*, 17:924–926, 1933.

[128] L.S. Da Rios. Sui vortici gobbi indeformabili (on hunched vortices of invariant shape). *Atti Pontificia Acc. Sci. Nuovi Lincei*, 86:162–168, 1933.

[129] Y. Fukumoto and T. Miyazaki. Three-dimensional distortions of a vortex filament with axial velocity. *Journal of Fluid Mechanics*, 222:369–416, 1991.

[130] G. L. Lamb Jr. *Elements of Soliton Theory*, volume 4. John Wiley and Sons, 1986.

[131] K. W. Schwarz. Generation of superfluid turbulence deduced from simple dynamical rules. *Physical Review Letters*, 49:283–285, 1982.

[132] D. Karp and S. M. Sitnik. Asymptotic approximations for the first incomplete elliptic integral near logarithmic singularity. *Journal of Computational and Applied Mathematics*, 205:186–206, 2007.

[133] A. Erdèlyi. *Asymptotic Expansions*. Dover, 1956.

[134] J. van der Corput. Asymptotic developments I: Fundamental theorems of asymptotics. *Journal d'Analyse Mathmatique*, 4:341–418, 1954.

[135] J. van der Corput. Asymptotic developments II: Generalization of the fundamental theorem on asymptotic series. *Journal d'Analyse Mathmatique*, 5:315–320, 1956.

[136] J. van der Corput. Asymptotic developments III: Again on the fundamental theorem of asymptotic series. *Journal d'Analyse Mathmatique*, 9:195–204, 1961.

[137] W. F. Vinen. Mutual Friction in a Heat Current in Liquid Helium II. IV. Critical Heat Currents in Wide Channels. *Proceedings of the Royal Society of London. Series A, Mathematical and Physical Sciences*, 243(1234):400–413, 1958.

[138] W. F. Vinen. Mutual friction in a heat current in liquid helium II III. Theory of the mutual friction. *Proceedings of the Royal Society of London A: Mathematical, Physical and Engineering Sciences*, 242(1231):493–515, 1957.

[139] W. F. Vinen. Mutual friction in a heat current in liquid helium II. II. Experiments on transient effects. *Proceedings of the Royal Society of London A: Mathematical, Physical and Engineering Sciences*, 240(1220):128–143, 1957.

[140] W. F. Vinen. Mutual friction in a heat current in liquid helium II I. Experiments on steady heat currents. *Proceedings of the Royal Society of London A: Mathematical, Physical and Engineering Sciences*, 240(1220):114–127, 1957.

[141] O. C. Idowu, A. Willis, C. F. Barenghi, and D. C. Samuels. Local normal-fluid helium II flow due to mutual friction interaction with the superfluid. *Physical Review B*, 62: 3409–3415, 2000.

[142] O. C. Idowu, D. Kivotides, C. F. Barenghi, and D.C. Samuels. Equation for self-consistent superfluid vortex line dynamics. *Journal of Low Temperature Physics*, 120: 269–280, 2000.

[143] J. Kim and P. Moin. Application of a fractional-step method to incompressible Navier-Stokes equations. *Journal of Computational Physics*, 59:308–323, 1985.

[144] F. H. Harlow and J. E. Welch. Numerical Calculation of Time-Dependent Viscous Incompressible Flow of Fluid with Free Surface. *Physics of Fluids*, 8:2182–2189, 1965.

[145] A. A. Wray. Very low storage time-advancement schemes. Internal Report, NASA Ames Research Center, Moffet Field, California, 1986.

[146] C. A. Kennedy, M. H. Carpenter, and R. M. Lewis. Low-storage, explicit runge-kutta schemes for the compressible navier-stokes equations. *Applied Numerical Mathematics*, 35 (3):177 – 219, 2000.

[147] S. A. Ragab and K. S. Youssef. Computational aspects of trailing vortices. *Journal of Wind Engineering and Industrial Aerodynamics*, 69-71:943 – 953, 1997.

[148] J. S. Hesthaven and T. Warburton. *Nodal Discontinuous Galerkin Methods Algorithms, Analysis, and Applications*. Springer, 2008.

[149] L. Liu, X. Li, and F. Q. Hu. Nonuniform time-step runge-kutta discontinuous galerkin method for computational aeroacoustics. *Journal of Computational Physics*, 229:6874–6897, 2010.

[150] T. F. Lemczyk and M. M. Yovanovich. Efficient evaluation of incomplete elliptic integrals and functions. *Computers & Mathematics with Applications*, 16(9):747 – 757, 1988.

[151] W. C. Hassenpflug. Elliptic integrals and the Schwarz-Christoffel transformation. *Computers & Mathematics with Applications*, 33(12):15–114, 1997.

[152] T. Fukushima and H. Ishizaki. Numerical computation of incomplete elliptic integrals of a general form. *Celestial Mechanics and Dynamical Astronomy*, 59:237–251, 1994.

[153] X. Yang. Efficient circular arc interpolation based on active tolerance control. *Computer-Aided Design*, 34(13):1037 – 1046, 2002.

[154] E. Hodby, G. Hechenblaikner, S. A. Hopkins, O. M. Maragò, and C. J. Foot. Vortex nucleation in Bose-Einstein condensates in an oblate, purely magnetic potential. *Phys. Rev. Lett.*, 88(1):010405, 2001.

[155] E. Varoquaux, O. Avenel, Y. Mukharsky, and P. Hakonen. The experimental evidence for vortex nucleation in ^{4}He. In C. F. Barenghi, R. J. Donnelly, & W. F. Vinen, editor, *Quantized Vortex Dynamics and Superfluid Turbulence*, volume 571 of *Lecture Notes in Physics, Berlin Springer Verlag*, 2001.

[156] R. B. Pelz. Locally self-similar, finite-time collapse in a high-symmetry vortex filament model. *Physical Review E*, 55:1617–1626, 1997.

[157] J. Koplik and H. Levine. Vortex reconnection in superfluid helium. *Physical Review Letters*, 71:1375–1378, 1993.

[158] T. Lipniacki. Evolution of quantum vortices following reconnection. *European Journal of Mechanics B Fluids*, 19:361–378, 2000.

[159] T. Lipniacki. From Vortex Reconnections to Quantum Turbulence. In C. F. Barenghi, R. J. Donnelly, & W. F. Vinen, editor, *Quantized Vortex Dynamics and Superfluid Turbulence*, volume 571 of *Lecture Notes in Physics, Berlin Springer Verlag*, 2001.

[160] T. Lipniacki. Evolution of the line-length density and anisotropy of quantum tangle in ^{4}He. *Physical Review B*, 64(21), 2001.

[161] D. Kivotides, C. F. Barenghi, and D. C. Samuels. Superfluid vortex reconnections at finite temperature. *Europhysics Letters*, 54:774–778, 2001.

[162] S. Gutierrez and L. Vega. Self-similar solutions of the localized induction approximation: singularity formation. *Nonlinearity*, 17:2091–2136, 2004.

[163] M. S. Paoletti, M. E. Fisher, and D. P. Lathrop. Reconnection dynamics for quantized vortices. *Physica D Nonlinear Phenomena*, 239:1367–1377, 2010.

[164] J. A. Seman, E. A. L. Henn, M. Haque, R. F. Shiozaki, E. R. F. Ramos, M. Caracanhas, P. Castilho, C. Castelo Branco, P. E. S. Tavares, F. J. Poveda-Cuevas, G. Roati, K. M. F. Magalhães, and V. S. Bagnato. Three-vortex configurations in trapped Bose-Einstein condensates. *Physical Review A*, 82(3), 2010.

[165] E. A. L. Henn, J. A. Seman, E. R. F. Ramos, M. Caracanhas, P. Castilho, E. P. Olímpio, G. Roati, D. V. Magalhães, K. M. F. Magalhães, and V. S. Bagnato. Observation of vortex formation in an oscillating trapped Bose-Einstein condensate. *Phys. Rev. A*, 79(4): 043618, 2009.

[166] E. Henn, J. Seman, G. Roati, K. Magalhãs, and V. Bagnato. Generation of vortices and observation of quantum turbulence in an oscillating Bose-Einstein condensate. *Journal of Low Temperature Physics*, 158:435–442, 2010.

[167] J. R. Abo-Shaeer, C. Raman, J. M. Vogels, and W. Ketterle. Observation of Vortex Lattices in Bose-Einstein Condensates. *Science*, 292(5516):476–479, 2001.

[168] K. W. Madison, F. Chevy, W. Wohlleben, and J. Dalibard. Vortex formation in a stirred bose-einstein condensate. *Phys. Rev. Lett.*, 84(5):806–809, 2000.

[169] M. Kobayashi and M. Tsubota. Quantum turbulence in a trapped Bose-Einstein condensate under combined rotations around three axes. *Journal of Low Temperature Physics*, 150:587–592, 2008.

[170] K. Kasamatsu, M. Tsubota, and M. Ueda. Nonlinear dynamics of vortex lattice formation in a rotating bose-einstein condensate. *Phys. Rev. A*, 67(3):033610, 2003.

[171] Y. Castin and R. Dum. Bose-einstein condensates in time dependent traps. *Phys. Rev. Lett.*, 77(27):5315–5319, 1996.

[172] H. E. Hall and W. F. Vinen. The Rotation of Liquid Helium II. I. Experiments on the Propagation of Second Sound in Uniformly Rotating Helium II. *Royal Society of London Proceedings Series A*, 238:204–214, 1956.

[173] H. E. Hall and W. F. Vinen. The Rotation of Liquid Helium II. II. The Theory of Mutual Friction in Uniformly Rotating Helium II. *Royal Society of London Proceedings Series A*, 238:215–234, 1956.

[174] H. E. Hall. The rotation of liquid helium II. *Advances in Physics*, 9:89–146, 1960.

[175] R. L. Ricca. Tropicity and Complexity Measures for Vortex Tangles. In C. F. Barenghi, R. J. Donnelly, & W. F. Vinen, editor, *Quantized Vortex Dynamics and Superfluid Turbulence*, volume 571 of *Lecture Notes in Physics, Berlin Springer Verlag*, 2001.

[176] C. F Barenghi, R. L. Ricca, and D. C. Samuels. How tangled is a tangle? *Phys. D*, 157 (3):197–206, 2001.

[177] D. R. Poole, H. Scoffield, C. F. Barenghi, and D.C. Samuels. Geometry and topology of superfluid turbulence. *Journal of Low Temperature Physics*, 132:97–117, 2003.

[178] D. Jou, M. S. Mongiovì, M. Sciacca, and C. F. Barenghi. Vortex length, vortex energy and fractal dimension of superfluid turbulence at very low temperature. *Journal of Physics A: Mathematical and Theoretical*, 43(20):205501, 2010.

[179] Annalisa Calini. Recent developments in integrable curve dynamics, 1997.

[180] P.G. Grinevich and M.U. Schmidt. Closed curves in $\mathbb{R}^3$: a characterization in terms of curvature and torsion, the hasimoto map and periodic solutions of the filament equation. arXiv:dg-ga/9703020, 1997

[181] A. Calini and T. Ivey. Finite-gap solutions tof the vortex filament equation: Genus one solutions and symmetric solutions. *Journal of Nonlinear Science*, 15:321–361, 2005.

[182] L. Uby. Strings, Rods, Vortices and Wave Equations. *Royal Society of London Proceedings Series A*, 452:1531–1543, 1996.

[183] R. L. Ricca. Physical interpretation of certain invariants for vortex filament motion under LIA. *Physics of Fluids*, 4:938–944, 1992.

[184] M. Tsubota and K. Kasamatsu. Quantized Vortices and Quantum Turbulence. In Alberto Bramati and Michele Modugno, editors, *Physics of Quantum Fluids: New Trends and Hot Topics in Atomic and Polariton Condensates*, 283–299. Springer Berlin Heidelberg, Berlin, Heidelberg, 2013.

[185] C. F. Barenghi, L. Skrbek, and K. R Sreenivasan. Introduction to quantum turbulence. *Proceedings of the National Academy of Sciences of the United States of America*, 111 Suppl 1, 4647–52, 2014.

[186] M. Leadbeater, T. Winiecki, D. C. Samuels, C. F. Barenghi, and C. S. Adams. Sound Emission due to Superfluid Vortex Reconnections. *Phys. Rev. Lett.*, 86(8):1410–1413, 2001.

[187] H. Salman. Breathers on Quantized Superfluid Vortices. *Phys. Rev. Lett.*, 111(16): 165301, 2013.

[188] P. Walmsley, D. Zmeev, F. Pakpour, and A. Golov. Dynamics of quantum turbulence of different spectra. *Proceedings of the National Academy of Sciences*, 111 Suppl 1, 4691–4698, 2014.

[189] A. L. Fetter and A. A. Svidzinsky. Vortices in a trapped dilute Bose-Einstein condensate. *Journal of Physics: Condensed Matter*, 13(12):R135–R194, 2001.

[190] Y. Fukumoto and T. Miyazaki. Three-dimensional distortions of a vortex filament with axial velocity. *Journal of Fluid Mechanics*, 222:369–416, 1991.

[191] A. J. Majda and A. L. Bertozzi. *Vorticity and Incompressible Flow.* Cambridge Texts in Applied Mathematics. Cambridge University Press, 2002.

[192] P. J. Olver. *Applications of Lie Groups to Differential Equations.* Applications of Lie Groups to Differential Equations. Springer New York, 2000.

[193] L. Faddeev, A. G. Reyman, and L. Takhtajan. *Hamiltonian Methods in the Theory of Solitons.* Classics in Mathematics. Springer Berlin Heidelberg, 2007.

[194] S. Dimas and D. Tsoubelis. A new Mathematica-based program for solving overdetermined systems of PDEs. In *8th International Mathematica Symposium*, 2006.

[195] D. Poole and W. Hereman. Symbolic computation of conservation laws for nonlinear partial differential equations in multiple space dimensions. *Journal of Symbolic Computation*, 46(12):1355–1377, 2011.

[196] N. Akhmediev and A. Ankiewicz. *Dissipative Solitons.* Lecture Notes in Physics. Springer Berlin Heidelberg, 2005.

[197] P. K. Newton and J. B. Keller. Stability of Periodic Plane Waves. *SIAM Journal on Applied Mathematics*, 47(5):959–964, 1987.

[198] D. Kivotides, J. C. Vassilicos, D. C. Samuels, and C. F. Barenghi. Kelvin Waves Cascade in Superfluid Turbulence. *Phys. Rev. Lett.*, 86(14):3080–3083, 2001.

[199] M. S. Paoletti, M. E. Fisher, and D. P. Lathrop. Reconnection dynamics for quantized vortices. *Physica D: Nonlinear Phenomena*, 239(14):1367 – 1377, 2010.

[200] R. Hänninen and A. W. Baggaley. Vortex filament method as a tool for computational visualization of quantum turbulence. *Proceedings of the National Academy of Sciences of the United States of America*, 111 Suppl 1, 4667–74, 2014.

[201] T. D. Andersen and C. C. Lim. *Introduction to Vortex Filaments in Equilibrium.* Springer Monographs in Mathematics. Springer New York, 2014.

[202] J. P. Mesirov, K. Schulten, and D. W. Sumners. *Mathematical Approaches to Biomolecular Structure and Dynamics.* The IMA Volumes in Mathematics and its Applications. Springer New York, 2012.

[203] A. Scott and E. P. M. A. Scott. *Encyclopedia of Nonlinear Science*. Taylor & Francis, 2006.

[204] Y. Shi and J. E. Hearst. The Kirchhoff elastic rod, the nonlinear Schrödinger equation, and DNA supercoiling. 1999.

[205] C. Lindemann, A. Visser, and P. Mariani. Dynamics of phytoplankton blooms in turbulent vortex cells. *Journal of The Royal Society Interface*, 14(136), 2017.

[206] W. M. Durham, E. Climent, M. Barry, F. De Lillo, G. Boffetta, M. Cencini, and R. Stocker. Turbulence drives microscale patches of motile phytoplankton. *Nature Communications*, 4:2148, 2013.

[207] R. A. Van Gorder. The Biot-Savart description of Kelvin waves on a quantum vortex filament in the presence of mutual friction and a driving fluid. *Proceedings of the Royal Society A: Mathematical, Physical and Engineering Science*, 471(2179), 2015.

[208] R. Klein and A. Majda. Self-stretching of a perturbed vortex filament I. The asymptotic equation for deviations from a straight line. *Physica D: Nonlinear Phenomena*, 49(3): 323–352, 1991.

[209] R. Klein and A. Majda. Self-stretching of perturbed vortex filaments: II. Structure of solutions. *Physica D: Nonlinear Phenomena*, 53(2-4):267–294, 1991.

[210] J. Laurie, V. S. L'vov, S. Nazarenko, and O. Rudenko. Interaction of Kelvin waves and nonlocality of energy transfer in superfluids. *Phys. Rev. B*, 81(10):104526, 2010.

[211] G. Boffetta, A. Celani, D. Dezzani, J. Laurie, and S. Nazarenko. Modeling Kelvin Wave Cascades in Superfluid Helium. *Journal of Low Temperature Physics*, 156(3):193–214, 2009.

[212] A. White, B. P. Anderson, and V. S. Bagnato. Vortices and turbulence in trapped atomic condensates. *Proceedings of the National Academy of Sciences of the United States of America*, 111 Suppl 1, 4719–26, 2014.

[213] E. V. Kozik and B. V. Svistunov. Comment on "Symmetries and Interaction Coefficients of Kelvin waves" byLebedev andL'vov. *Journal of Low Temperature Physics*, 161(5): 603–605, 2010.

[214] V. V. Lebedev, V. S. L'vov, and S. V. Nazarenko. Reply: On Role of Symmetries in Kelvin Wave Turbulence. *Journal of Low Temperature Physics*, 161(5):606–610, 2010.

[215] E. Fonda, D. Meichle, N. T. Ouellette, S. Hormoz, and D. P. Lathrop. Direct observation of Kelvin waves excited by quantized vortex reconnection. *Proceedings of the National Academy of Sciences of the United States of America*, 111 Suppl 1, 4707–10, 2014.

[216] L. C Berselli and H. Bessaih. Some results for the line vortex equation. *Nonlinearity*, 15(6):1729–1746, 2002.

[217] A. J. Callegari and L. Ting. Motion of a Curved Vortex Filament with Decaying Vortical Core and Axial Velocity. *SIAM Journal on Applied Mathematics*, 35(1):148–175, 1978.

[218] J. Parsley. The Biot-Savart operator and electrodynamics on subdomains of the three-sphere. *Journal of Mathematical Physics*, 53(1):013102, 2012.

[219] D. DeTurck and H. Gluck. Electrodynamics and the Gauss linking integral on the 3-sphere and in hyperbolic 3-space. *Journal of Mathematical Physics*, 49(2):023504, 2008.

[220] G. K. Batchelor. *An Introduction to Fluid Dynamics*. Cambridge University Press, Cambridge, 2000.

[221] B. Khesin. Symplectic structures and dynamics on vortex membranes. *Mosc. Math. J.*, 12(2):413–434, 2012.

[222] R. G. Burns, B. A. Dubrovin, A. T. Fomenko, and S. P. Novikov. *Modern Geometry Methods and Applications: Part I: The Geometry of Surfaces, Transformation Groups, and Fields*. Graduate Texts in Mathematics. Springer New York, 1991.

[223] K. W. Schwarz. Three-dimensional vortex dynamics in superfluid ^{4}He: Line-line and line-boundary interactions. *Phys. Rev. B*, 31(9):5782–5804, 1985.

[224] T. Fukushima. Series expansions of symmetric elliptic integrals. *Mathematics of Computation*, 81:957–990, 2012.

[225] D. Karp and S. M. Sitnik. Asymptotic approximations for the first incomplete elliptic integral near logarithmic singularity. *Journal of Computational and Applied Mathematics*, 205(1):186–206, 2007.

[226] B. C. Carlson and J. L. Gustafsoni. Asymptotic approximations for symmetric elliptic integrals. *SIAM J. Math. Anal.*, 25(2):288–303, 1994.

[227] D. W. Moore and P. G. Saffman. The Motion of a Vortex Filament with Axial Flow. *Philosophical Transactions of the Royal Society of London. Series A, Mathematical and Physical Sciences*, 272(1226):403, 1972.

[228] A. A. Svidzinsky and A. L. Fetter. Dynamics of a vortex in a trapped Bose-Einstein condensate. 62(6):63617, 12 2000.

[229] E. J. Hinch. *Perturbation Methods*. Cambridge Texts in Applied Mathematics. Cambridge University Press, 1991.

[230] A. Georgescu. *Asymptotic Treatment of Differential Equations*. Applied Mathematics. Taylor & Francis, 1995.

[231] W. Kühnel. *Differential Geometry: Curves - Surfaces - Manifolds*. Student mathematical library. American Mathematical Society, 2006.

[232] J. Langer and R. Perline. Poisson geometry of the filament equation. *Journal of Nonlinear Science*, 1(1):71–93, 1991.

[233] J. Langer and R. Perline. The Hasimoto transformation and integrable flows on curves. *Applied Mathematics Letters*, 3(2):61–64, 1990.

[234] V. I. Arnold and B. A. Khesin. *Topological Methods in Hydrodynamics*. Applied Mathematical Sciences. Springer New York, 1999.

[235] J. Holmer and M. Zworski. Geometric structure of NLS evolution. arXiv:0809.1844, 2008.

[236] user153764 (https://mathoverflow.net/users/110090/user153764). Infinitesimal generators and conserved quantities (Schrödinger type evolution). MathOverflow:q/270157

[237] O. Bühler. *A Brief Introduction to Classical, Statistical, and Quantum Mechanics*. Courant Institute of Mathematical Sciences [New York University], 2006.

[238] A. Ludu. *Nonlinear Waves and Solitons on Contours and Closed Surfaces*. Springer Series in Synergetics. Springer Berlin Heidelberg, 2012.

[239] E. F. Toro. Notions on Hyperbolic Partial Differential Equations. In *Riemann Solvers and Numerical Methods for Fluid Dynamics: A Practical Introduction,*. Springer Berlin Heidelberg, Berlin, Heidelberg, 2009.

[240] S. E. Buckley and M. C. Leverett. Mechanism of Fluid Displacement in Sands. 1942.

[241] T. Fukushima. Precise and fast computation of a general incomplete elliptic integral of second kind by half and double argument transformations. *Journal of Computational and Applied Mathematics*, 235(14):4140–4148, 2011.

[242] E. D. Bloch. *A First Course in Geometric Topology and Differential Geometry*. Modern Birkhäuser Classics. Birkhäuser Boston, 1997.

[243] P.G. Grinevich and M.U. Schmidt. Closed curves in $\mathbb{R}^3$: a characterization in terms of curvature and torsion, the hasimoto map and periodic solutions of the filament equation. arXiv:dg-ga/9703020, 1997

[244] L. Onsager. Reciprocal Relations in Irreversible Processes. I. *Physical Review*, 37(4): 405–426, 1931.

[245] L. Onsager. Reciprocal Relations in Irreversible Processes. II. *Physical Review*, 38(12): 2265–2279, 1931.

[246] T. Drivas and G. Eyink. An Onsager Singularity Theorem for Turbulent Solutions of Compressible Euler Equations. *Communications in Mathematical Physics*, 2017.

[247] R. McKeown, R. O. Monico, A. Pumir, M. P. Brenner, and S. M. Rubinstein. The Emergence of Small Scales in Vortex Ring Collisions, 2017.

[248] Y. Kimura and H. K. Moffatt. Scaling properties towards vortex reconnection under BiotSavart evolution. *Fluid Dynamics Research*, 50(1):011409, 2 2018.

[249] Y. Kimura and H. K. Moffatt. A tent model of vortex reconnection under BiotSavart evolution. *Journal of Fluid Mechanics*, 834:R1, 1 2018.

[250] T. Tao. Can the Navier-Stokes Equations Blow Up in Finite Time?, youtube:DgmuGqeRTto, 2015.

[251] T. Tao. Finite time blowup for Lagrangian modifications of the three-dimensional Euler equation. arXiv:1606.08481, 2016.

[252] M. P. Brenner, S. H. , and A. Pumir. Potential singularity mechanism for the Euler equations. *Phys. Rev. Fluids*, 1(8):84503, 2016.

[253] G. A. El and M. A. Hoefer. Dispersive shock waves and modulation theory. *Physica D: Nonlinear Phenomena*, 333:11 – 65, 2016.

[254] L. P. Pitaevskii and S. Stringari. *Bose-Einstein Condensation*. International Series of Monographs on Physics. Clarendon Press, 2003.

[255] E. Gügercinoğlu. Glitches as probes of neutron star internal structure and dynamics: Effects of the superfluid-superconducting core. *Journal of Physics: Conference Series*, 932:012037, 2017.

[256] P. W. Anderson and N. Itoh. Pulsar glitches and restlessness as a hard superfluidity phenomenon. *Nature*, 256:25, 1975.

[257] B. Audoly and Y. Pomeau. *Elasticity and Geometry: From hair curls to the non-linear response of shells*. OUP Oxford, 2010.

[258] C. H. Wiggins and R. E. Goldstein. Flexive and Propulsive Dynamics of Elastica at Low Reynolds Numbers. 1997.

[259] R. E. Goldstein and S. A. Langer. Nonlinear Dynamics of Stiff Polymers. *Phys. Rev. Lett.*, 75(6):1094–1097, 1995.

[260] A. J. Taylor and M. R. Dennis. Vortex knots in tangled quantum eigenfunctions. *Nature Communications*, 7:12346, 2016.

APPENDIX A

OVERVIEW HANDOUT FOR THESIS DEFENSE

Geometric Quantum Hydrodynamics and Bose-Einstein Condensates: Non-Hamiltonian Evolution of Vortex Lines

Context

Fluid turbulence at large Reynolds number is a subject where nontrivial exact results are rare, which is due to the fact that Navier-Stokes equations exhibit stronger nonlinearity at fine scales than coarse ones. Quantum liquids are essentially inviscid fluids whose vortical structure is restricted to thin filaments whose homogeneous circulation is a consequence of quantum effects. Here turbulence looks like a tangle of vortex lines.

Research Problem

Free decay in an ultracold quantum tangle occurs when turbulent vortices dissipate energy through phonons excited by Kelvin wave motion along the vortex line. A complete understanding quantum turbulence requires a vortex line model that supports cascade processes by allowing energy transfer between helical modes.

Geometric Quantum Hydrodynamics

Geometric quantum hydrodynamics merges geometric hydrodynamics with quantum hydrodynamics to study the geometric properties of vortex structures in superfluid states of matter. Here the vortex line acts as the fundamental building block and is a topological defect of the fluid medium about which the otherwise irrotational fluid circulates. This theory predicts that the simplest flow of curved regions on a vortex line generates Kelvin waves, providing a route to the anomalous dissipation first predicted by Onsager.

Biot-Savart Induced Velocity Field

The Kelvin-Helmholtz theorem states that the vortex flows with the ambient fluid velocity. The Biot-Savart integral constructs the ambient velocity due to a vortex source. Using this, we derive an asymptotic expression for the velocity induced by a vortex line to arrive at an equation of motion.

First, we find that the Biot-Savart integral over the vortex line, $\gamma = \boldsymbol{\gamma}(s,t)$, can be decomposed into an axial, circulatory and binormal flow

$$\mathbf{v}(\mathbf{r},t) = \frac{\Gamma}{4\pi}\int_0^L \frac{(\mathbf{r}-\boldsymbol{\gamma})\times d\boldsymbol{\gamma}}{|\mathbf{r}-\boldsymbol{\gamma}^3|} = \mathbf{v_T} + \mathbf{v}_\Gamma + \mathbf{v_B}. \tag{1}$$

It can be shown that the the binormal component arises only when the vortex is bent. For a plane circular arc, $\boldsymbol{\gamma}(s,t) = (R\sin(\kappa s), R - R\cos(\kappa s), 0)$ where $\kappa^{-1} = R = R(s,t)$ and $\kappa s = \theta \in (-\pi,\pi)$, we find that the integral of interest,

$$\mathbf{v_B} = -\frac{\Gamma\kappa}{4\pi}\int_0^L \frac{\cos(\theta)-1}{(c_1+c_2\cos(\theta))^{3/2}}\,d\theta, \tag{2}$$

$$c_1 = \epsilon^2 - 2\epsilon\cos(\phi) + 2, \tag{3}$$

$$c_2 = 2\epsilon\cos(\phi) - 2, \tag{4}$$

where $\epsilon = |\mathbf{r}|\kappa$. This integral is elliptic and for $\epsilon \ll 1$ known asymptotic formula can be applied to arrive at

$$\mathbf{v_B} = -\frac{\Gamma a_0}{4\pi}\left(1 + a_2\kappa^2 + a_4\kappa^4 + \dots\right)\kappa\mathbf{B} \tag{5}$$

As this velocity field is responsible for the evolution of the vortex line, we conclude that

$$\frac{\partial\boldsymbol{\gamma}}{\partial t} = \frac{\Gamma a_0}{4\pi}\alpha(\kappa)\frac{\partial\boldsymbol{\gamma}}{\partial s}\times\frac{\partial^2\boldsymbol{\gamma}}{\partial s^2}, \tag{6}$$

where $\boldsymbol{\gamma}_s \times \boldsymbol{\gamma}_{ss} = \kappa\mathbf{B}$. When $\alpha = 1$ we have the well-known local induction approximation.

Evolution of the Vortex Geometry

The Hasimoto transformation assumes that the local velocity field is responsible for the global dynamics of the vortex line and maps the vector problem onto the two degrees of freedom provided by the curvature and torsion. In fact, by studying the dynamics of new orthogonal frame consistent with Eq. (6) one finds that the curvature, κ, and torsion, τ are evolved by

$$i\psi_t + A(\alpha\psi)_{ss} + \frac{\alpha A}{2}|\psi|^2\psi + \frac{A\psi}{2}\int_0^s \alpha_{s'}|\psi|^2 ds' = 0 \tag{7}$$

where $A = \dfrac{\Gamma a_0}{4\pi}$ and $\psi(s,t) = \kappa(s,t)\,\mathrm{Exp}\left[i\displaystyle\int_0^s \tau(s',t)ds'\right]$. Using the previous expansion of α in terms of κ we can reduce the previous evolution to a perturbative regime where $a_{2n} = 0$ for $n \geq 2$,

$$i\psi_t + \psi_{ss} + \frac{1}{2}|\psi|^2\psi + a_2\left(\left[|\psi|^2\psi\right]_{ss} + \frac{3}{4}|\psi|^4\psi\right) = 0 \tag{8}$$

and ask the question of how the corrective term given by a_2 affects the Hamiltonian and integrable cubic focusing nonlinear Schrödinger base. From Eq. (8) we find three interesting modifications of the integrable theory associated with the local induction approximation. First, Eq. (8) and all higher order generalizations are non-Hamiltonian since no functional can be found whose variational derivative can accommodate the the fully nonlinear term, $[|\psi|^2\psi]_{ss}$. Next, we find that wave function norm, $|\psi|^2 = \kappa^2 = \rho$, is no longer conserved,

$$\frac{d}{dt}\int_{s_0}^{s_1}\kappa^2 ds = -2\int_{s_0}^{s_1}(a_2 + 2a_4\rho + 3a_6\rho^2 + \cdots)\rho_s\rho\tau ds, \tag{9}$$

resulting in gain/loss of bending along the vortex. Additionally, we find a nonlinear dispersion relation for helical modes, $\psi = \mathcal{A}e^{i(ks-\omega t)}$, for an initially localized curvature disturbance,

$$\omega(k,\mathcal{A}) = k^2(1 + a_2\mathcal{A}^2) - \frac{\mathcal{A}^2}{2} - \frac{3}{4}a_2\mathcal{A}^4, \tag{10}$$

which enhances the group velocity of low wavenumber modes.

Predictions

Moving past the lowest order approximation given by the local induction approximation, we find that a non-Hamiltonian evolution of the curvature and torsion along a vortex line supports the dispersion of long wavelength Kelvin modes necessary for relaxing post-reconnection events occurring in an ultracold quantum tangle.

Vortex Line Diagram

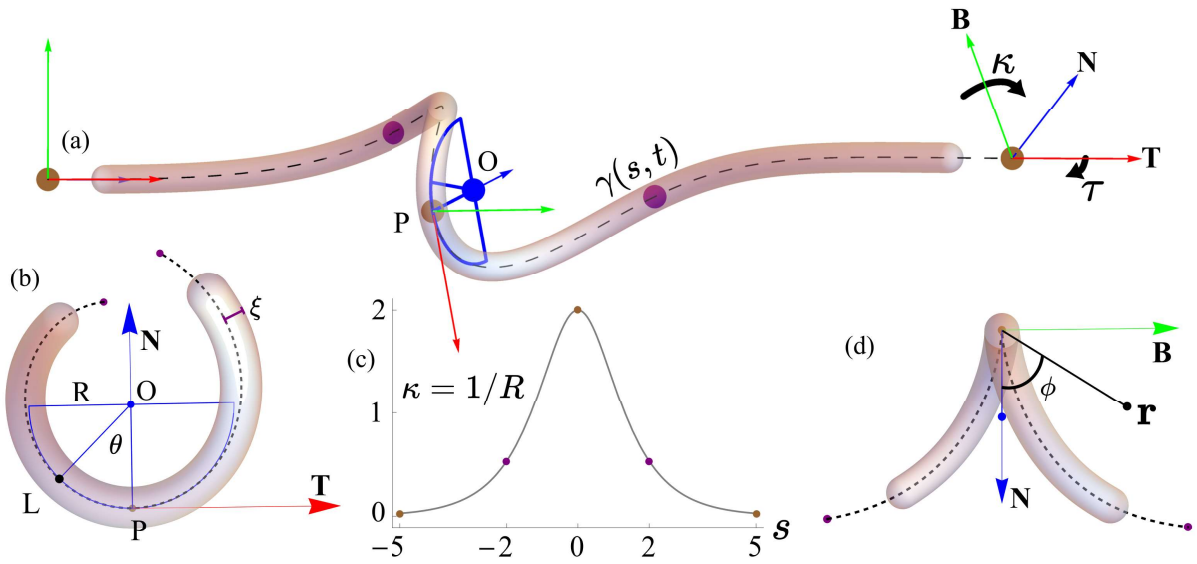

Conclusions

What was done?

We derive a model for the wave motion of an isolated vortex line consistent with Bose-Einstein condensation. Our model describes the motion of the vortex through its Biot-Savart integral and is adaptable to standard vortex filament methods. Through the Hasimoto transformation, we investigate the induced velocity field by considering the evolution of the curvature and torsion along the vortex line. The scalar evolution of the geometric properties predicts that curvature abnormalities seek to decompose themselves into traveling helical waves. Specifically, an emergent non-Hamiltonian gain/loss mechanism works in concert with enhanced dispersion to support the generation of Kelvin waves capable of emitting energy, found through vortex reconnection, as phonon excitations of the fluid. Additionally, we connect the Biot-Savart integral to continuum fluids in the high Reynolds number limit for circulatory flows whose spatial variation in the density field is suitably controlled by the potential flow.

Why was it done?

Classical turbulence undergoes free decay by allowing energy to cascade from large to small scales where molecular diffusion results in viscous dissipation. For an inviscid superfluid, an altogether unique cascade where Kelvin waves couple the vortex medium to the fluid so that turbulent energy can be dissipated via phonon emission. Currently, there are statistical theories focused on helical wave interaction. However, the only model focused on the geometric properties of a vortex line is integrable and prohibits a robust transfer of energy between Kelvin modes. Using the Biot-Savart integral, we generalize this theory and in doing so produce a model capable of Kelvin wave motion. Since it is not clear how the Biot-Savart integral fits into hydrodynamic theory, we also outline a derivation with continuum fluid mechanics as a starting point.

How was it done?

After connecting the Biot-Savart integral to hydrodynamic theory, we consider a plane circular arc and derive an expansion of the fluid velocity in powers of the local curvature. This flow is then transformed into a scalar evolution of the vortex geometry. Analysis of this evolution indicates a primitive mechanism of Kelvin wave generation, which is corroborated by numerical simulation.

What was found?

Using this analysis we find that vortex lines in Bose-Einstein condensate can be thought of as a manifestation of continuum fluid mechanics in the large Reynolds number limit and that the process of Kelvin wave generation leading to phonon emission is a direct realization of Onsager's conjecture.

What does it mean?

If the local induction approximation is a linear theory (in the curvature variable) of wave motion on a vortex line, then generalized local induction nonlinearly perturbs the problem to allow for energy transport between helical modes. This dynamic is the principal mechanism of Kelvin wave cascade in the ultracold regime of high Reynolds number turbulence, which furthers our understanding of Newtonian fluid phenomenon and vortex dominated flows in Bose-Einstein condensates.

APPENDIX B

ATTRIBUTIONS FOR IMAGES IN MIND MAP

In Figure 1.3 we provide a mind map that was used at the defense of this dissertation. The maps shows how the different topics and tools joins together to form geometric quantum hydrodynamics. Additionally, the map also shows where these materials are discussed within this thesis. Public domain graphics were used in the mind map and most request proper attribution, which we outline here. The following list starts at the upper left and cites the authors going from left to right and top to bottom.

- Silly Rabbit, Frenet Serret moving frame, *Wikipedia*, 2007
- Silly Rabbit, TNB frame momenta, *Wikipedia*, 2007
- NIST/JILA/CU-Boulder, A vortex structure emerges within a rotating Bose-Einstein condensate, *NIST*, 1995
- NIST/JILA/CU-Boulder, Bose Einstein condensate, *Wikipedia*, 1995
- Sanpaz, Components stress tensor cartesian, *Wikipedia*, 2009
- C. Fukushima and J. Westerweel, color image of the far field of a submerged turbulent jet, *Wikipedia*, 2007
- George Kenneth Lucey Jr. and Dr. D. Lyon (Army Research Laboratory), Frank Dindl (Armament Research, Development and Engineering Center), Vortex Ring Gun Schlierin, *Wikipedia*, 1997
- Jorge Stolfi, IrrotationalVortexFlow-anim-frame, *Wikipedia*, 2012
- A.C. Norman, Vortextangle, *Wikipedia*, 2009

APPENDIX C

PERMISSIONS TO USE COPYRIGHTED MATERIAL

1. Chapter 3. *Generalized Local Induction Equation, Elliptic Asymptotics, and Simulating Superfluid Turbulence*, S. A. Strong and L. D. Carr, Journal of Mathematical Physics **53**, 033102 (2012), doi:10.1063/1.3696689. Copyright (2012) by AIP Publishing. Permission is provided by AIP according to the AIP Publishing copyright policy.

2. Chapter 4. *Non-Hamiltonian Dynamics of Quantized Vortices in Bose-Einstein Condensates*, S. A. Strong and L. D. Carr, Physical Review Letters (2017), under review arXiv:1712.05885. Copyright (2017) by APS Publishing. Permission is provided by APS Publishing according to the APS copyright notice.

3. Chapter 5. *Non-Hamiltonian Kelvin wave generation on vortices in Bose-Einstein condensates*, S. A. Strong and L. C. Carr, Physical Review Fluids (2018), arXiv:1803.00147. Copyright (2018) by APS Publishing. Permission is provided by APS Publishing according to the APS copyright notice.